Nonlinear dyamics of cracked structures for non-destructive evaluation

Nonlinear Dynamics of Cracked Structures for Non-Destructive Evaluation

by

Vikrant Hiwarkar

A Doctoral Thesis

Submitted in partial fulfilment of the requirements for the award of Doctor of Philosophy of Loughborough University

2010

Dedicated to my parents

Abstract

The power plant and aerospace industries have been facing a huge loss, due to structural failure. The structural failure occurs due to the presence of the crack in it. Hence, it becomes necessary to monitor the structural health under operating condition. Most of the techniques, for structural health monitoring are used for a specific purpose. Some of these techniques require structure dismantling, which is very much expensive and time consuming. So the vibration based structural health monitoring is advantageous, compared to other techniques. Most of the vibration based Structural Health Monitoring (SHM) approaches, use linear vibration theory. But, these linear vibration based procedures, have inherently low sensitivity to crack. Since crack introduces nonlinearities in the system, their merits in damage detection need to be investigated for SHM.

In this thesis, the problem is focused on studying nonlinear dynamics of cracked structures for Structural Health Monitoring. For this, simulations and experiments are performed. The new procedure for the simulation is developed using Matlab-Simulink. It uses the numerical approximation for dynamic compliance operators and a nonlinear model of cracks contact faces interaction to study the dynamic behaviour of the cracked bar. Furthermore, the finite element model of the cracked cantilever bar with crack- tip plasticity is developed and the dynamic behaviour of the elasto-plastic bar is studied. Additionally, numerous experiments are performed to study the dynamics of cantilever bar with the fatigue crack in it.

The results from Matlab-Simulink simulation shows the distribution of higher harmonics generated along the bar length, as a function of distance from the crack. In finite element simulation, comparison is made between the resonance frequency of cracked cantilever bar with and without crack-tip plasticity. It is found that, there is decrease in resonance frequency of the cracked bar with cracked tip plasticity, when compared with the resonance frequency of cracked bar without crack-tip plasticity. This reduction in resonance frequency is due to the crack-induced plasticity near the crack tip which affects the overall stiffness of bar. In experiments, the response is measured at four different points on the cracked cantilever bar at a given resonant frequency of excitation at lower and higher vibration amplitude. For lower vibration amplitude, it is found that the response obtained near the vicinity of the crack shows the presence of higher harmonics of resonant frequency, which disappears in the response obtained far away from the crack. For higher vibration amplitude, it is found that the response obtained near the vicinity of the crack shows the presence of higher harmonics along with the low frequency component. This low frequency component causes modulation, which leads to the generation of side band frequencies near the resonant frequency. The occurrence of low frequency component and side band frequencies is due to the vibro-impact behaviour of crack. The amplitude of these side band frequencies and higher harmonics are reduced in the response obtained far away from the crack. This indicates that crack-induced nonlinearity has a localized effect on the dynamics of bar. It is also observed that the magnitude of low frequency component is proportional to the magnitude of resonant frequency of excitation. This indicates that crack behaves like a signal modulator, detector of low frequency component and amplifier as the magnitude of low frequency component is proportional to the magnitude of resonant frequency excitation. From the Matlab-Simulink simulation and experimental results, it is concluded that crack-induced nonlinearity affects the dynamic behaviour of the cracked bar significantly, which will be effective in structural health monitoring.

Keywords: vibro-impact, crack, dynamic compliance, harmonics, modulator, detector, amplifier, crack-tip plasticity, resonance frequency, structural health monitoring.

Acknowledgements

I would like to express my deep gratitude to my supervisor Prof. Vladimir I. Babitsky for his continuous support in Ph.D program. He was always there to listen and to give advice. He always encouraged me to explore my own ideas and gave me valuable suggestion when required. His valuable suggestion gave me a very good insight about the mathematics involved in my research problem and the physics behind it. His encouragement and useful suggestion made possible the successful completion of this thesis.

I am also grateful to my second supervisor Prof. Vadim V. Silberschmidt for his guidance and support at all levels. His knowledge, patience, understanding made possible the successful completion of this thesis.

I wish to recognize Wolfson School of Mechanical and Manufacturing Engineering of Loughborough University for providing the generous financial support without which my postgraduate studies would not have been possible.

I am also grateful to Dr. Alan Meadows for his suggestion for experiments.

I would also like to thank Dick Price, Dave Britton, Andy Sandaver , Alan Trahar, Brian Mace and John Dorman for technical support.

I am also indebted to many of my colleagues for their support from dynamics research group and mechanics of advanced material group.

Finally, I would like to thank my parents for their continual support during my post graduate years of study.

Notations and Abbreviations

Symbols	Meaning
P	Harmonic Force
E	Modulus of Elasticity
S	Area of Cross Section
ϵ	Strain
ρ	Density of Material
γ	Wave Velocity
b	Linearised Coefficient of Force of Internal Damping
χ	Absorption Coefficient
ω	Frequency of Excitation
s	Complex Variable
$u(x,t)$	Vibrational Displacement
$L(x,j\omega)$	Receptance Coupling Between Force and Displacement
$\overline{K}$	Displacement of a Cross Section of Rod
$y(x)$	Static Deflection
$f(q), P(q,t)$	Load Intensity
F_k	Concentrated Force
α_{ik}	Static Factors of Influence
$m(x)$	Mass or Moment of Inertia of Unit Length of Rod
$\bar{A}(x)$,$A(x)$	Amplitude or Modal function
Ω	Eigenvalues
$F(x,\dot{x})$	Contact Force
NDE	Non-Destructive Evaluation
FEM	Finite Element Method
SHM	Structural Health Monitoring

Publications

Vikrant Hiwarkar , Vladimir Babitsky, Vadim Silberschmidt "Damage Assessment of a Cracked Bar: Effect of Material Nonlinearity on Vibro-Impact Response." *Key Engineering Materials* Vols. 413-414 (2009) pp 237-244.

Vikrant R. Hiwarkar , Vladimir I. Babitsky, Vadim V.Silberschmidt "Vibro-Impact Response of a Cracked Bar." *Proc. 2nd International Conference on Vibro-Impact Systems,* Sanya , P.R. China, 2010, pp 1-11

Vikrant R. Hiwarkar , Vladimir I. Babitsky, Vadim V.Silberschmidt "Vibro-Impact Response of a Cracked Bar." *Journal of Shock and Vibration, special edition for 2nd ICoVIS.* In press, submitted 16.2.2010.

Table of Contents

Chapter 1 Introduction

1.1 General Introduction

Structural Health Monitoring (SHM) is receiving much attention due to the possible failure occurring in structures under operating conditions. In most of the cases, failure is caused by the growth of crack present in the structure. In order to prevent the failure due to the crack, structures need to be designed with higher safety margins. But due to the increasing demands for the energy and material conservation structures have to be designed with smaller safety margins. At these conditions, it becomes necessary to have the accurate quantitative estimates of flaw tolerance of structure in load bearing components of all kinds. Hence, it becomes necessary to design a structure which will avoid large stress concentration coupled with Non-Destructive Evaluation (NDE) techniques to find the defects in structures under working condition.

Presence of crack in structure does not mean that it is at the end of its useful service life. Hence the repair and replacement of damaged components can be balanced for the optimum utilization of the structure under working conditions with the help of NDE techniques. These techniques can help minimize the risk of failure, but problem exists due to poor design, deterioration, over loading, inadequate or nonexistent maintenance and the low bid syndrome. Identifying and rectifying all the problems which can cause structural failure is an impossible task but through the effective use of NDE techniques, failures can be reduced. Hence, there is a need for new NDE techniques to monitor the crack in the structures, so that structure can be optimally utilized. In recent years, there has been an increase in crack detection methodologies and online techniques. Some of the crack detection methodologies includes visual inspection, ultrasonic technique, eddy current technique, acoustic emission technique, X-rays etc. However these methods are inoperative and unsuitable for some particular cases, since they require minutely detailed periodic inspections, which are very costly. In order to avoid this cost, new methods have been developed for online SHM based on the vibration characteristics of the structure. These vibration characteristics of structure can help to monitor the structural health globally when compared with other NDE techniques. These vibration characteristics of the structures are dependent on physical parameters such as mass, stiffness or damping. The presence of cracks in a structure affects these parameters which results in change in vibration characteristics of the structure such as natural

frequency and mode shapes. But these linear vibration based procedures do not always come up with practical results because of its inherently low sensitivity to defects. Since cracks introduce nonlinearities in the system, their merits in damage detection need to be investigated for SHM.

1.2 Aim and Objectives

1.2.1 Aim

The aim of this project is to study the effect of crack-induced nonlinearity on the dynamics of the structure for SHM.

1.2.2 Objectives

The objectives of this research are:

1) To investigate the effect of material nonlinearity on the dynamic response of the structure.
2) To study the nonlinear resonant phenomena due to vibro-impact interaction within a cracked bar.
3) To make recommendations on structural health monitoring of cracked bar due to the presence of contact nonlinearity.

1.3 Outline of Thesis

The work incorporates six chapters, summary of which is as follows:

Chapter 1 is introduction to the problem.

Chapter 2 deals with the literature review on various crack monitoring techniques at present and about various mathematical and finite element models developed for studying the dynamic behaviour of structures with crack in it.

Chapter 3 is devoted to developing the dynamic model of the cracked cantilever bar. The developed new procedure uses numerical approximation for dynamic compliance operators and a nonlinear model of cracks contact faces interaction to study the dynamic behaviour of the cracked bar. Nonlinear resonant phenomena due to vibro-impact interaction within cracked bar are obtained and analysed. A distribution of the higher harmonics generated due to the crack along the bar length is revealed as a function of

the distance from the crack. Recommendations on structural health monitoring of cracked bar due to contact nonlinearity are presented.

Chapter 4 presents the damage assessment for a component using an example of a crack in the cantilever bar under longitudinal harmonic loading. The finite element simulation is used to perform this analysis. For nonlinear materials, their properties in terms of the plastic behaviour are introduced. The effects of the crack size and position along the beam length are studied. An observed change in frequency response is used to characterize the damage state of the cracked cantilever bar.

Chapter 5 discusses experiments performed on the cracked cantilever bar under longitudinal harmonic loading excitation. In experiments piezo-strain gauges are used for measuring a response of the uncracked and cracked bar. The dynamic response of the system obtained is used to characterize the structural health of the bar under consideration.

Chapter 6 summarises the outcome of the present work, draws conclusions and recommends areas for future work.

Chapter 2 Crack Monitoring Techniques

2.1 Introduction

In recent years, there has been increase in crack detection methodologies and online techniques. These techniques for crack detection are conventional and non conventional Non-Destructive Evaluation (NDE) techniques. The conventional NDE methods have unacceptable limits in terms of their applications for online crack detection. Some of these conventional NDE techniques are time consuming and inconvenient. Almost all the conventional NDE techniques require that vicinity of the damage be known in advance and they can provide only local information with no indication of structural strength at component and system level. In addition to this, the effectiveness of these techniques is affected by the high measurement noise level. Hence there is a need for new non-conventional NDE techniques. In this chapter various available NDE techniques have been discussed on the basis of their application in different sections.

2.1.1 Visual Inspection

Visual inspection is a method in which the structural integrity of the material component is assessed by the eye. This method is effective for the detection of the damage on the surface of the component. It is most commonly used for assessing the damage in aircraft in service. Visual inspection by the eye can be assisted by a microscope to provide detailed information on micro crack in metals and delamination areas in composites. However this procedure is not helpful in finding the subsurface crack in the material component.

2.1.2 Eddy Current Technique

The eddy current technique is the most widely used technique for monitoring the damage in aircraft. This method is based on the principle of detecting the changes in electromagnetic impedance due to the strain in the material. In this technique a circular coil carrying current is placed in the proximity of an electrically conductive specimen. The alternating current in the coil generates changing magnetic field which interacts with the conductive specimen and generates eddy currents. The presence of any flaw causes a change in the eddy current flow and a corresponding change in phase and amplitude of the measured current. This technique is widely used because of its

simplicity to implement and inexpensive equipment for performing test. However, disadvantages of this technique is that large power requirements and complicated data.

2.1.3 Ultrasonic Technique

Ultrasonic technique used high frequency sound energy for flaw detection and the material characterization. This technique can be classified as linear and nonlinear ultrasonic technique. The conventional (linear) ultrasonic techniques utilize wave attenuation, reflection, and refraction for the damage detection. But in non conventional (non-linear) ultrasonic technique Lamb waves are used for damage detection. Lamb waves are guided waves governed by the same wave equations as bulk waves having infinite number of modes associated with propagation. In this technique, an external source of energy is used to open and close the crack while it is isonified with the Lamb waves. This results in the interaction between the Lamb wave and the frequency of the energy which opens and closes the crack. This interaction occurs only in the presence of crack. Thus non-linear method based on Lamb waves provides a quick and reliable method of determining a crack for SHM [McGravie *et al.*, 2000] when compared with conventional ultrasonic technique.

Nagy, 1998 used nonlinear ultrasonic to study effect of fatigue on nonlinear behaviour of materials. The comparisons were made between different linear and nonlinear parameters to the degradation of material strength during long term fatigue cycling. It was found that just before the failure, nonlinearity caused by fatigue cracks were as much as one order of magnitude higher than the intrinsic nonlinearity of the intact material. From the results obtained, it was concluded that acoustic nonlinearity was uniquely sensitive to the fatigue damage, which could be exploited for non-destructive characterization of plastics, plastic joints, epoxy matrix composites, adhesive joints as well as metals and metal matrix composites.

Solodov, 1998 investigated acoustic non-linear phenomena on contact boundaries. He performed simulation and experiments to study this phenomenon. It was found that contact vibrations led to threshold nonlinear distortion due to clapping and kissing mechanism, multiple bifurcations and chaos development. It was also observed that Hertzian contact nonlinearity increased with the decrease in contact load and was predominated by a clapping mechanism in mixed mode vibrations. Also, the author has

proposed many modes of non-linear NDE to detect small fractured defects invisible by linear NDE techniques.

Donskoy *et al.*, 2001 developed a vibro-acoustic modulation technique based on modulation of ultrasonic signal by low frequency vibration in the presence of a flaw such as a crack, delamination or poor quality bonding. They found that the resulting modulated signal contained new frequency components which were associated with the flaw. They indicated that the method developed could be expanded and enhanced for non-destructive testing and characterization by providing discriminating and quantitative capabilities.

Donskoy *et al.*, 2003 suggested the vibro-modulation technique for the detection of contact type interfaces such as cracks. The principle of vibro-modulation technique is shown in Fig. 2.1. In this technique, the excitation of low frequency vibrations at f_1 and

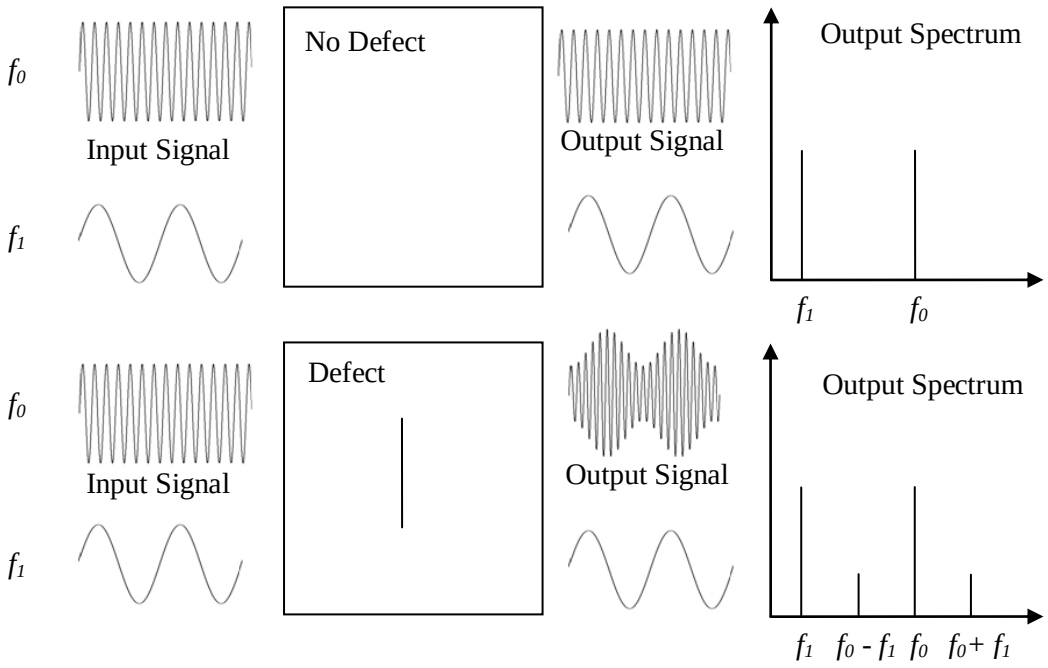

Figure 2.1 Principle of vibro-modulation technique
Modified, after [Donskoy *et al.* , 2003]

high ultrasound at frequency f_o were given to the damaged and undamaged sample of linear elastic material. It was found that the output spectrum of sample with no defect showed only f_o and f_1 frequency components. However in the case of the sample with a crack, applied low frequency vibrations vary a contact area of cracks faces effectively modulating a high frequency ultrasonic wave passing through it. From Fig. 2.1 it is clear

that modulation leads to additional spectral components at the combination frequencies of $f_o \pm f_1$ which serve as indicators of material imperfection. They have shown that spectral amplitude as the sum and difference of frequencies were proportional to the crack size and could be used for defect characterization as well as monitoring.

Staszewski *et al*., 2004 developed structural health monitoring technique using Lamb waves based on guided waves introduced to a structure at one point and sensed at different location. The technique utilized a laser Doppler velocitimeter for sensing the Lamb waves. The study showed that there is a potential of laser vibrometry for Lamb wave sensing. This sensing technique was utilized for the damage detection using low frequency Lamb waves [Mallet *et al.*, 2004]. It was found that scanning laser vibrometry could be used to analyse the 3D Lamb wave propagation field, which allowed for automated damage detection and location. This technique was further extended for fatigue crack detection in metallic structures [Leong *et al*., 2005]. It was shown that the method developed could be used for non-contact measurements of local amplitude and time of flight variations of Lamb waves that cannot be achieved with a smaller number of traditional contact transducers. The experimental results obtained clearly located the crack at the centre of an aluminium plate.

Palit Sagar *et al.*, 2006 used nonlinear ultrasonic technique to assess the fatigue damage in low carbon steel. They considered percentage of harmonic distortion, ratio of the second harmonic and the fundamental as the measurement parameter in this study. They observed that second harmonic amplitude becomes comparable to the amplitude of fundamental at nearly 95% of expended fatigue life, which could be used as a signature of fatigue crack initiation of in-service components. Their results were analyzed in the light of dislocation theory for harmonic generation during material degradation.

Zaitsev *et al.*, 2006 discussed nonlinear modulation acoustic technique for crack detection. This technique was based on the cross modulation effect consisting in transfer of modulation from an intensive, initially slowly amplitude modulated pump to probe signal. The carrier frequency of the latter may be either lower or comparable or higher than that of the pump signal. The principle of cross modulation is schematically shown in Fig.2.2. Their investigation revealed that the modulation technique was sensitive to the presence of crack like defect. Their result indicated that in contrast to conventional role of the elastic part of the sample nonlinearity, the effect of amplitude dependent

dissipation might play a dominant role for modulated effect in weakly damaged samples.

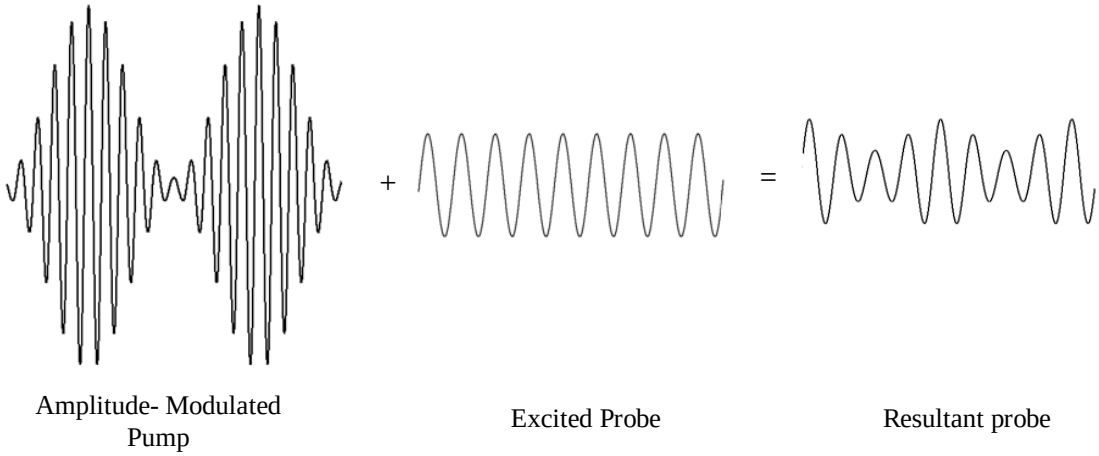

Figure 2. 2 Cross modulation of a probe wave caused by an amplitude modulated pump excitation
Modified, after [Zaitsev *et al.* , 2006]

Parsons *et al.,* 2006 developed a technique based on acoustic wave propagation in structures for crack detection. They used piezoelectric excitation in the nonlinear acoustic technique for the detection of fatigue cracks. Their results showed the encouraging potential of piezoelectric excitation for the nonlinear acoustic technique.

The ultrasonic damage detection techniques discussed in this section show that nonlinear ultrasonic technique is quite advantageous as compared to the linear ultrasonic technique because of its high sensitivity to the defects like crack. It can be observed from the literature that the nonlinear ultrasonic's can be used to characterize the material properties of the damaged specimens, predict the extent of damage in the specimen and to locate the position of the crack in the specimen. The nonlinear ultrasonic technique offers an advantage for SHM whereas conventional ultrasonic technique is quite expensive, time consuming and it needs the dismantling of the machines for testing. This conventional technique is useful for NDE has limited application and cannot be used for online structural health monitoring.

2.1.4 Acoustic Emission Technique

Acoustic Emission (AE) is one of the early and widely used NDE techniques for structural damage detection. This technique relies on the transient sound waves generated by the material during fracture which then propagates through the analyzed

material. Most of these waves are short-time transient events (burst signals) of significant energy between 100-1000 kHz. The waves can propagate long distances in circles, i.e. in all possible directions. Therefore AE testing can cover large, often inaccessible, monitored areas. The distance of propagation depends on material properties, geometry, frequency and environment. Acoustic events at their origin are high-frequency (in MHz) wideband impacts emitted internally by micro cracks and/or inclusion de-cohesion (e.g. metallic inclusions, bubbles) under external loading applied to monitored specimens. These material defects release elastic energy due to rapid local stress redistribution as a result of loading. The energy results from growing cracks, rubbed surfaces of cracks or dislocations. In this section literature is focussed on the new developments in the acoustic emission technique.

Paget *et al.*, 2003 developed a very efficient way to determine the location of a damage using Tobias algorithm. However, this algorithm is restricted to the quasi isotropic composites. To overcome this, they developed an analytical triangulation algorithm adapted to composites including quasi-isotropic materials. They experimentally verified the results using damage monitoring system based on modified acoustic emission called BALRUE. It was concluded that new algorithm was very effective in damage location with good accuracy and fast processing time.

Carpinteri *et al.*, 2007 used acoustic emission technique to identify defects and damage in reinforced concrete structures and masonry buildings. They developed a methodology for crack propagation monitoring and damage assessment in structural elements under service conditions. This technique allowed to estimate the energy released during fracture propagation and to obtain information on the criticality of the ongoing process. This made them possible to ascertain stability or instability conditions and to forecast the extent of damage in structures.

This technique is used for monitoring the bridges, masonry buildings, pipelines, pressure vessels, storage tanks and reinforced structures. This technique offers good advantage of continuously gathering the data and detecting the changes due to the damage in structure under consideration. But the acoustic emission signals are quite weak. In noisy environment it becomes difficult to discriminate between the signal due to the damage and signal due to the surrounding environment.

2.1.5 Vibration Based Technique

Vibration based technique offers an effective and fast means of detecting the cracks in the structures under working condition. Several researchers have used this technique for various problems. This technique has several advantages over other crack monitoring techniques. This technique can be used for online crack monitoring. Moreover this technique is economical as compared to other NDE techniques. This technique has been classified on the basis of the type of vibration and the behaviour of crack.

2.1.5.1 Transverse Vibration of Cracked Beams

This section discusses the transverse vibration of the cracked beam. The literature considered in this section deals with the different approaches used by researchers for the modelling of the cracked beam and their findings.

Cawley *et al.*, 1979 developed a method of non-destructively assessing the structural integrity by measuring the natural frequency. They have shown that measurement made at single point in the structure can be used to detect, locate and quantify the damage. The results obtained showed good agreement between the predicted and actual damage sites useful for the indication of the magnitude of defect.

Gounaris *et al.*, 1988 modelled cracked prismatic beam using finite element method by using local flexibility introduced by the crack in beam section. They used strain energy concentration argument which led to the development of a compliance matrix for the behaviour of beam in the vicinity of the crack. This matrix was used to develop the stiffness matrix for the cracked beam element and the consistent mass matrix. The element was used to evaluate the dynamic response of a cracked cantilever beam to a harmonic point excitation. The results obtained showed that the resonant frequencies and vibration amplitudes were considerably affected by the existence of the moderate cracks.

Ostachowicz *et al.*, 1990 modelled a beam with a transverse crack by triangular disk finite elements. They studied the effects of crack locations and sizes on the vibration behaviour of the beam. They determined the location of the crack by determining the deflection shape of the beam. It was found that vibration amplitude was three times bigger than vibration amplitudes without a crack.

Shen *et al.*, 1990 suggested an approximate Galerkin solution to the one-dimensional cracked beam theory developed by Christides *et al.*,1984 for free bending beams with pairs of symmetric open cracks. In Galerkin's procedure, series of comparison functions were considered to be consisting of mode shapes of the corresponding uncracked beam. The number of terms in the expansion was determined by convergence of natural frequencies and was confirmed by studying the stress concentration profile near the crack. This approach allowed them to determine the higher natural frequencies and the mode shape of the cracked beam. A finite element approach, predicted the changes in eigen frequencies and eigen modes due to cracks. Results obtained for the first three natural frequencies and mode shapes agreed well with the finite element results and experimental findings.

Rizos *et al.*, 1990 analyzed flexural vibrations of a cantilever beam with rectangular cross-section having a transverse surface crack extending uniformly along the width of the beam. They measured amplitudes at two points on the structure vibrating at one of its natural modes. This helped them to predict the crack location and the crack depth with satisfactory accuracy. The identification method was based on the assumption of a transverse surface crack, extending uniformly along the width of the structure. The proposed method can be developed into a simple, non-invasive technique and a useful tool for preventive maintenance and non-destructive testing of structures.

Ostachowicz *et al.*, 1991 proposed a method to study the effects of two open cracks on the natural flexural vibrations of a cantilever beam. They considered two types of crack: double sided, occurring in the case of cyclic loadings and single sided, occurring as a result of fluctuating loads. They assumed that the cracks occurred in the first mode of fracture i.e. the opening mode. They developed an algorithm which indicated the relationship between the position, the magnitude of the crack and the first natural frequency of the cantilever beam. The results obtained showed that the positions of the cracks in relation to each other significantly affected the natural frequency in the case of equal relative depth of the cracks. It was also found that a decrease in the natural frequency was the largest if the cracks are near to each other. When the distance between cracks increased, the natural frequencies of the beam tend to the natural frequencies of a system with a single crack. Moreover in case of two cracks with different depths, the larger crack had more significant effect on the natural frequency. They also concluded from the algorithm that double sided cracks affected the vibration

frequencies to a smaller degree than a single crack with the same relative depth of crack and the same position.

Shen *et al.*, 1991 developed the procedure to determine the crack characteristics from the dynamic measurements. Their procedure was based on minimization of either the ‘‘mean-square’’ or the ‘‘max’’ measure of difference between the measured data such as natural frequency and mode shape. They obtained a necessary condition for formulations and simulated damage in the form of one-side or symmetric cracks in a simply supported Bernoulli-Euler beam. The results obtained indicated the uniqueness and reliability of the developed procedure.

Kam *et al.*, 1992 used modal test data for identifying the crack in a cantilever beam. They discretized the cantilever beam into a set of elements and assumed the crack to be located within one of these elements. They used vibration frequencies and mode shapes to identify the cracked element based on the simple reduced stiffness model. They performed static deflection analysis of the structure with and without a crack and constructed a strain energy equilibrium equation for determining the size of the crack. They suggested that the procedure in general can be applied to more complex structures containing a crack.

Kam *et al.*, 1994 developed an expanded mode method based on modal analysis and energy method for crack identification at a given location in a damaged structure. The result obtained indicated that the use of frequency and mode shape of only one vibration mode of cracked structures could yield good results as long as the crack was not located at the nodes of the mode.

Cheer Germ Go *et al.*, 1994 formulated a super element by using infinitely small elements for analyzing the dynamic behaviour of a cracked beam. They used the concept of matrix condensation, using the characteristic properties of stiffness for the plane elements. This element approach for determining the stress field in the immediate neighbourhood of a singular point was found to be excellent. The sub-element around the crack tip was subdivided to be arbitrarily small to model the stress singularity with sufficient accuracy. The results obtained indicated that it was economical in terms of computer memory and programming.

Shen *et al.*, 1994 presented a formulation for the flexural motion of a Bernoulli – Euler beam containing a single edge crack. They used generalized variational principle. They represented strain concentration by introducing a crack function in to the beams compatibility relations. A displacement function was also introduced to modify the in-plane displacement and its slope near the crack. Both functions were chosen to have a maximum value at the cracked section and to decay exponentially along the longitudinal direction. They solved the resulting equation of motion for simply supported and cantilevered beams with a single-edge crack by Galerkin and a local Ritz procedure. It was found that the effects of cracks on frequency and mode shape were very sensitive to crack location and mode number.

Bamnios *et al.*, 1995 studied the influence of a transverse surface crack on the dynamic behaviour of a cracked cantilever beam. They modelled the crack as a rotational spring; relations linking to the change in natural frequency and mechanical impedance to the location and depth of crack were obtained. It was shown that the change in the mechanical impedance due to the presence of the crack was substantial and exhibited definite trends depending upon the location of the crack and the driving point. The method was based on the combined examination of both natural frequencies and mechanical impedance that allowed an estimation of both the location and size of the crack.

Gounaris *et al.*, 1996 developed a new method for the determination of the depth and location of a transverse surface crack in a beam. They found that the direct responses changed very little due to the presence of small cracks, while the coupled responses changed substantially allowing the diagnosis of the presence of small cracks. It was also observed that the coupled response was only due to the existence of cracks, which disappeared in the absence of cracks.

Gounaris *et al.*, 1997 developed a new method for crack identification in structures in fluid environments such as offshore installations, ship and others. In this method, they correlated the mode differences with the crack depth and location. The correlated differences were chosen to be the ratio of two amplitude measurements in two positions and the distance of node of the vibrating mode from the left end, while the structure was vibrating under harmonic excitation in resonant condition. Their findings suggested that this method could have application in diagnosis of cracked bone restoration process.

Dado, 1997 developed a comprehensive algorithm for crack identification in different boundary conditions. In this study he assumed crack as a torsional spring and calculated the torsional stiffness using the expression of local crack compliance. For developing the algorithm he considered natural frequencies of the first two bending modes .The algorithm developed helped to give the initial estimate of severity and the proper location of the cracks. The algorithm was developed for pinned-pinned beams, clamped-free beams, clamped-pinned beams and clamped-clamped beams. From the results, it was found that in the case of pinned-pinned beams for a given first mode frequency ratio, as the crack location moved towards the middle of the beam, the second mode frequency ratio gets closer to unity and the crack got deeper as it moved closer to support. In clamped-free beams as the crack location moved towards the root of the beam, the second mode frequency ratio got closer to unity and the crack got deeper as it moved closer to the free end. In clamped-pinned beams as the crack location moved towards the clamped end or the middle of the beam, the second mode frequency ratio got closer to unity and the crack depth got smaller near the clamped end and the middle of the beam. Finally, in clamped-clamped beams the crack location came near the end or the middle of the beam as the second mode frequency ratio gets closer to unity and the crack depth got smaller near the end and the middle of the beam.

Chondros *et al.*, 1998 proposed a vibration theory for the lateral vibration of continuous cracked Euler-Bernoulli beams with single edge or double edge open cracks. They used the Hu-Washizu-Barr variational formulation [Barr, 1966] to develop a differential equation and the boundary conditions of the cracked beam as a one dimensional continuum. The crack was modelled as a continuous flexibility using the displacement field in the vicinity of the crack found by fracture mechanics methods. They compared the lowest natural frequency of the bar obtained from the continuous cracked bar vibration theory and the experimental results. They found that the analytical results and experimental results showed very good correlation.

Shifrin *et al.*, 1999 introduced a new technique for calculating the natural frequencies of vibrating beams with an arbitrary finite number of transverse open cracks. They considered the crack as a mass-less spring and used a continuous mathematical model of the beam in transverse vibration. The main feature of this technique was related to the reduction of the dimensions of the matrix involved in the calculation to reduce computation time for evaluating the natural frequencies compared to alternative

methods which also make use of a continuous model of the beam. Utilising this approach, they have showed that it was possible to write a determinantal equation whose roots were the eigen frequencies of the beam. They showed that just (n+2) equations were sufficient to solve the problems for a beam with n number of cracks. Hence, a key feature of the procedure was to evaluate a small dimension of the determinant which enabled reduction of computation time. As a consequence, this procedure opened new possibilities in the reduction of computation time needed for solving the inverse problem through advanced optimisation techniques.

Viola *et al.*, 2001 used a cracked beam element method to study the dynamic behaviour of a cracked cantilever beam. They developed a special finite element for a cracked Timoshenko beam and used shape functions for rotational and translational displacements to obtain consistent mass matrix for the cracked beam element. They investigated the effect of the crack on stiffness and consistent mass matrix. Their study proposed that the finite element model of a cracked beam, coupled with identification methodology might be useful for detecting the cracks in engineering applications.

Saavedra *et al.*, 2001 proposed a new modelling approach for cracked beam structures. The additional flexibility that crack generated in its vicinity was evaluated by using the strain energy density function given by the linear fracture mechanic theory. Based on this flexibility, a new cracked finite element stiffness matrix was deduced, which was used subsequently in the FEM analysis of crack systems.

Bamnios, 2002 studied the influence of a transverse open crack on the mechanical impedance of cracked beams under various boundary conditions. They found that driving point impedance changed substantially due to the presence of the crack. This change depended on the location and the size of the crack and on the location of the excitation force. The results obtained indicated the change in first anti-resonance as a function of location of measurement point along the beam for different boundary conditions. It was found that there was a jump in a slope of plot in the vicinity of the crack.

Sinha *et al.*, 2002 modelled cracks in beams undergoing transverse vibration. They used Euler-Bernoulli beam elements with small modifications to the local flexibility in the vicinity of the cracks. This crack model was used to estimate crack location and sizes. It

was observed that estimation of crack location was more accurate than the estimation of crack depth.

Dilena *et al.,* 2002 presented a technique of crack location in vibrating beams from the changes in node positions. They focussed on detecting a single crack when the damaged-induced shift in the nodes of mode shapes of a beam in bending vibration was known. It was shown that the direction by which the nodal points shifted might be used to estimate the location of damage. The analytical results agreed well with the experimental tests performed on cracked steel beams. The results obtained represented the first step of a line of research on the damage-induced changes in the null set of eigen functions of vibrating systems.

Dado *et al.,* 2003 addressed the problem of linear crack quantification, crack depth estimation and localization in structures. They obtained the modal data for cracked structures by solving the corresponding eigenvalue problem. The error in the modal data was simulated by an additive noise that followed the normal distribution. The simulated modal data was expanded using eigenvector projection method. The results obtained showed that this technique gave good results with high depth ratio.

Dado *et al.,* 2003 investigated the vibrational behaviour of a cracked cantilever beam carrying end mass and rotary inertia. They coupled transverse and axial vibrations of beam through the crack model. They found that the coupling between transverse and axial vibration was weak for the first two modes for the moderate values of the crack depth ratio. For the higher crack depth ratio there was a strong coupling between the modes.

Dilena *et al.,* 2004 investigated the influence of single open crack in a vibrating beam. They showed that how an appropriate use of frequencies and anti-resonances might be useful to avoid non-uniqueness of damage location problem which occurred in symmetrical beams when only one frequency data was used.

Dharmaraju *et al.,* 2004 suggested a general identification algorithm to estimate crack flexibility coefficients and crack depth based on the force–response information. This technique required that the crack location and the force acting on the beam were known. They used a harmonic force of known amplitude and frequency to excite the beam. For finite element modelling, Euler-Bernoulli beam element was used. They considered an

open transverse surface crack and modelled the crack by a local compliance matrix of four degrees of freedom. This compliance matrix contained diagonal and off diagonal terms. To simulate the cracked-beam response, they assumed the coefficients of the compliance matrix due to the crack, which was evaluated by the fracture mechanics approach for a given crack depth. However, for measuring responses at all the nodes, general identification algorithm had practical limitations. To overcome this they incorporated the static reduction technique in the identification algorithm to eliminate some of the degrees of freedom. The results for the cracked beam response showed splitting of the natural frequency due to the coupled motion of the beam in two orthogonal directions in the presence of the crack. It was also found that the splitting of natural frequency was more intensive when the location of crack was at the anti-nodal point of the mode shapes.

Douka *et al.,* 2004 studied the effects of two transverse open cracks on the anti-resonances of a double cracked cantilever beam analytically and experimentally. They found that far from the expected changes in natural frequencies, the anti-resonance frequencies changed substantially due to the presence of the cracks. They concluded that anti-resonance could be used as an additional information carrier for crack appearance which was complementary to natural frequency changes.

Çam *et al.,* 2005 used impact-echo method to excite the natural frequencies of a cracked beam. It was found from this study that when the position of the crack changed starting from the clamped end of the beam, natural frequencies of the beam and the amplitude of the high frequency vibration increased, but the amplitude of low frequency vibration decreased. It was also shown that as the depth of the crack increased, the amplitude of vibration also increased at high frequencies but the natural frequencies decreased as expected because of stiffness reduction which is inversely proportional to the depth of the crack. From this they concluded that more sensitive results may be obtained by optimizing the impact point.

Dharmaraju *et al.,* 2005 developed an algorithm for the estimation of beam crack parameters. The result showed the separation of its natural frequencies due to coupled motion of the beam in two orthogonal directions in the presence of the crack. The separation of the natural frequency was found to be more when the location of crack was at the anti-nodal point as compared to nodal points of the mode shape.

Nahvi *et al.*, 2005 studied a crack cantilever beam to establish a method for predicting the location and depth of the crack. To avoid non-linearity, it was always assumed that crack was open. To identify the crack, contours of the normalized frequency in terms of the normalized crack depth and location were plotted. The intersection of the contours with constant modal natural frequency planes were used to relate the crack location and its depth. A minimization approach was employed for identifying the cracked element within the cantilever beam.

Orhan, 2007 analyzed the free and forced vibration of a cracked cantilever beam using a finite element program in order to locate the crack. This study was carried on a single and two edge crack. The natural frequencies were calculated by the free vibration analysis. The sinusoidal harmonic force was applied on the free end of the beam and the harmonic response was obtained at the point of application of the force. The changes in natural frequencies and the harmonic responses corresponding to the change in crack depth and location were evaluated for crack detection analysis. The study indicated that the harmonic response analysis was more suitable than the free vibration analysis in the case of a single crack on the top and the bottom surfaces. On other hand, free vibration analysis seemed to be a more effective method of detection as compared to the harmonic response analysis for two cracks on the top and bottom surfaces of the beam.

Bayissa *et al.*, 2008 developed a new damage identification technique based on statistical moments of the energy density function of the vibration in the time-frequency domain. They concluded that the time-frequency analysis conducted using wavelet transform provided a powerful tool to characterize deterministic as well as random responses and could be used to detect slight changes in the response characteristics and local variations. The results obtained from this method showed that it was more sensitive than the non-model based damage identification techniques.

Manoach *et al.*, 2008 studied the sensitivity of nonlinear vibration response parameters to the presence of damage on geometrically nonlinear vibrations of a fully clamped rectangular plate. They represented damage as a stiffness reduction in a small area of the plate and obtained plate vibration response by a pseudo-load mode superposition method. Numerical results obtained for large amplitude vibrations of damaged and healthy rectangular and square plates showed good abilities to detect and localize damage.

Shih *et al.*, 2009 used dynamic computer simulation techniques to develop and apply a multi-criteria procedure using non-destructive methods for damage assessment in beams and plates. In addition to changes in natural frequency, this multi-criteria procedure incorporated two methods called modal flexibility and the modal strain energy based on vibration characteristics of the structure. The results obtained showed that multi-criteria method incorporating modal flexibility and modal strain energy method was effective in multiple damage assessment in beam and plate structures

From the literature, it can be observed that researchers considered the open crack for the purpose of modelling. They used different approaches to derive the stiffness matrix for the behaviour of a beam in the vicinity of a crack and established a finite element model having different boundary condition. They showed that the presence of a crack in the beam affected the resonance frequencies and the vibration amplitude considerably. Few researchers used the Galerkin's solution to the cracked beam theory. Their approach allowed them to determine the higher natural frequencies and the mode shapes of the cracked beam. Some researchers used a variational approach to model the cracked beam. They modelled crack as a continuous flexibility using the displacement field in the vicinity of the crack using the fracture mechanics method. This allowed them to estimate the damage in the beam with the use of eigen frequencies and mode shapes. Some of them observed that there were damage-induced shifts in the nodes of mode shape which could be used for determining the location of damage. Few of them suggested that the coupled response and the shift in the anti-resonance frequency could be used for predicting the presence of crack and estimating the severity of damage. It was also observed by some researchers that due to the presence of a crack, splitting of the frequencies takes place. It was also found by a few of them that combined examination of both natural frequency and mechanical impedance allowed an estimation of both location and size of the crack.

It is clear from discussion in above section that the presence of crack significantly affects resonant frequency, mode shape, and vibration amplitude, position of node in a mode shape, anti-resonance frequency and mechanical impedance. All this parameters can be used for determining the location and the size of crack. But in all this research carried by researchers the crack was considered as an open crack to avoid the nonlinearity in the cracked beam. The crack closure effect was neglected. However, the opening and closing of the crack has the significant effect on the dynamics of a cracked

beam. So it becomes necessary to study the effect of the breathing crack on the dynamics of the cracked beam.

2.1.5.2 Longitudinal Vibration of Cracked Beams

This section deals with the longitudinal vibration of cracked beams. The literature considered over here discusses the different approaches used by the researchers for modelling of the open crack and their findings.

Gudmundson, 1982 considered a bar with a free end and a transverse crack at the centre. He presented a perturbation method which predicted the changes in resonance frequencies of a structure resulting from cracks, notches or other geometrical changes. He had shown that eigen frequency changes due to crack depend on the strain energy static solution. The results compared well with the values obtained by experiments and finite element method for small cracks.

Chondros *et al.*, 1998 developed the continuous cracked bar vibration theory. They analyzed a fixed-free bar with single open edge crack. In this study, the stress and displacement field about the crack was used to modify the stress and displacement field throughout the bar; reduction to one spatial dimension was achieved by integrating the stress and displacement fields throughout the bar cross-sections so that total displacement would be exact. They obtained differential equation with variable coefficients with the modified displacement field due to the embedded crack. The displacement field about the crack was computed using fracture mechanics methods. The results obtained from numerical solution and a first order perturbation solution showed changes in natural frequencies. These results obtained had very close correlation with the experimental results.

Chondros *et al.*, 1998 proposed a vibration theory for the longitudinal vibration of rods with an edge crack. They analyzed a free-free bar with single open edge crack. They used Hu-Washizu-Barr variational formulation [Barr, 1966] to develop the differential equation and boundary conditions for a cracked bar as a one dimensional continuum. The crack was modelled as a continuous flexibility using the displacement field in the vicinity of the crack with the fracture mechanics methods. They have compared the lowest natural frequency of the bar obtained from continuous cracked bar vibration theory, the lumped crack bar vibration analysis and the experimental results. They

found that experimental results fall between the values predicted by the two analytical methods. Moreover, they found that continuous bar theory agreed better with the experimental results.

Viola *et al.,* 2007 investigated the changes in the magnitude of natural frequencies and modal response introduced by the presence of a crack on an axially loaded uniform Timoshenko beam using a particular member theory. The results indicated that when the effects of shear deformation and rotary inertia were neglected, the errors associated with them became increasingly large as the beam thickness and the modal index increased. They also found that natural frequency decreased when shearing effect was included.

As discussed in the previous section about the study of cracked beams under transverse vibration researchers also studied and proposed the vibration theory for the longitudinal vibration of the cracked bar. They used similar techniques of modelling the crack bar as used for the transverse vibration problem. Their findings suggested that resonant frequencies and the mode shape were significantly affected in cracked bar when compared with the response of the uncracked bar.

2.1.5.3 Vibration of Cracked Rotors

In every machine we come across rotors and the reciprocating parts. For example steam turbine in the power plant has to operate continuously for the power generation. This machine is quite expensive costing billions of pounds. Moreover, single day's loss of power generation can cost millions of pounds. So it becomes necessary to continuously monitor the health of the rotor to avoid the loss caused due to its failure. There is a need for good fault diagnostic techniques so that the loss caused due to the failure can be minimized. In this section, literature is focussed on the vibration of cracked rotors. It deals with the different approaches used by researchers for modelling and analyzing the behaviour of cracked rotors.

Dimarogonas *et al.,* 1983 investigated a de-Laval rotor with a crack by the way of application of the theory of shaft with dissimilar moments of inertia. They obtained the analytical solution for closing crack under the assumption of large static deflections, a common situation in turbo machinery. This realistic assumption for turbo machinery led to a bilinear spring behaviour of the cracked section of the shaft. For a rotating shaft, this led to equations with periodic coefficients and appropriate analytical solutions for

natural and forced vibrations. As expected, higher harmonics were identified. They also found the local flexibility of a cracked section using a Paris energy equation for crack. Their computation of local flexibility was based on the plane strain assumption for the shaft and the stress intensity factors used for the plane strip. Furthermore, they investigated the case of uncoupled bending vibration of a de-Laval rotor with an open surface crack. Their results showed that near the half critical speed it was possible to clearly identify the crack in an isotropic cylindrical shaft. Hence, this speed was used as the primary source of information for identification of the existence of a crack in turbo machinery rotors.

Papadopoulos *et al.,* 1987 analyzed the coupling of longitudinal and bending vibrations of a rotating shaft due to an open transverse crack. Their assumption of open crack led to a system behaviour similar to that of a rotor with dissimilar moment of inertia along two perpendicular directions. They represented the local flexibility due to the presence of a crack by way of a 6x6 matrix for six degrees of freedom in a short shaft element which included crack. The matrix had off-diagonal terms which caused coupling along the directions which were indicated by these terms. They neglected shear and used three degrees of freedom i.e. bending in two directions and extension. This led to 3x3 stiffness matrix with coupling terms. They considered undamped free and forced coupled vibrations as well as damped free and forced vibrations. They investigated the coupling and examined the effects of unbalance and gravity. Their results indicated variations of eigen frequencies for a small crack depth. A much more pronounced manifestation of the existence of the crack appeared in the vibration spectrum where both the longitudinal and lateral vibration frequencies coexisted in the same spectrum. It was only due to the surface crack and could be used for an unambiguous identification of the existence of the crack. Similarly for the damped system coupling of the motion was clearly observed for moderate crack depths.

Sekhar *et al*, 1992 used the approach of a flexibility matrix developed by Papadopoulos *et al.*, 1987. They used finite element method for the crack detection. They detected the cracks in a shaft by measuring the changes in the adequate number of natural frequency using the finite element method. Their results showed that the changes in natural frequencies due to crack were appreciable in case of shafts with low slenderness ratio.

Tsai *et al.*, 1996 developed a diagnostic method for determining the position and size of a transverse open crack on a stationary shaft without disengaging it from the machine system. They modelled the crack as a joint of a local spring. They employed the transfer matrix method on the basis of Timoshenko beam theory to obtain the dynamic characteristics of a stepped shaft and a multi disc shaft. It was combined with beam segments to derive a frequency equation for the assembly and was then solved for the frequency as well as the corresponding mode shape of the cracked shaft. The position of the crack was predicted by comparing the fundamental mode shapes of the shaft with and without a crack. Furthermore, the depth of the crack was obtained by the change of natural frequency of the shaft with and without a crack. The result showed that the bending term in the crack compliance matrix was dominant. Therefore, the proposed method, which excluded the coupled flexibility at the crack point, was considered reliable.

Gounaris *et al.*, 2002 investigated a rotating cracked shaft to identify the depth and location of a transverse surface crack. They used local compliance matrix of different degrees of freedom to model the transverse crack of circular cross-section, based on the expressions of the stress intensity factors and associated expressions for strain energy release rates. Their findings suggested the possibility to detect the existence of cracks in rotating shafts by measuring the axial response for two or three different rotational speeds and loadings.

Sinou *et al.*, 2005 studied the influence of cracks in rotating shafts. They addressed the two distinct issues of change in modal properties and the influence of the breathing crack on dynamic response during operation. Their investigation of evolution of the orbit of a cracked rotor near half of the first resonance frequency provided a possible basis for an online monitoring.

Chondros *et al.*, 2007 analyzed the torsional vibration of a circumferentially cracked shaft. In this analysis, the crack was assumed as an open crack in order to avoid nonlinearity. They used Hu-Washizu-Barr variational [Barr,1966] formulation to develop the differential equation and the boundary conditions of the cracked shaft. They modelled the crack as a continuous flexibility based on the fracture mechanics principle. They used Rayleigh quotient to approximate the natural frequencies of the cracked shaft. Furthermore, they used the finite element method and compared the results

obtained from the variational formulations. They concluded that the behaviour of this damaged model led to the extension of their utility for the fault detection of the cylindrical shaft and rotors.

It can be seen from this section that researchers have tried to model the crack in the rotor. Their findings have suggested that the presence of a crack in the rotor significantly affects the modal properties of the rotor during the operating condition.

2.1.5.4 Breathing Crack

Breathing crack as defined in the literature is the crack which opens and closes during vibration process. This opening and closing of crack has the character of the bilinear spring which introduces the nonlinearity in the system. The research based on open crack consideration has given the good insight about the dynamic behaviour, but in real situation opening and closing of crack during vibration process has a significant effect on the dynamic behaviour. Researchers have tried to address this issue by modelling the breathing crack as a bilinear spring to study its effect on the dynamics of beam /bar. Below are the few sources from the literature in which researchers have tried to address the issue of the breathing crack.

Gudmundson, 1983 studied a dynamic behaviour of cracked cantilever beam. He had shown that a crack could be represented by a consistent, static flexibility matrix. He used two different methods for the determination of the flexibility matrix. In the first method he considered that if the static stress intensity factors were known, the flexibility matrix could be determined from integration of these stress intensity factors. Alternatively, he used static finite element calculations for the determination of the flexibility matrix. The mathematical model developed for edge-cracked cantilevered beam was used to determine the eigen frequencies for different crack lengths and crack positions. The obtained results compared well with dynamic finite element calculations. The results from experiments showed that crack closure effect in a vibrating beam was of considerable importance. It was found that the eigen frequencies decreased, as functions of crack length, at much slower rate than in case of an open crack.

Actis *et al.*, 1989 used the finite element method to study the simply supported beam with a breathing crack. They used beam finite elements to model the uncracked portions of the beam. They determined the flexibility of cracked beam when crack is open using

fracture mechanics considerations. The crack was modelled as a rotational spring in between the two uncracked beam segments. So that they can simulate the behaviour of fully open and fully closed crack.

Qian *et al.*, 1990 derived the element stiffness matrix of a beam with a crack. They established a finite element model by integrating the stress intensity factor. The model established was applied to the cracked cantilever beam with an edge crack and the eigen frequencies were determined for different crack lengths and locations. Results obtained were well in agreement with the experimental results

Krawczuk *et al.*, 1990 studied the transverse vibrations of a cracked beam with a time-varying stiffness. The periodic time-varying stiffness was simulated by a square-wave function with a fundamental frequency equal to the forcing frequency. The equation of motion was solved by employing the harmonic balance technique. It was shown that, when a breathing crack was present, higher harmonics in the frequency spectrum were generated revealing the non-linear behaviour of the system.

Friswell *et al.*, 1992 simulated the nonlinear behaviour of a beam with a closing crack, vibrating in its first mode of vibration, through a simple single degree of freedom model with bilinear stiffness. The response due to harmonic excitation was obtained using numerical integration. Integral multiples of the forcing frequencies were found in the frequency spectrum.

Chu *et al.*, 1992 proposed a closed form solution based on the use of two square wave functions to model the stiffness change for bilinear oscillators under low frequency excitation. They extended the solution procedure to the cases of bilinear forcing function which usually occurs in the dynamics of damaged structures. The results showed that the proposed solution might be used to predict spectral patterns of damaged structures efficiently.

Shen *et al.*, 1992 formulated the equation of motion and associated boundary conditions for vibration of a uniform beam containing one single edge fatigue crack. They introduced the fatigue crack in the form of breathing crack. The Galerkin procedure was used to formulate a bilinear equation of motion for each mode of vibration of simply supported beam. The dynamic response of the bilinear equation under a concentrated excitation force was calculated through a numerical analysis. The results clearly showed

the nonlinear behaviour in the time history and frequency spectrum for each mode of vibration. They suggested that changes in the dynamic behaviour of structure could be used to deduce the size and location of crack.

Sundermeyer *et al.,* 1995 studied a single degree of freedom bilinear spring mass system. They excited the system at two frequencies, the difference of which was the resonant frequency of the system. The Fourier transform of the steady state spectra showed the presence of nonlinearity. When the crack was open a simply supported beam was modelled using an appropriate rotational spring between two segments of uncracked portions of the beam. When the crack was closed the whole beam was assumed to be a continuous beam. Modal expansions were employed to compute the beam response at any excitation with proper incorporation of continuity of displacement and velocity when the crack was in a state of transition. Again, a similar nonlinear effect was found in the Fourier spectra of displacement. This was then correlated with the location and depth of the crack.

Brandon *et al.,* 1995 proposed a model for the opening and closing of a breathing crack in which two uncracked portions of the beam were considered as two subsystems. The connection between these two systems ensured continuity of normal force, bending moment and shear force. A discontinuity of axial displacement, transverse displacement and slope was permitted at the crack section. The two subsystems in a cantilever beam were considered as two Timoshenko beams, one with clamped-free boundary conditions and the other with free-free boundary conditions. The two subsystems of the cantilever beam, separated by a crack, were related to one another by time varying connection matrices representing the interaction forces. The natural frequencies and mode shapes were determined and compared with those available in literature

Ruotolo *et al.,* 1996 extended the work of Krawczuk *et al.* they assumed that the crack changes from a state of fully open to fully close instantaneously, which gave rise to bilinear stiffness nonlinearity. The bilinear stiffness was approximated using a higher order polynomial. Beam curvature at the crack section was checked to determine whether the crack is open or closed. When the crack was open, flexibility was introduced using cracked beam elements. Higher order frequency response functions were defined using Volterra series for systems having polynomial type nonlinearity. A damage assessment procedure was suggested, based on a quantitative comparison of

higher order frequency response functions.

Lamonaca *et al.*, 1997 proposed the crack identification procedure in vibrating beams. They made use of the concept of model updating that were recast to include an evolutionary modal model capable to deal with the non-stationarity of the dynamic response arising from the nonlinearity of the problem. The outcome of this identification suggest that evolutionary stiffness of the damaged elements and their time variations and global excursions were used to assess the crack type and severity

Chati *et al.*, 1997 used modal analysis to study the nonlinear dynamics of the cantilever beam with a transverse crack edge. They modelled nonlinearity produced by opening and closing of crack as a piece wise linear system. To define effective natural frequencies for piece wise linear system they used the idea of bilinear frequency. They obtained the bilinear frequency by computing associated frequencies of each of the

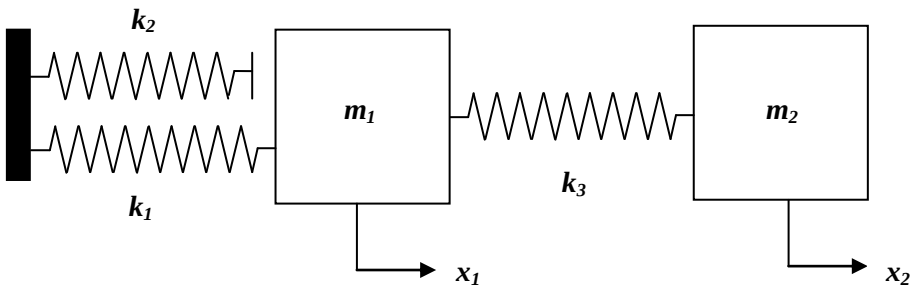

Figure 2.3 The Two Degree of Freedom System
Modified, after [Chati *et al.*, 1997]

linear pieces of the piecewise-linear system. They used finite element method to obtain the natural frequencies in each linear region. In order to understand essential nonlinear dynamics of the cracked beam, a piecewise linear two degree of freedom model was studied as shown in Fig. 2.3. They used a perturbation method to obtain the nonlinear normal modes of vibration and the associated period of motion. It was found that the bilinear frequency formula was a good approximation for the effective natural frequency.

Chondros *et al.*, 1998 investigated the dynamics of a cracked fixed-free bar with a breathing crack in longitudinal vibration. They used Hu-Washizu-Barr variational [Barr, 1966] formulation to develop the equation of motion and the boundary conditions of the cracked bar as a one-dimensional continuum. The crack was modelled as a continuous

flexibility using the displacement field in the vicinity of the crack found by fracture mechanics methods. They presented an analytical approach to the non-linear dynamic problem of cracked fixed–free bar and examined the effect of the breathing crack. They used the bilinear character of the system for the prediction of changes in longitudinal vibration of a bar. The result obtained analytically was compared with the experimental results from bars with open cracks. It was found that breathing cracks result in a smaller drop in the dominant system frequency as compared to the natural frequencies of linear system with open cracks.

Rivola *et al.*, 1998 used a different approach to study the vibration of a beam with a breathing crack. They modelled the beam as an oscillator with a bilinear restoring force (Fig.2.4) and applied bi-spectral analysis to the response. The bi-spectral analysis showed high sensitivity to the non-linear behaviour of the system compared to other techniques.

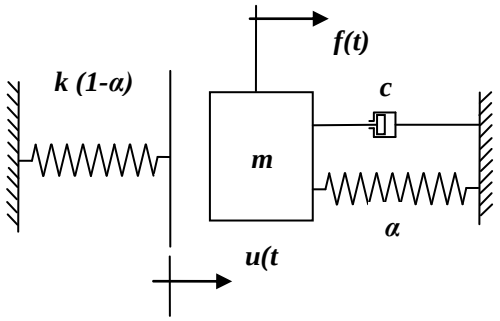

Figure 2.4 Bilinear Model
Modified, after [Rivola *et al.*, 1998]

Cheng *et al.*, 1999 developed a simple nonlinear fatigue crack model. For simplicity they analyzed the dynamic behaviour of a cracked beam vibrating at its first mode. They carried the analysis in both time domain and frequency domains, which was aimed to identify the distinguishing features of the dynamic response associated with the existence of the fatigue crack. They found that the side peaks appeared in frequency response functions near the resonance peak due to the fatigue crack. There were also pronounced anti-resonance frequency shifts and super/sub-harmonic vibration phenomena observed in the experimental study of naturally grown fatigue cracks.

Tsyfansky *et al.*, 2000 simulated the bending vibrations encountered in an aircraft wing under external harmonic excitation. They have shown that due to the influence of the elastic non-linearity of typical cracks, super-harmonic vibration regimes appear in

system response. By utilizing specific features of these regimes they developed a new method for the detection of the crack. This method showed capability of high detection sensitivity and testing reliability.

Pugno *et al.*, 2000 presented a technique capable of evaluating the response of a beam with several breathing cracks perpendicular to its axis subjected to harmonic excitation. The method described by them was based on the assumption that the response was periodic and cracks open and close continuously. They defined a non-linear system of algebraic equations and solved it iteratively using numerical integration. They analyzed the vibrational response of a cantilever beam with cracks of different size and location using the harmonic balance method. The results obtained by harmonic balance approach compared well with those obtained through numerical integration.

Matveev *et al.*, 2002 analyzed the vibration of damaged structures. They modelled bending vibrations of a beam with closing crack and evaluated the distribution functions of vibration characteristics of damage based on the estimation of non-linear distortions of the displacement, acceleration and strain waves of a cracked beam for first three mode shapes. The results showed that the amplitudes of concomitant modes of vibration were heavily dependent on the crack depth. Furthermore, a closing crack essentially caused non-linearity of these distribution functions; this fact might serve as a diagnostic indication of damage.

Sinha *et al.*, 2002 developed a finite element approach to study the vibration behaviour of free-free beam with a breathing crack. Their simulation results were in good agreement with the experimental results.

Douka *et al.*, 2005 studied the free vibration response of a beam with breathing crack. They have used Hilbert transform and empirical mode decomposition for evaluating the instantaneous frequency of a mono component signals. Their analysis revealed that the instantaneous frequency (IF) allowed an efficient and accurate description of nonlinearities of the system and could be used to improve the reliability and effectiveness of vibration based crack diagnosis technique.

Loutridis *et al.*, 2005 investigated the dynamic behaviour of a cantilever beam with a breathing crack under harmonic excitation theoretically and experimentally. They developed a simple model of single degree of freedom with varying stiffness to simulate

the dynamic behaviour. They analysed both the simulated and experimental response data by applying empirical mode decomposition and Hilbert transform. The results obtained by them indicated that the instantaneous frequency oscillates between frequencies corresponding to the open and closed states of the crack. The variation of the instantaneous frequency increased with increasing crack depth following a polynomial law which could be used for estimation of crack size. They have also showed that the harmonic distortion increased with crack depth following definite trends and could be used as an effective indicator of crack size.

Andreaus *et al.*, 2007 simulated the problem of nonlinear dynamics of cracked cantilever beam under harmonic loading using finite element technique. They used two dimensional finite elements for the analysis. Their investigation revealed that the frequency does not change with the oscillation amplitude but the steady state response obtained was very rich of sub and super-harmonic components (Fig. 2.5). They also found that when the forcing frequency coincides with any one of the integer sub-multiples of the first system frequency ω_0, then the nth harmonic component of the forcing frequency, which was close to ω_0 would be significantly exalted. Moreover, within the super-harmonic resonance ranges the phase portraits were characterized by significant wiggles due to impact between cracks (Fig. 2.6).

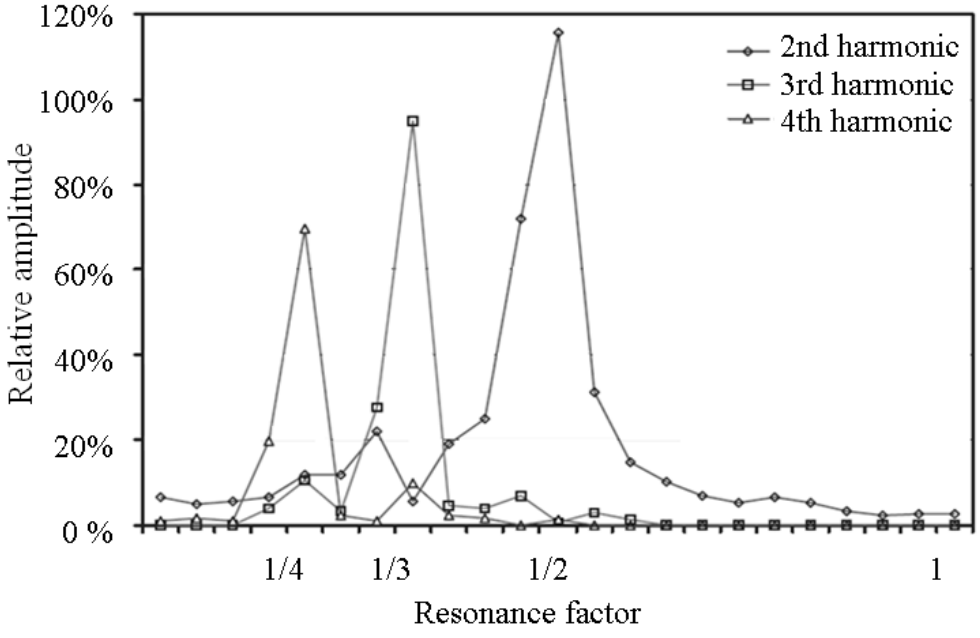

Figure 2. 5 A Sub Harmonic and Super Harmonic Frequencies
Modified, after [Andreaus *et al.* , 2007]

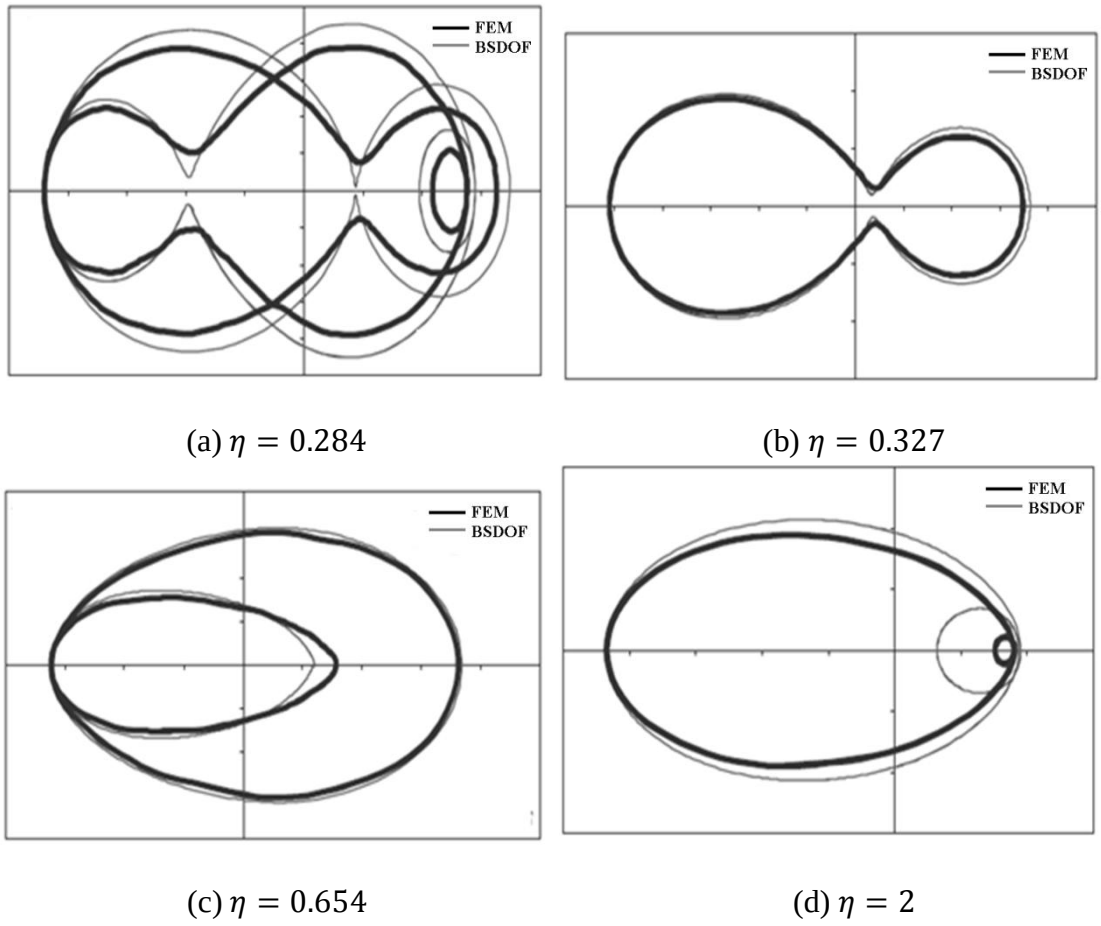

Figure 2. 6 Phase Portrait for Different Values of $\boldsymbol{\eta}$
Where η is excitation to system frequency ratio $(\eta = \Omega/\omega_0)$
Modified, after [Andreaus *et al.* , 2007]

Sinha, 2009 used bi-coherence and tri-coherence and applied it on acceleration response of structures having fatigue cracks. The results obtained indicated that higher order coherence has tremendous potential for the detection of fatigue cracks even in presence of noisy environment.

This section was focussed on the modelling of the breathing crack in the cracked beam/ bar. As breathing crack behaves like a bilinear spring, researchers have used the different approaches to model the crack having bilinear characteristics. Few researchers used Galerkin's procedure and formulated a bilinear equation of motion for each mode of vibration. Their results clearly indicated the nonlinear behaviour on the time history and frequency spectrum for each mode of vibration. Some of them used periodic time varying stiffness for modelling the breathing crack. Their findings suggested that higher harmonics in the frequency spectrum were generated revealing the non-linear behaviour of system. Few of them modelled crack as a piecewise linear two degree of freedom

system and used perturbation methods to obtain nonlinear normal modes of vibration. They suggested that bilinear frequency formula was good approximation for effective natural frequency.

It is clear from the above section that the breathing crack introduces nonlinearity in the system. This shows that crack-induced nonlinearity significantly affects the dynamic behaviour of system.

2.2 Discussion

From the literature review above it can be seen that several researchers have used vibration characteristics as a tool for crack identification. Researchers have considered transverse vibration, and longitudinal vibration of a cracked beam/bar with open and breathing cracks. Their findings have suggested that presence of the open crack in the structure significantly affected the modal properties of the beam/bar. But in the actual situation under the action of dynamic force crack opens and closes. This opening and closing of the crack has characteristics of a bilinear spring. This bilinear nature of the crack introduces nonlinearity in the system. The results obtained by them considering the bilinear model of the spring indicate the distortion of the time history and the presence of the higher harmonics in the frequency response. Moreover, few researchers modelled bilinear behaviour of the crack as a bilinear spring with single degree of freedom system or two degree of freedom system to study the nonlinear vibration characteristics. This has given valuable information about the behaviour of breathing crack. This can be extended to the continuous system with infinite degrees of freedom. In the next chapter a special mathematical technique is developed to study the dynamics of the continuous structure with discontinuities. In this technique developed local discontinuity (crack) is implanted as a nonlinear feedback and continuous elements as the operators of the dynamic compliance of the media at the contact point.

2.3 Summary

This chapter was focussed on the various linear and nonlinear methods of crack monitoring. The methods such as visual inspection, eddy current technique, acoustic emission technique and linear ultrasonic technique are useful for some application. But these techniques cannot be used for online monitoring of the structures. Nonlinear ultrasonic technique when compared with linear ultrasonic technique provides added

advantage for online SHM. Though they can be used for detecting cracks they cannot predict the structural strength. On the contrary, vibration based techniques can be used for online crack monitoring and it can also be used for getting the information about the structural strength. So the vibration based techniques need to be explored for crack monitoring of structures under working conditions.

Chapter 3 Vibro-Impact Response of a Cracked Bar

3.1 Introduction

The presence of discontinuity in the structure affects its dynamic behaviour under working conditions. A crack in structure behaves like a discontinuity and it drastically changes the general dynamic characteristics of the structure which results in the excitation of significant additional perturbations. It occurs mainly due to the generation of intensive forces of impact between the contact surfaces. In order to simulate and study the dynamics of the cracked bar a special mathematical technique for proper matching of local and distributed elements of the resulting structure has been developed. This has been effectively implemented with the use of the force characteristics of contact interaction for the discontinuous elements and Green's function for media, calculated in the contact areas. This description leads to application of integral equation. Laplace transformation of the integral equation produces an operator for the simulation of the interaction, where local discontinuity is implanted as a nonlinear feedback and continuous elements as the operators of dynamic compliance (receptance) of the media at the contact points. Effective numerical simulation of such structures with Matlab-Simulink software needs implementation of realistic models for contact phenomena and transformation of the transcendental operators of dynamic compliances into rational functions of complex variable. This has been made with the help of modal representation for the dynamic compliances. Uniform convergence of the modal approximation leads to high accuracy of simulation within the use of first few initial modes. This also produces a convenient calculation scheme for accurate estimation of system response. In this chapter, a model of the one-dimensional cracked cantilever bar subjected to longitudinal harmonic excitation is used to analyse a vibro-impact response as a way to monitor the structural health. Nonlinear resonant phenomena due to vibro-impact interaction within the cracked bar are obtained and analysed.

3.2 Differential Equation of Motion of a Cantilever Bar

Consider a cantilever bar as shown in the Fig. 3.1 of length l with plane cross sectional area S having modulus of elasticity E and mass density ρ. The exciting force $P(x,t) = a_p cos\omega t$ is applied at the free end of the bar with co-ordinate $x = l$ measured from the

fixed end. Let there be any arbitrary section dx at the distance x measured from the fixed end of the bar. The absolute displacement of this arbitrary section can be written as a function of $u(x,t)$, and the axial force acting on it is called $P(x,t)$. This axial force $P(x,t)$ results in strain in the arbitrary section dx which is represented by ϵ [Babitsky,1998].

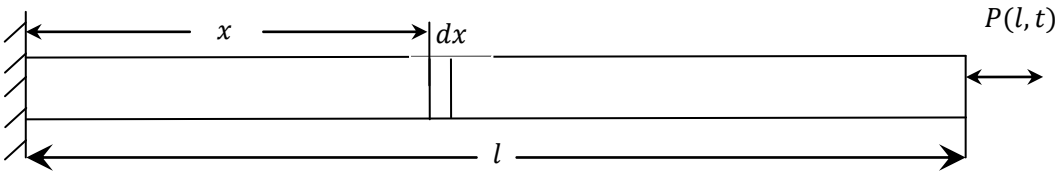

Figure 3.1 Schematic of the cantilever bar

According to Hooke's law

$$P(x,t) = ES\epsilon = ES\frac{\partial u(x,t)}{\partial x} \tag{3.1}$$

The change in axial force over an element dx is as follows

$$P(x+dx,t) - P(x,t) = ES\frac{\partial^2 u(x,t)}{\partial x^2}dx \tag{3.2}$$

The force difference produces an acceleration $\partial^2 u(x,t)/\partial t^2$ transferred to the element $\rho S dx$. Therefore from Newton's second law, we can write

$$\rho S dx\frac{\partial^2 u(x,t)}{\partial t^2} = ES\frac{\partial^2 u(x,t)}{\partial x^2}dx \tag{3.3}$$

Dividing both sides of Eq. (3.3) by Sdx, we have

$$\frac{\partial^2 u(x,t)}{\partial t^2} = \frac{E}{\rho}\frac{\partial^2 u(x,t)}{\partial x^2} \tag{3.4}$$

Eq. (3.4) can be rewritten as

$$\frac{\partial^2 u(x,t)}{\partial t^2} = \gamma^2\frac{\partial^2 u(x,t)}{\partial x^2} \tag{3.5}$$

Where

$$\gamma = \sqrt{E/\rho} \tag{3.6}$$

The Eq. (3.5) doesn't take into account the internal damping of the material. Internal damping is common to range of mechanism's that occur in the deformation of the materials that are cyclically strained, in particular, internal damping is the cause of hysteresis loops that occur in the stress/strain curve. Several experimental results have shown that under a periodic deformation the area of hysteresis loops for most materials depends on the amplitude of deformation for a wide range of change but not on frequency. For this reason, in the study of a periodic process an equivalent force, proportional to the velocity of strain, is introduced selecting a suitable factor β so that the general dissipative effect corresponds to the experimental data [Panovko, 1960]. Considering an equivalent force proportional to the velocity of strain Eq. (3.1) can be written as:

$$P(x,t) = ES\epsilon + ES\beta\frac{\partial\epsilon}{\partial t} \tag{3.7}$$

Where

$$\epsilon = \partial u(x,t)/\partial x\ ;\quad \beta = \chi/2\pi\omega$$

Therefore, we have

$$P(x,t) = ES\frac{\partial u(x,t)}{\partial x} + ES\beta\frac{\partial^2 u(x,t)}{\partial x\partial t} \tag{3.8}$$

The change in axial force over an element dx is as follows

$$P(x+dx,t) - P(x,t) = ES\frac{\partial^2 u(x,t)}{\partial x^2}dx + ES\beta\frac{\partial^3 u(x,t)}{\partial x^2\partial t}dx \tag{3.9}$$

The force difference produces an acceleration $\partial^2 u(x,t)/\partial t^2$ transferred to the element $\rho S dx$. Therefore from Newton's second law, we can write

$$\rho S dx\frac{\partial^2 u(x,t)}{\partial t^2} = ES\frac{\partial^2 u(x,t)}{\partial x^2}dx + ES\beta\frac{\partial^3 u(x,t)}{\partial x^2\partial t}dx \tag{3.10}$$

Dividing both sides of Eq. (3.10) by Sdx, we have

$$\frac{\partial^2 u(x,t)}{\partial t^2} = \frac{E}{\rho}\frac{\partial^2 u(x,t)}{\partial x^2} + \frac{E\beta}{\rho}\frac{\partial^3 u(x,t)}{\partial x^2\partial t} \tag{3.11}$$

Using Eq. (3.6) we have

$$\frac{\partial^2 u(x,t)}{\partial t^2} - \gamma^2 \frac{\partial^2 u(x,t)}{\partial x^2} - \gamma^2 \beta \frac{\partial^3 u(x,t)}{\partial x^2 \partial t} = 0 \tag{3.12}$$

As a result, Eq. (3.12) for the study of periodic vibration of the rod can be written in the following form

$$\frac{\partial^2 u(x,t)}{\partial t^2} - \gamma^2 \frac{\partial^2 u(x,t)}{\partial x^2} - b \frac{\partial^3 u(x,t)}{\partial x^2 \partial t} = 0 \tag{3.13}$$

where $b = \gamma^2 \beta = \gamma^2 \chi / 2\pi\omega$ is the linearised coefficient of force of internal damping; ω is the frequency; χ is the absorbtion coefficient found from the test as the ratio of energy absorbtion during the cycle (proportional to the hysteresis loop) to the basic deformation energy. Because of internal damping, the periodic process can only be established in a case with a regular addition of energy into system.

3.3 Expression of Dynamic Compliance for a Cantilever Bar

The expression of the dynamic compliance can be derived by solving a suitable boundary value problem. As the complete details of the derivation of the dynamic compliance has not been given in the monograph [Babitsky V.I., 1998] referred it has been given over here with minute details. The differential Eq. (3.13) for cantilever bar can be written in the following form:

$$s^2 u - (\gamma^2 + bs)\, \partial^2 u / \partial x^2 = 0 \tag{3.14}$$

Where $u = u(x,t)$, $s = \partial/\partial t$ the expression for dynamic compliance can be obtained by applying the boundary conditions to Eq. (3.14).

Fixed End:

$$u(0,t) = 0 \tag{3.15}$$

Free End:

$$ES\left(1 + \frac{b}{\gamma^2} s\right)\left[\frac{\partial u(x,t)}{\partial x}\right]_{x=l} = \exp(j\omega t) \tag{3.16}$$

Assuming the solution of form

$$u(x,t) = u_x(t) = L_l(x, j\omega) \exp(j\omega t) \tag{3.17}$$

Substituting Eq. (3.17) in Eq. (3.14), Eq. (3.15) and Eq. (3.16) we have

$$(j\omega)^2 L_l(x, j\omega) - (\gamma^2 + \mathrm{j}\omega\mathrm{b})\frac{d^2 L_l(x, j\omega)}{dx^2} = 0 \tag{3.18}$$

$$L_l(0, j\omega) = 0 \tag{3.19}$$

$$ES\left(1 + j\omega\frac{b}{\gamma^2}\right)\left[\frac{dL_l(x, j\omega)}{dx}\right]_{x=l} = 1 \tag{3.20}$$

The solution of differential Eq. (3.18) of second order with constant coefficients satisfying the boundary conditions Eq. (3.19) and Eq. (3.20) takes the form

$$L_l(x, j\omega) = c_1 e^{\lambda x} + c_2 e^{-\lambda x} \tag{3.21}$$

Where

$$\lambda = \frac{j\omega}{\sqrt{\gamma^2 + bj\omega}} \tag{3.22}$$

Applying the boundary conditions Eq. (3.19) and Eq. (3.20) to Eq. (3.21) we have

$$c_2 = -c_1 \tag{3.23}$$

$$c_1 = -\frac{\lambda\gamma^2}{\omega^2 ES}\left[\frac{1}{e^{\lambda l} + e^{-\lambda l}}\right] \tag{3.24}$$

From Eq. (3.21), Eq. (3.23) and Eq. (3.24) we have

$$L_l(x, j\omega) = -\frac{\lambda\gamma^2}{\omega^2 ES}\left[\frac{e^{\lambda x} - e^{-\lambda x}}{e^{\lambda l} + e^{-\lambda l}}\right] \tag{3.25}$$

The Eq. (3.22) can be rewritten by substituting $b = \gamma^2\chi/2\pi\omega$ as

$$\lambda = \frac{j\omega}{\gamma}\left(1 + j\frac{\chi}{2\pi}\right)^{-1/2} \tag{3.26}$$

Taking in account smaller value of damping coefficient χ the solution can be simplified by expanding Eq. (3.26) as a series in χ and neglecting higher order terms we have

$$\lambda = \frac{j\omega}{\gamma} + \frac{\chi\omega}{4\pi\gamma} \tag{3.27}$$

Substituting Eq. (3.27) in Eq. (3.25) we have

$$L_l(x, j\omega) = -\frac{\lambda\gamma^2}{\omega^2 ES}\left[\frac{e^{\left(\frac{j\omega}{\gamma}+\frac{\chi\omega}{4\pi\gamma}\right)x} - e^{-\left(\frac{j\omega}{\gamma}+\frac{\chi\omega}{4\pi\gamma}\right)x}}{e^{\left(\frac{j\omega}{\gamma}+\frac{\chi\omega}{4\pi\gamma}\right)l} + e^{-\left(\frac{j\omega}{\gamma}+\frac{\chi\omega}{4\pi\gamma}\right)l}}\right] \tag{3.28}$$

For $x = l$, we obtain

$$L_l(l, j\omega) = -\frac{\lambda\gamma^2}{\omega^2 ES}\left[\frac{e^{\left(\frac{j\omega}{\gamma}+\frac{\chi\omega}{4\pi\gamma}\right)l} - e^{-\left(\frac{j\omega}{\gamma}+\frac{\chi\omega}{4\pi\gamma}\right)l}}{e^{\left(\frac{j\omega}{\gamma}+\frac{\chi\omega}{4\pi\gamma}\right)l} + e^{-\left(\frac{j\omega}{\gamma}+\frac{\chi\omega}{4\pi\gamma}\right)l}}\right] \tag{3.29}$$

Let

$$\zeta = \frac{\omega l}{\gamma} \tag{3.30}$$

Substituting Eq. (3.30) in Eq. (3.29) we have

$$L_l(l, j\omega) = -\frac{\lambda\gamma^2}{\omega^2 ES}\left[\frac{e^{\left(j\zeta+\frac{\chi}{4\pi}\zeta\right)} - e^{-\left(j\zeta+\frac{\chi}{4\pi}\zeta\right)}}{e^{\left(j\zeta+\frac{\chi}{4\pi}\zeta\right)} + e^{-\left(j\zeta+\frac{\chi}{4\pi}\zeta\right)}}\right] \tag{3.31}$$

Simplifying the expression in bracket we get

$$\therefore L_l(l, j\omega) = -\frac{\lambda\gamma^2}{\omega^2 ES}\left[\frac{\left(\frac{x\zeta}{2\pi}\right)^2 + 2\left(\frac{x\zeta}{2\pi}\right) + j\left(\frac{x\zeta}{2\pi}+1\right)4\sin\zeta\cos\zeta}{\left(\frac{x\zeta}{2\pi}\right)^2 + \left(\frac{x\zeta}{2\pi}+1\right)4\cos^2\zeta}\right] \tag{3.32}$$

Using Eq. (3.27) we have

$$\therefore L_l(l, j\omega) = -\left(\frac{j\omega}{\gamma} + \frac{\chi\omega}{4\pi\gamma}\right)\frac{\gamma^2}{\omega^2 ES}\left[\frac{\left(\frac{x\zeta}{2\pi}\right)^2 + 2\left(\frac{x\zeta}{2\pi}\right) + j\left(\frac{x\zeta}{2\pi}+1\right)4\sin\zeta\cos\zeta}{\left(\frac{x\zeta}{2\pi}\right)^2 + \left(\frac{x\zeta}{2\pi}+1\right)4\cos^2\zeta}\right] \tag{3.33}$$

Rearranging the terms in Eq. (3.33) we get

$$\therefore L_l(l, j\omega) = -\frac{l}{ES}\left(\frac{j\gamma}{\omega l} + \frac{\chi\gamma}{4\pi\omega l}\right)\left[\frac{\left(\frac{x\zeta}{2\pi}\right)^2 + 2\left(\frac{x\zeta}{2\pi}\right) + j\left(\frac{x\zeta}{2\pi}+1\right)4\sin\zeta\cos\zeta}{\left(\frac{x\zeta}{2\pi}\right)^2 + \left(\frac{x\zeta}{2\pi}+1\right)4\cos^2\zeta}\right] \tag{3.34}$$

Neglecting the second order term in Eq. (3.34) and using Eq. (3.30), we have

$$L_l(l,j\omega) = -\frac{l}{ES}\left(\frac{j}{\zeta}+\frac{\chi}{4\pi\zeta}\right)\left[\frac{x\zeta}{4\pi\cos^2\zeta}+j\frac{\sin\zeta\cos\zeta}{\cos^2\zeta}\right] \tag{3.35}$$

Simplifying Eq. (3.35) we have

$$L_l(l,j\omega) = \frac{l}{ES\zeta}\left[\tan\zeta - j\frac{\chi}{4\pi}\frac{\zeta+{}^1\!/_2\sin 2\zeta}{\cos^2\zeta}\right] \tag{3.36}$$

Eq. (3.36) represents the expression of the closed form dynamic compliance for the cantilever bar under longitudinal vibration. This closed form of dynamic compliance cannot be implemented numerically in the Matlab-Simulink model. So to implement this numerically the equivalent of the closed form dynamic compliance is used, which is derived from the basics of the general linear theory of integral equations for straight rods [Babakov, 1958]. The derivation of the dynamic compliance using theory of integral equation for the straight rods is given in appendix A. The expression of the dynamic compliance is as follows:

$$L_{pq}(s) = \sum_{i=1}^{\infty}\frac{A_v(p)A_v(q)}{s^2+\Omega_v^2} \tag{3.37}$$

Eq. (3.37) represents the expression of the dynamic compliance for the straight rods. In this, expression of the dynamic compliance internal damping has not been considered. This will cause the rod to vibrate continuously for the given excitation. But in reality the rod will not vibrate continuously because the energy of excitation will be absorbed by internal damping of material, which will bring the rod to stand still. Hence, we need to take into consideration internal damping of material which will represent the real system. Hence Eq. (3.37) can be modified to the following form [Babitsky, 1998]:

$$L_{pq}(s) = \sum_{v=1}^{\infty}\frac{A_v(p)A_v(q)}{s^2+2r_v\Omega_{\mathrm{v}}\mathrm{s}+\Omega_{\mathrm{v}}^2}, \tag{3.38}$$

Where

$$r_v = \chi\Omega_v/4\pi\omega$$

The expression in Eq. (3.38) consists of infinite number of vibration modes and the coefficients of each mode remain functions of the continuous coordinate x which represents the position of the section under consideration. This coefficient $A_v(x)$ represents the transferring action to the section $x = p$ from the concentrated force

applied at the section $x = q$. The mechanism of energy dissipation in the form of internal friction in the material is taken into consideration in terms of absorption coefficient χ in the parameter r_v.

3.4 Dynamic Model of a Cracked Bar

Consider a cantilever bar of length l with a plane cross-sectional area S excited by the harmonic force $P(l,t) = a_p cos\omega t$. The crack is considered at the free end of the bar and is modelled as a limiter stop with a distance Δ from the free end (Fig.3.2). The dimensions of the cantilever bar are given in Table 3.1. Under the application of the

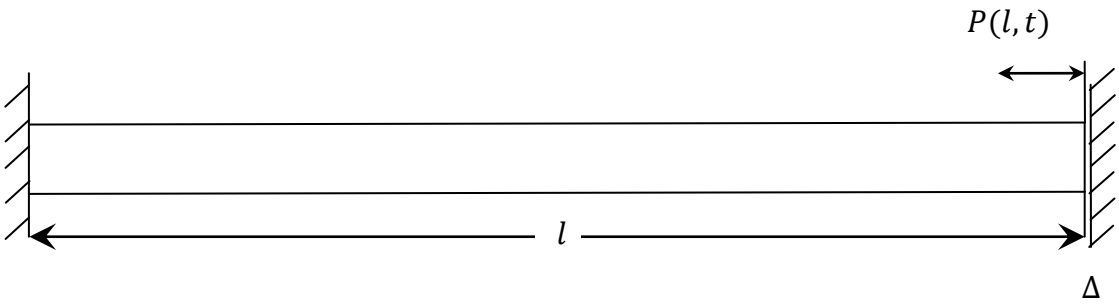

Figure 3.2 Schematic of cantilever bar with crack at free end

harmonic force the crack's faces interact. This interaction of the bar with the limiter (considered as a crack in this case) leads to generation of the contact force due to opening and closing of the crack. The concept of dynamic compliance and the contact force characteristics of impact interaction are considered for analysing the dynamics of the bar due to the crack [Babitsky, 1998]. The blocks of the dynamic compliance and

Material	Steel
Length(L) [mm]	300
Width(b) [mm]	10
Height(h) [mm]	25

Table 3.1 Dimensions of the bar

the contact force are modelled in Matlab-Simulink software. From the schematic shown in Fig.3.3 it is clear that when the harmonic loading is acting on the bar it starts to interact with a limiter, generating the contact force that affects deformation of the bar.

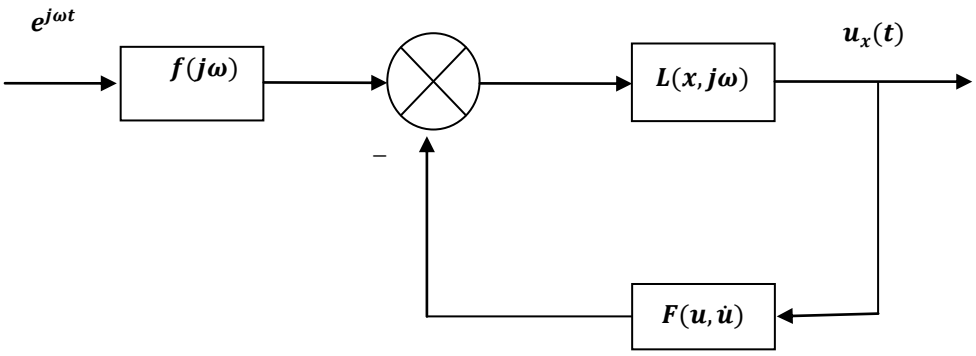

Figure 3.3 Block Diagram

This contact force generated is implanted as the nonlinear feedback. When the cantilever bar interacts with the limiter, the vibrational displacement of an arbitrary section x is defined as a function of $u_x(t)$. By introducing the contact force characteristics $F(u,\dot{u})$ and dynamic compliance operator $L(x,j\omega)$, the coupling displacement $u_x(t)$ due to the force acting at $x = l$ can be written in terms of compliance operator in the following form:

$$u_x(t) = L_l(x,s)P_l(t) - L_l(x,s)F(u,\dot{u})\,. \tag{3.39}$$

3.5 Dynamic Compliance (Receptance)

Eq. (3.36) represents the expression of dynamic compliance of rod under longitudinal vibration. Effective numerical simulation of structures needs transformation of the transcendental operators of dynamic compliance as a function of complex variable into rational function of complex variable. This can be made with the help of modal representation for the dynamic compliances. Uniform convergence of the modal approximation leads to high accuracy of simulation within the use of first few initial modes. The equivalent of transcendental dynamic compliance can be obtained by comparing following expression Eq. (3.36) and Eq. (3.38)

$$L_l(l,j\omega) = \frac{l}{ES\zeta}\left[\tan\zeta - j\frac{\chi}{4\pi}\frac{\zeta + {}^1\!/_2 \sin 2\zeta}{\cos^2\zeta}\right] = \sum_{v=1}^{\infty}\frac{A_v(l)A_v(l)}{s^2 + 2r_v\Omega_{\mathrm{v}}\mathrm{s} + \Omega_{\mathrm{v}}^2} \tag{3.40}$$

The Fig. 3.4 shows the comparison between the transcendental operators of dynamic compliance (closed form) with the rational form of dynamic compliance (summation form). It is clear that the rational form of dynamic compliance gives the very good approximation for the transcendental form of dynamic compliance for the first three

modes of vibration. Hence the rational form of the dynamic compliance can be effectively used for the simulation of continuous structures.

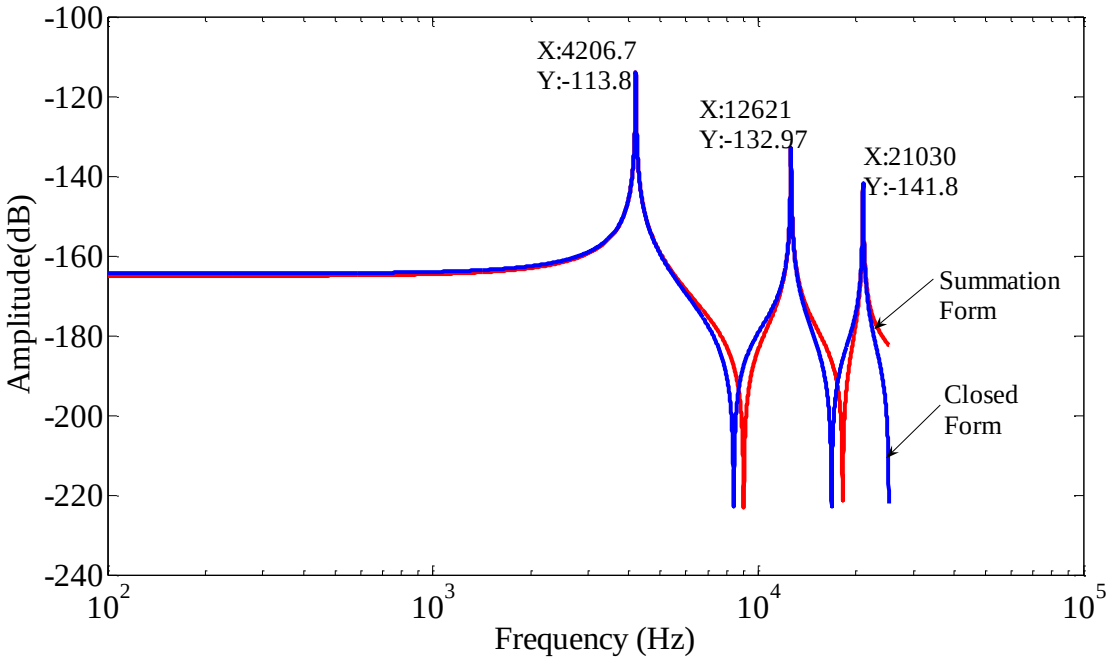

Figure 3.4 Comparison of frequency response

3.6 Characteristics of Contact Force

Under harmonic loading the bar interacts with the limiter (Fig.3.2). This interaction with the limiter transforms the continuous process into successive impulses modulated by the velocity of the input process at the instant when the process reaches the threshold value. Such nonlinear components of the structural scheme are called the *impact elements* [Babitsky, 1998]. These impact elements have positional impulse effects, which specifically combine the effects of the relayed and impulse elements. Fig.3.5 shows an example of transformations of deformation into the force by impact elements. This force characteristic of the contact interaction is given by an expression called *static force characteristics of the impact pair*:

$$F(x) = \psi(x-\Delta)\eta(x-\Delta) \tag{3.41}$$

Where

$$\eta(x) = \begin{cases} 0, & x < 0 \\ 1, & x \geq 0 \end{cases} \tag{3.42}$$

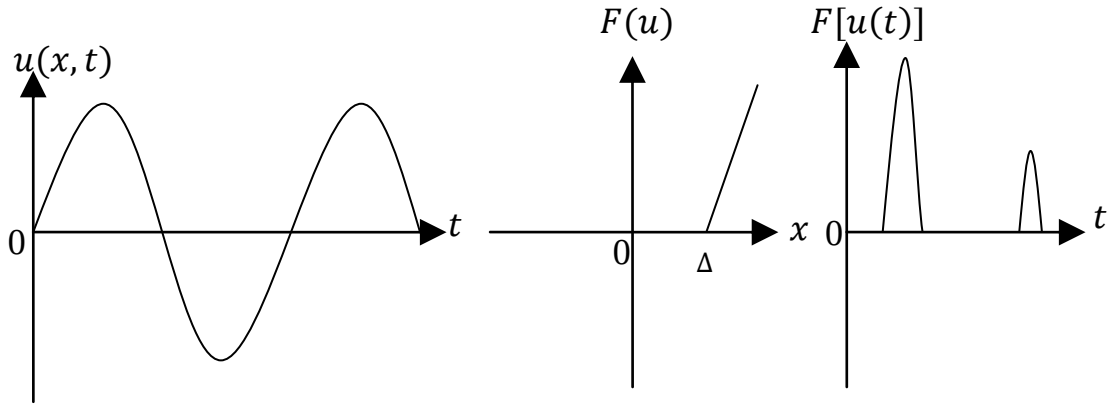

Figure 3.5 Contact force characteristics

3.7 Flow Chart of a Matlab-Simulink Program

Fig. 3.6 shows the general procedure for generating the simulation model of the continuous structure with discontinuities in Matlab-Simulink software. This algorithm has been used for generating the one-dimensional model of the cracked bar for studying the effect of crack on dynamics of the bar. The procedure developed requires deriving differential equations of motion of linear substructure and solving it considering the boundary condition of the problem. The expression of eigen frequencies and eigen modes are obtained after solving the differential equation. The values obtained for eigen frequencies, eigen modes and experimental values of absorption coefficients of material is used to construct the expression of the dynamic compliance of the structure under consideration. After obtaining the expression of dynamic compliance next step is to construct the model of discontinuity which is responsible for the generation of contact force. When all the blocks are ready they are arranged in the logical form to model the dynamic system having discontinuities. This has been implemented for the analysis of one-dimensional model of cracked cantilever bar. External force in the form of harmonic force is given as input to the system and the output response obtained is given as input to the contact force block which is again given as a feedback to the system. These contact force and the harmonic force are summed up at the summation block and the output response for the system is obtained. This output in the form of time response $u(x,t)$ is then transformed into the frequency response using the Fast Fourier Transform program.

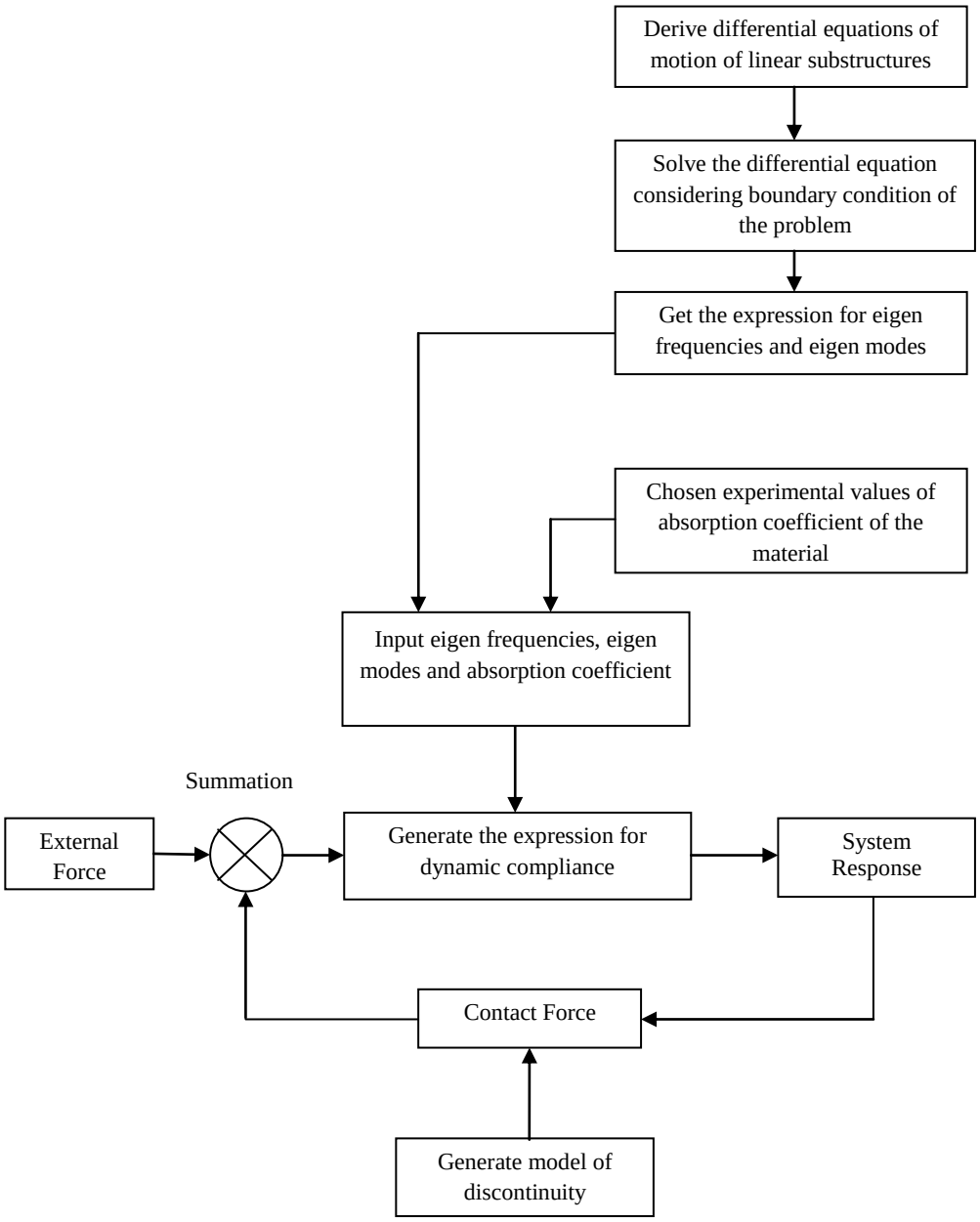

Figure 3.6 Flow chart of the program

3.8 Simulation Results

3.8.1 Response of Cantilever Bar without Crack

The forced longitudinal vibration was performed on a cantilever bar without crack. The frequency sweep was performed from 3500 Hz to 35000 Hz in the Matlab-Simulink model of cantilever bar. The results in Fig. 3.7(a) and Fig. 3.7 (b) shows the time and frequency response of the cantilever bar respectively. From the time response it was

observed that it was symmetric about the x-axis. The frequency response of the system clearly shows that the first three resonances occur at the frequencies of 4206 Hz, 12619 Hz and 21031 Hz.

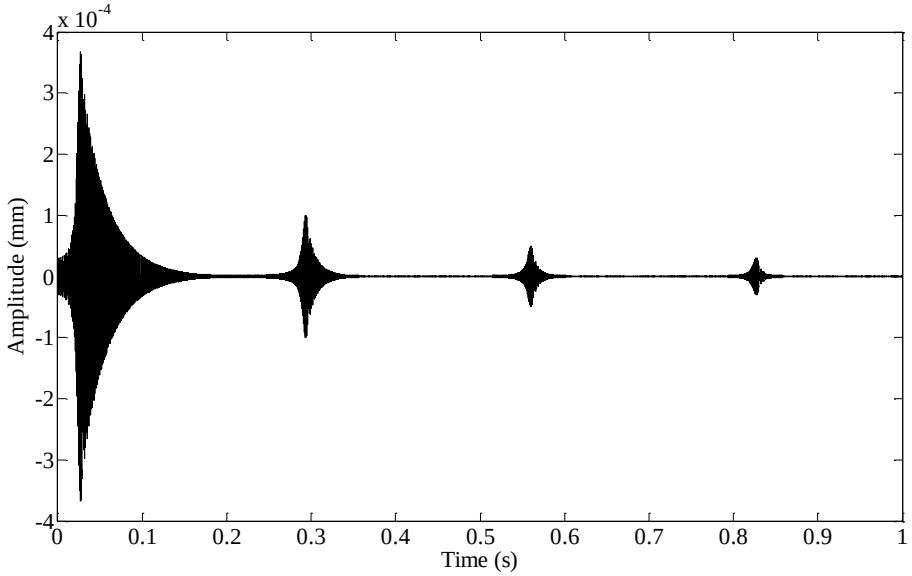

(a) Time response

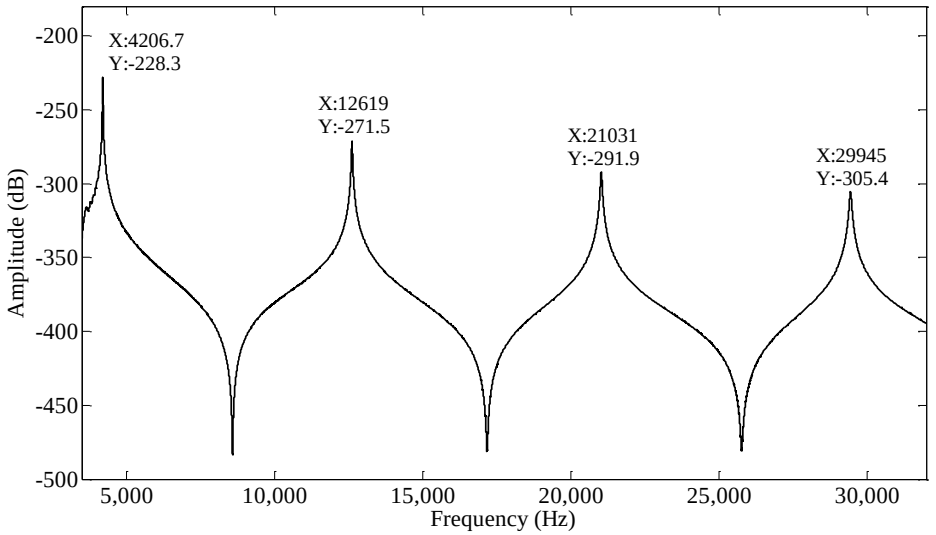

(b) Frequency response

Figure 3.7 Response of cantilever bar (linear case)

3.8.2 Response of Cantilever Bar with Crack

Similarly, for a cantilever bar with a crack, the frequency sweep was performed from 3500 Hz to 35000 Hz in the Matlab-Simulink model. The result in Fig.3.8 (a) and Fig. 3.8 (b) shows the time response and frequency response of the cracked cantilever bar

respectively. From the time response it was observed that the it has lost the symmetry, indicating distortion. This distortion in time response was an indication of nonlinearity due to opening and closing of the crack. In frequency response (Fig.3.8 (b)) it can be observed that there has been shift in the frequencies when compared with the frequency response of the uncracked bar (Fig.3.7 (b)) along with the generation of higher harmonics. This indicates the crack-induced nonlinearity causes frequency shift and generation of higher harmonics (Fig.3.9).

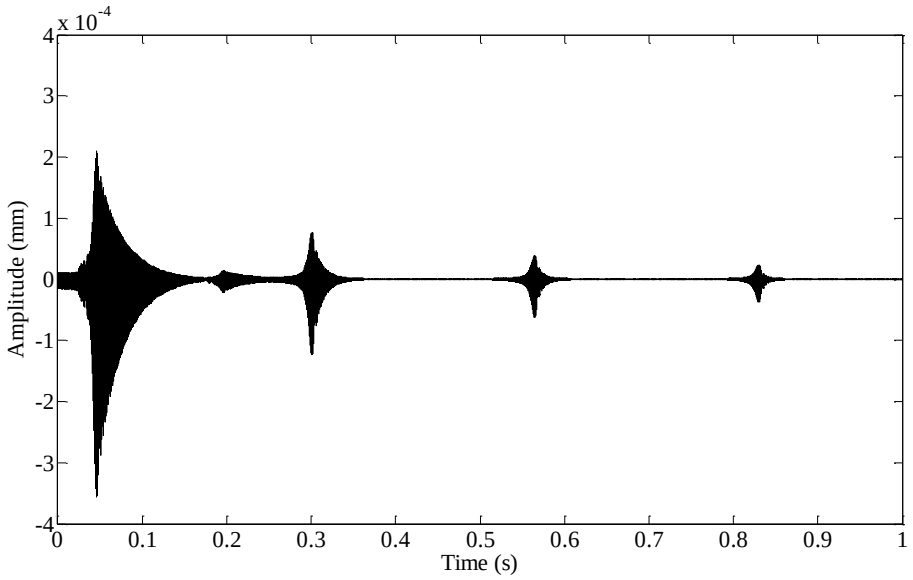

(a) Time response

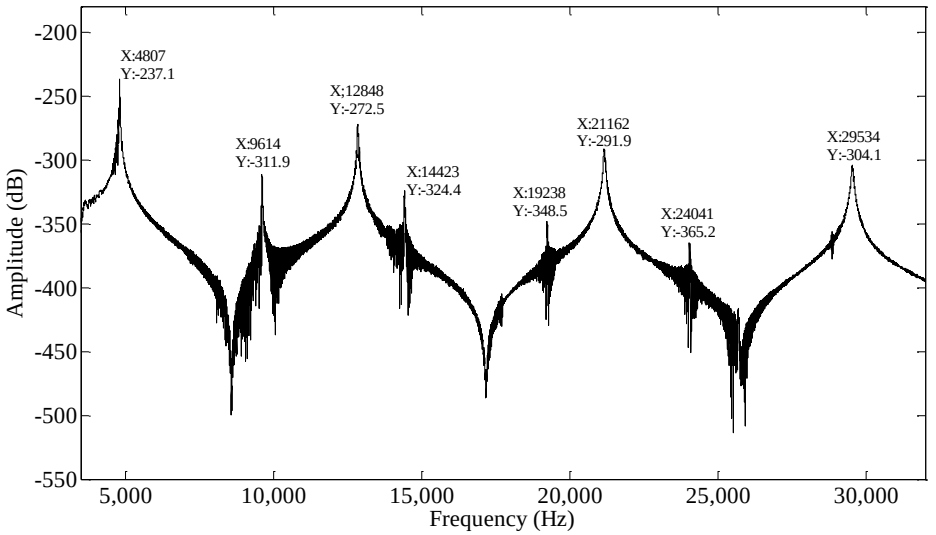

(b) Frequency response

Figure 3.8 Response of cracked cantilever bar (nonlinear case)

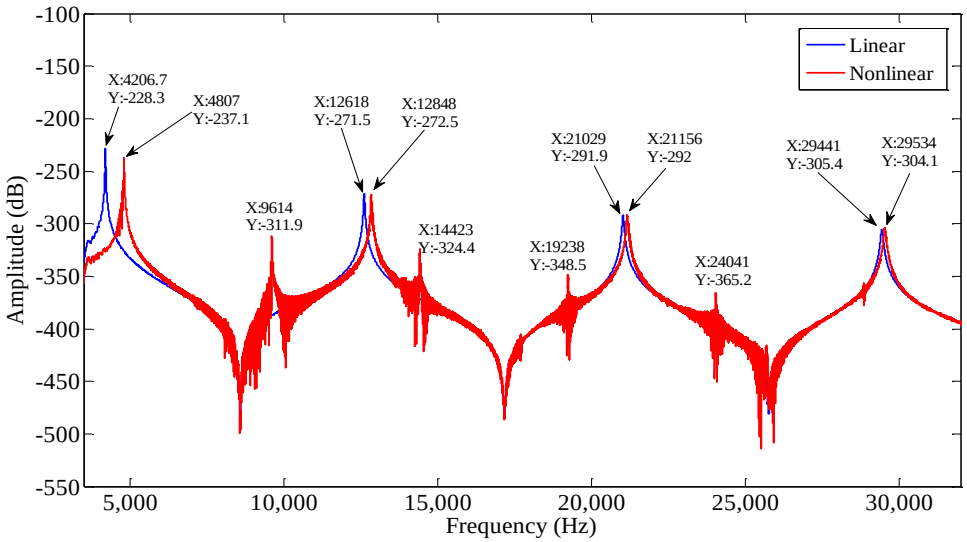

Figure 3.9 Comparison of frequency response of cracked and uncracked bar

3.8.3 Effect of Changing Clearances at Constant Contact Stiffness

The simulation was performed for the different values of the clearances (Δ) by keeping the contact stiffness constant. The frequency sweep was performed from 3500 to 35000 Hz. It was performed for the three different values of clearances. The values of clearance for three different cases were $\Delta = 0, \Delta = 1 \times 10^{-6}\ mm$ and $\Delta = -1 \times 10^{-6}\ mm$. The contact stiffness used for all the three cases was $2 \times 10^{8}\ N/m$. The

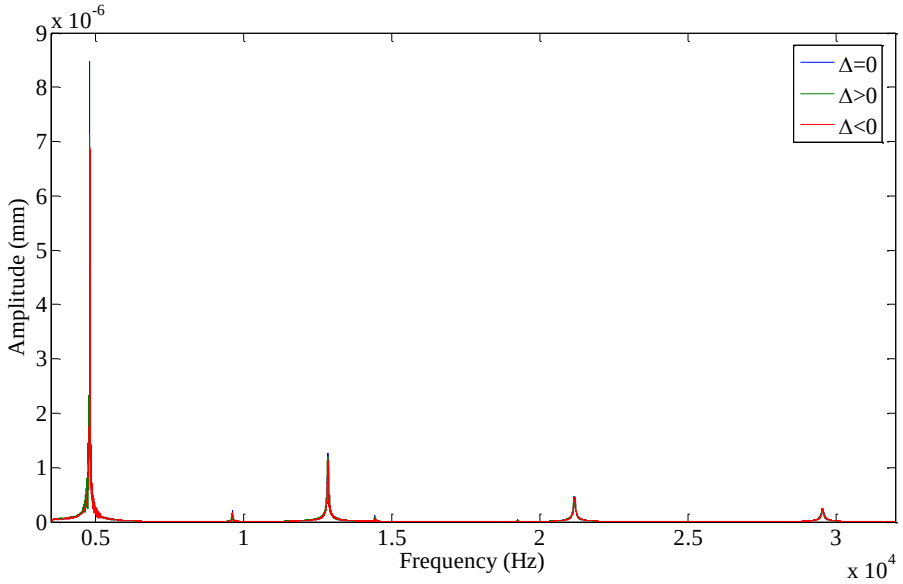

Figure 3.10 Frequency response for different values of clearance (Δ)

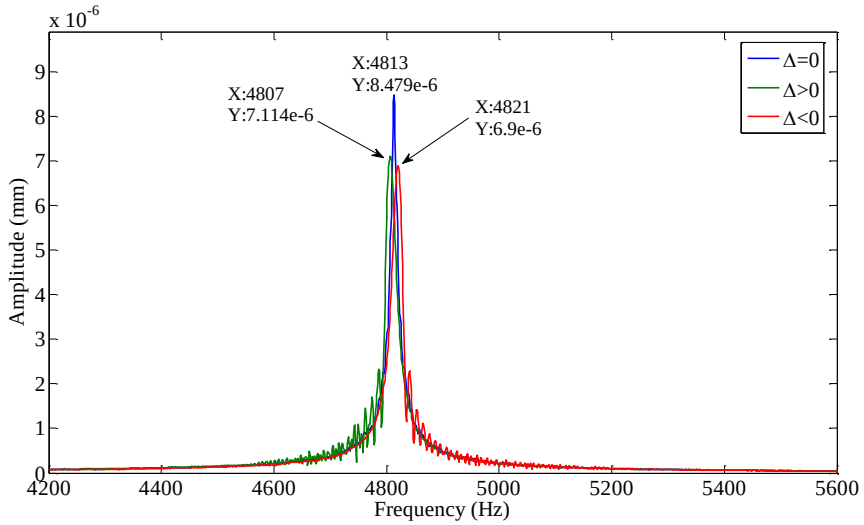

Figure 3.11 First nonlinear resonance frequency

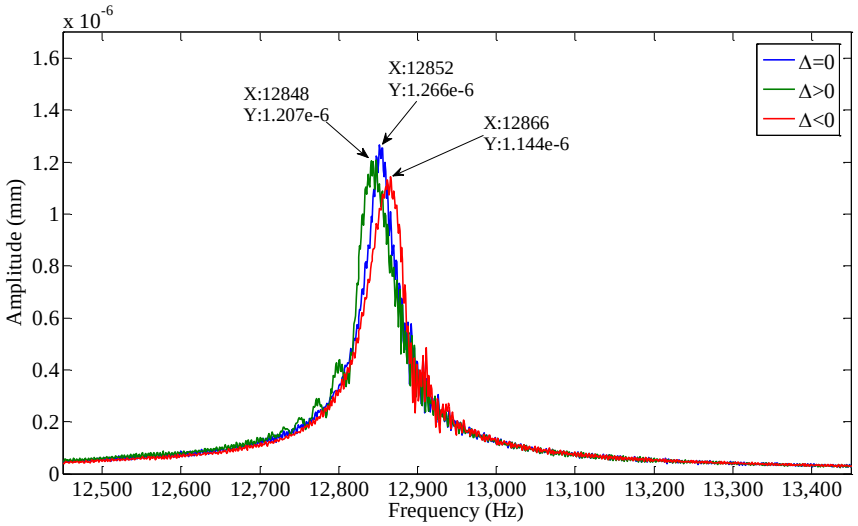

Figure 3.12 Second nonlinear resonance frequency

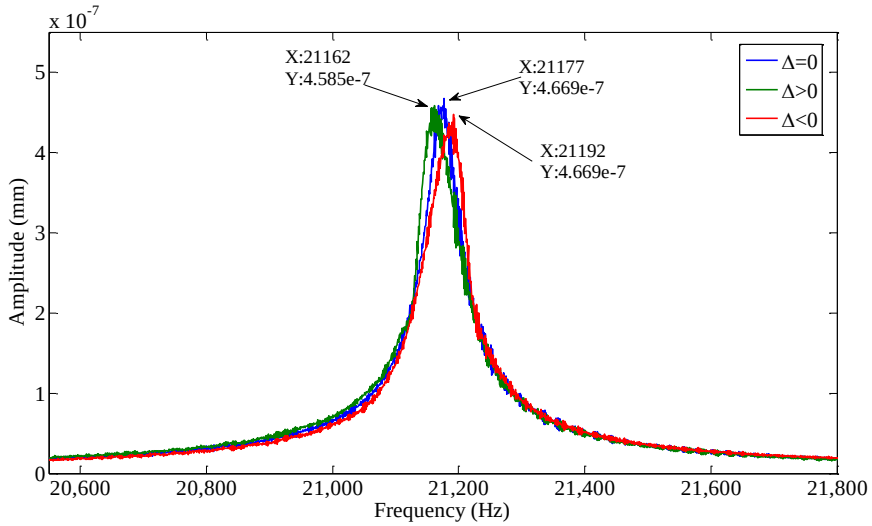

Figure 3.13 Third nonlinear resonance frequency

result in Fig.3.10 shows the comparison of frequency response of the system for different values of clearance. Fig. 3.11, Fig 3.12 and Fig. 3.13 shows the close up view of the each mode for the clearances $\Delta < 0$, $\Delta = 0$ and $\Delta > 0$. The case $\Delta = 0$ corresponds to an isochronous system in which frequency was independent of amplitude retaining the nonlinear vibration character. For the system with clearance ($\Delta > 0$) for each mode had a hard character while for system with interference ($\Delta < 0$) the curve was of soft type.

3.8.4 Effect of Changing Contact Stiffness

3.8.4.1 Case (A) $\Delta = 0$

In this case simulation was performed by keeping the clearance value zero and varying the contact stiffness. The frequency sweep was performed from 3500 Hz to 35000 Hz. Fig. 3.14 shows the comparison between the frequency responses for different values of contact stiffness. It was found that as the contact stiffness increases frequency shift goes on increasing significantly indicating the strong nonlinear response. Fig. 3.15, Fig 3.16 and Fig.3.17 show the close up view of each prominent mode. It was observed that frequency shift for first mode varies from 9.03 % to 22.56 % with increase in contact stiffness when compared with linear system response. For second mode it varies from 1.06 % to 3.3 % with increase in contact stiffness. Similarly for third mode it varies from 0.38 % to 1.25%. It clearly showed that the frequency shift for the first mode was quite significant when compared with second and third mode.

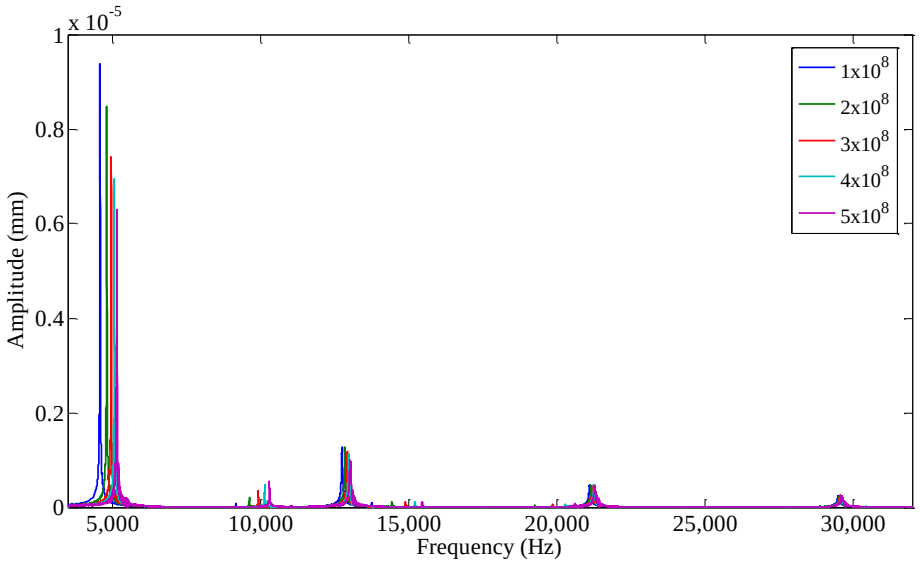

Figure 3.14 : Frequency response for different values of constant stiffness

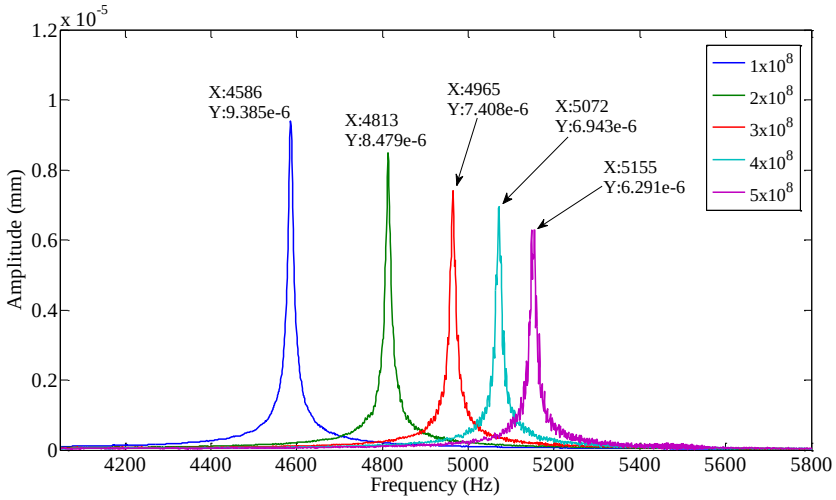

Figure 3.15 First nonlinear mode of vibration

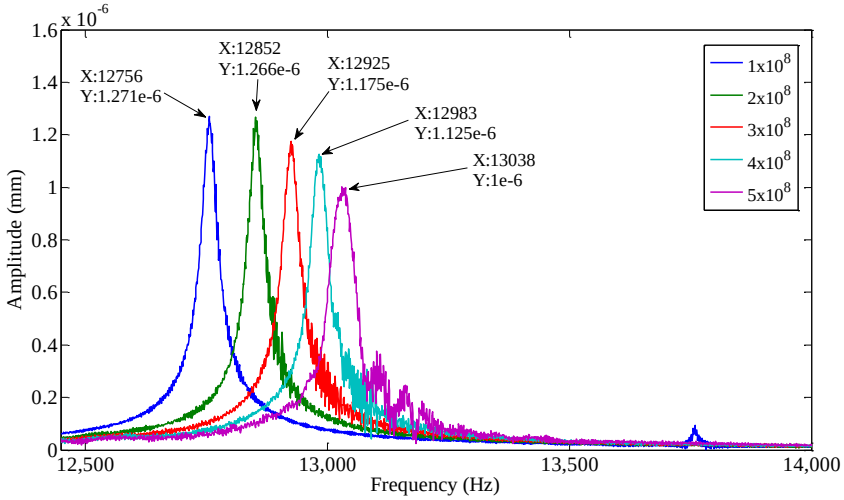

Figure 3.16 Second nonlinear mode of vibration

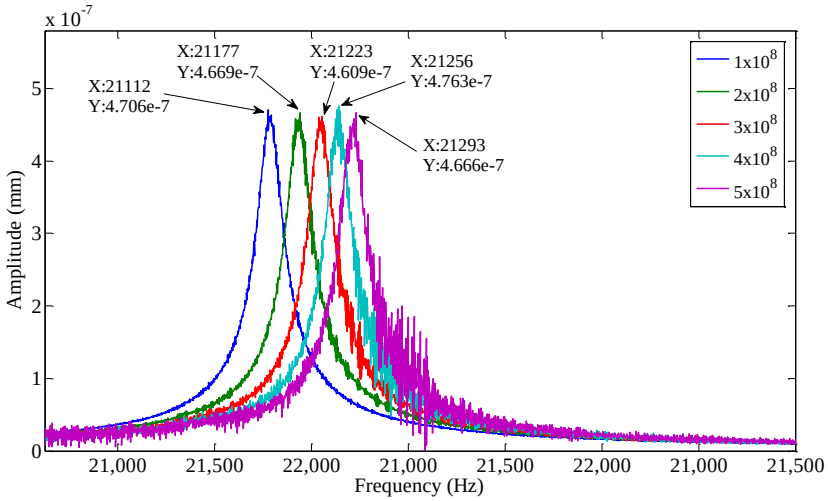

Figure 3.17 Third nonlinear mode of vibration

3.8.4.2 Case (B) $\Delta > 0$

In this case simulation was performed by keeping the clearance value greater than zero and varying the contact stiffness. The frequency sweep was performed from 3500 Hz to 35000 Hz. Fig.3.18 shows the comparison between the frequency responses for different values of contact stiffness. It was found that as the contact stiffness increases frequency shift goes on increasing significantly indicating the strong nonlinear response. Fig.3.19, Fig.3.20 and Fig.3.21 shows close up view of each prominent mode. It was observed that frequency shift for first mode varies from 8.9 % to 22.23 % with

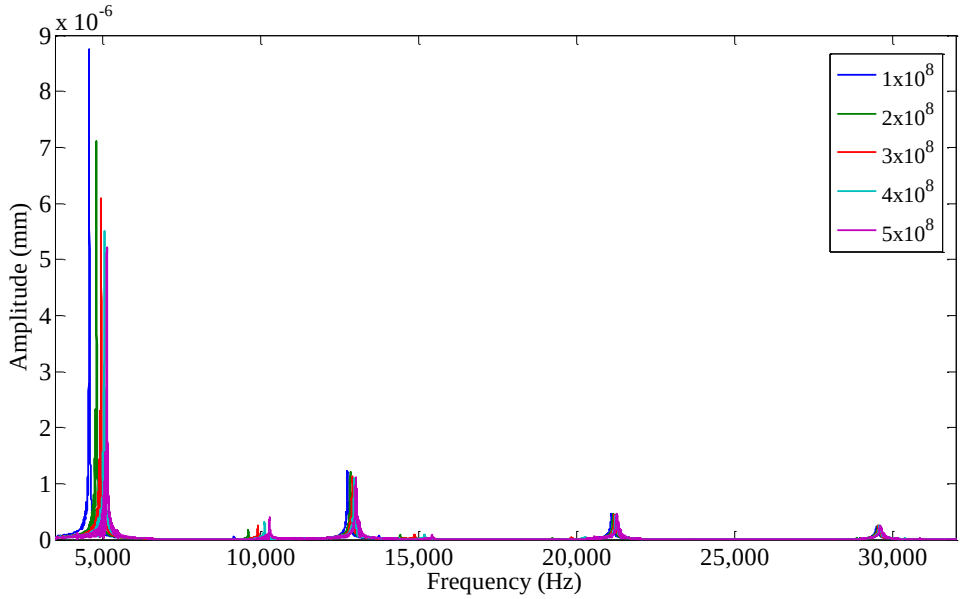

Figure 3.18 Frequency response for different values of constant stiffness

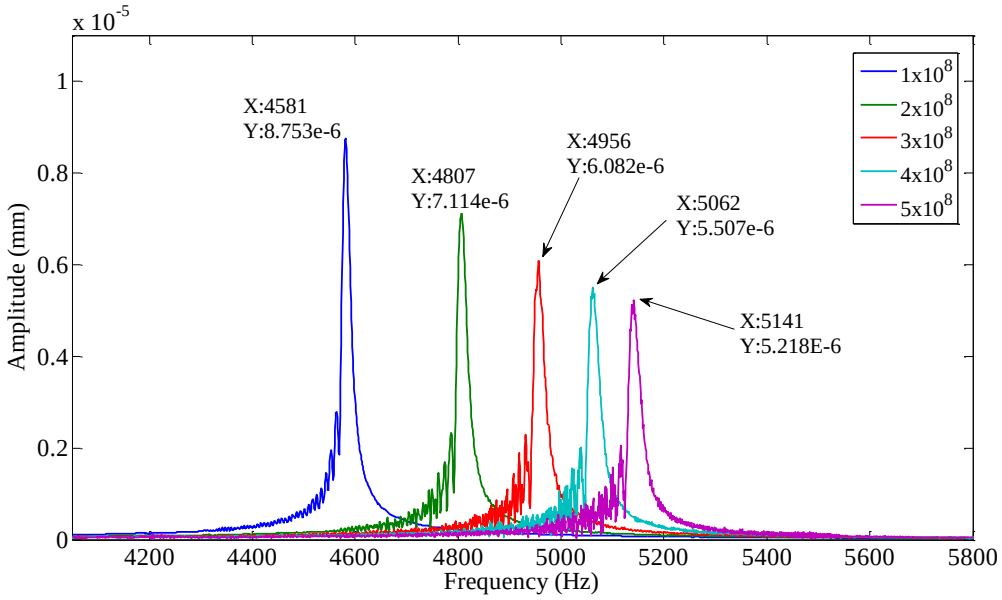

Figure 3.19 First nonlinear mode of vibration

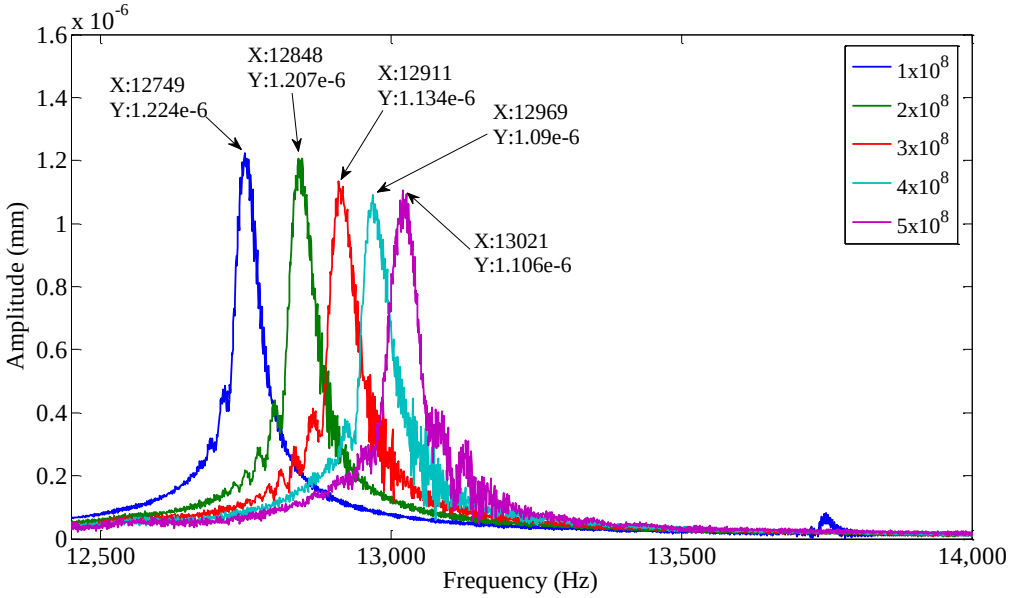

Figure 3.20 Second nonlinear mode of vibration

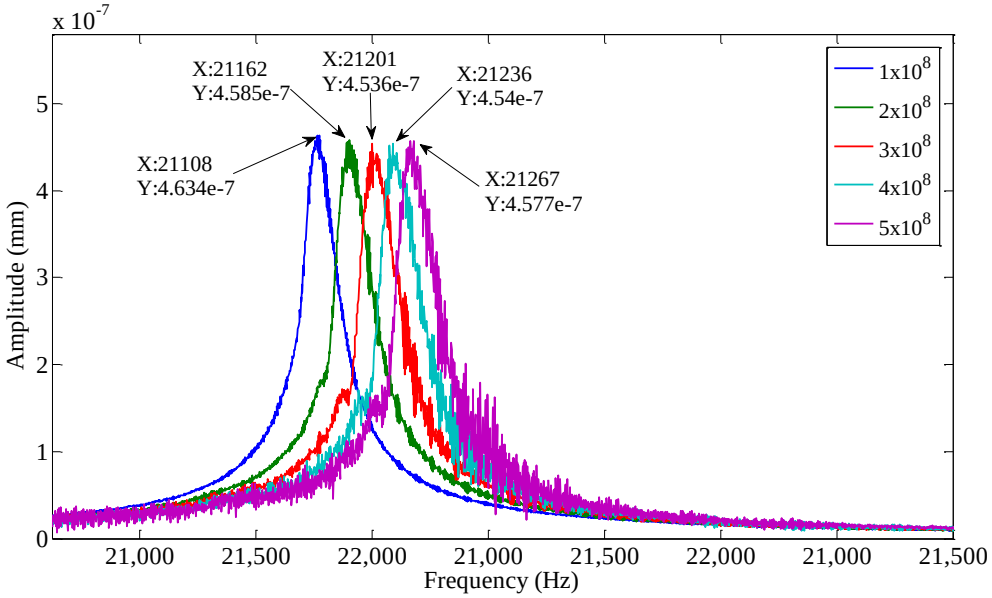

Figure 3.21 Third nonlinear mode of vibration

increase in contact stiffness when compared with linear system response. For second mode it varies from 1.01 % to 3.16 % with increase in contact stiffness. Similarly for third mode it varies from 0.37 % to 1.12%. It clearly showed that the frequency shift for the first mode was quite significant when compared with second and third mode.

3.8.4.3 Case (C) $\Delta < 0$

In this case simulation was performed by keeping the clearance value less than zero and varying the contact stiffness. The frequency sweep was performed from 3500 Hz to 35000 Hz. Fig.3.22 shows the comparison between the frequency responses for different values of contact stiffness. It was found that as the contact stiffness increases frequency shift goes on increasing significantly indicating the strong nonlinear response. Fig.3.23, Fig.3.24 and Fig.3.25 shows close up view of each prominent mode. It can be observed that frequency shift for first mode varies from 9.17 % to 22.75 % with increase in contact stiffness when compared with linear system response. For second mode it varies from 1.15 % to 3.35 % with increase in contact stiffness.

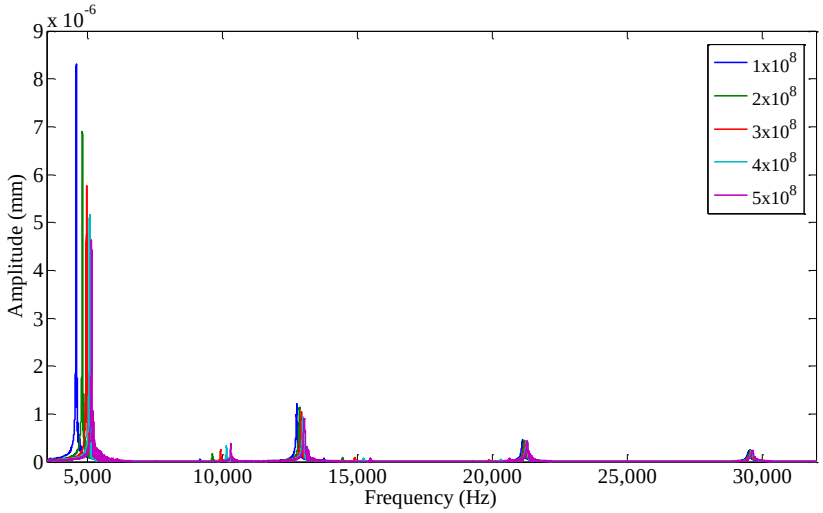

Figure 3.22 Frequency response for different values of contact stiffness

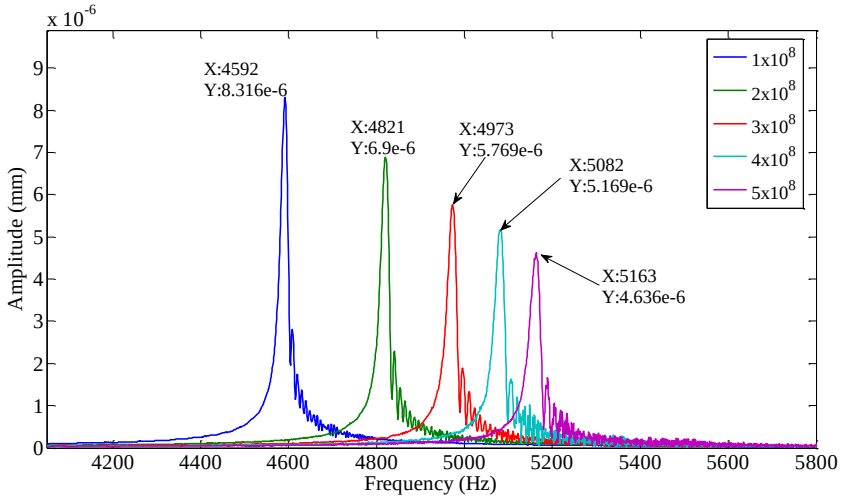

Figure 3.23 First nonlinear mode of vibration

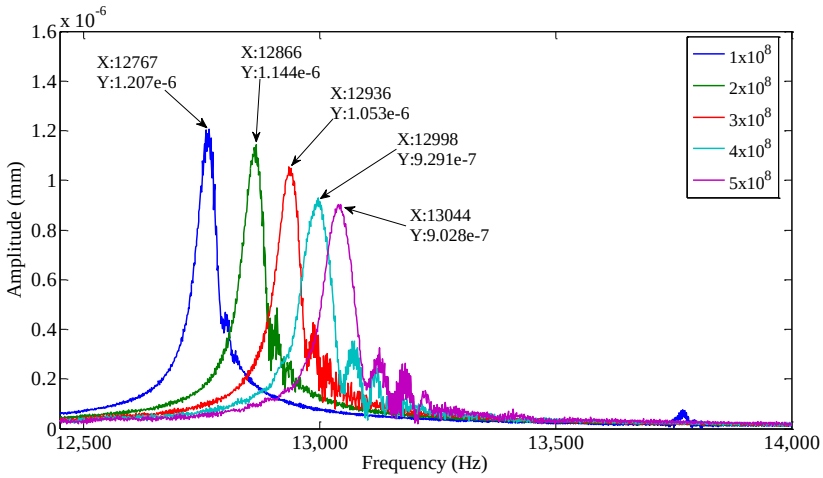

Figure 3.24 Second nonlinear mode of vibration

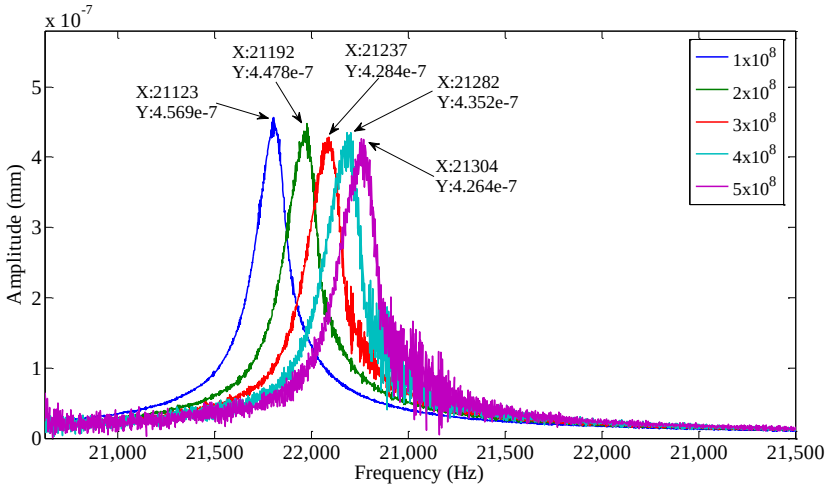

Figure 3.25 Third nonlinear mode of vibration

Similarly for third mode it varies from 0.44 % to 1.30%. It clearly showed that the frequency shift for the first mode was quite significant when compared with second and third mode.

3.8.5 Effect of Linear Resonance Frequency of Excitation on the Cracked Bar

3.8.5.1 Effect of First Linear Resonance Frequency of Excitation

The cracked bar was excited at the first linear resonance frequency 4206 Hz to obtain the time response. The result in Fig. 3.26 (a) shows the plot of amplitude $u(x,t)$ versus time. From Fig.3.26 (a) it was observed that there was modulation of time response indicating the presence of some additional frequency component. The FFT of time response was taken at the sampling frequency of 10 MHz. From frequency response (Fig. 3.26(b)) obtained it was clear that along with the frequency of excitation there was

an additional frequency component coupled with it. This additional frequency component was due to the free vibration taking place during the process of forced excitation, i.e. the interaction between cantilever bar and limiter.

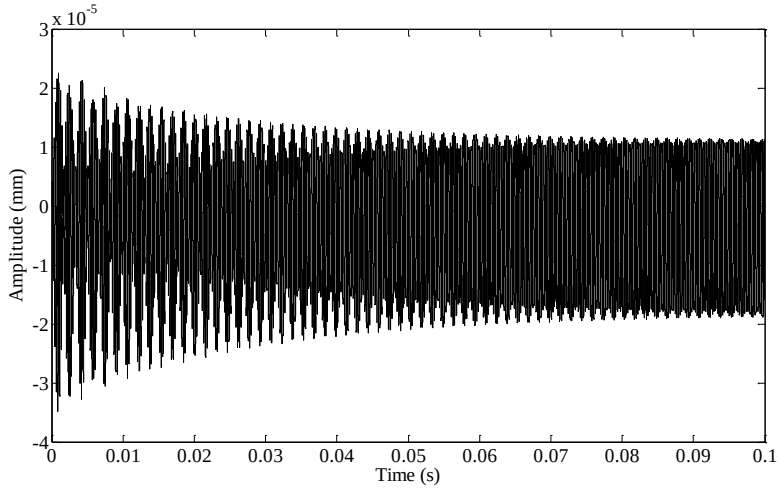

(a) Time response

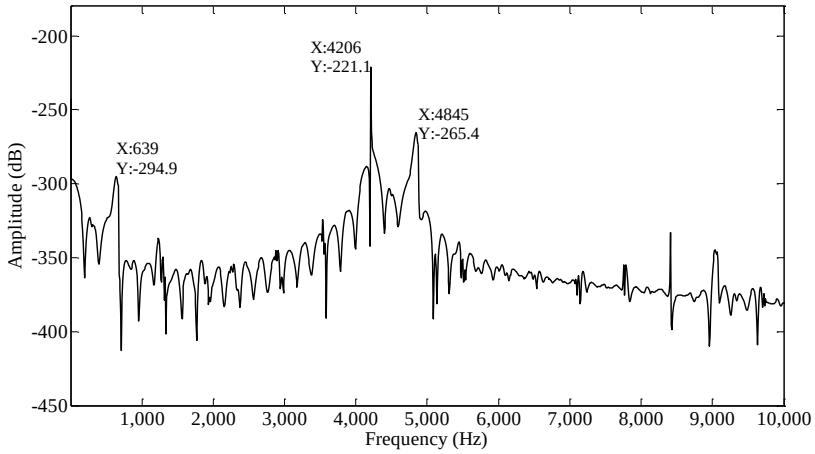

(b) Frequency response

Figure 3.26 Response at first linear resonance frequency of excitation

3.8.5.2 Effect of Second Linear Resonance Frequency of Excitation

The cracked bar was excited at the second resonance frequency 12617 Hz to obtain the time response. The result in Fig. 3.27 (a) showed that there was a modulation of the time response indicating the presence of some additional frequency. The FFT of time response was taken at the sampling frequency of 10 MHz. From frequency response (Fig. 3.27(b)) obtained it was clear that along with the frequency of excitation there was

an additional frequency component coupled with it. This additional frequency component was due to the free vibration taking place during the process of forced excitation, i.e. the interaction between cantilever bar and limiter.

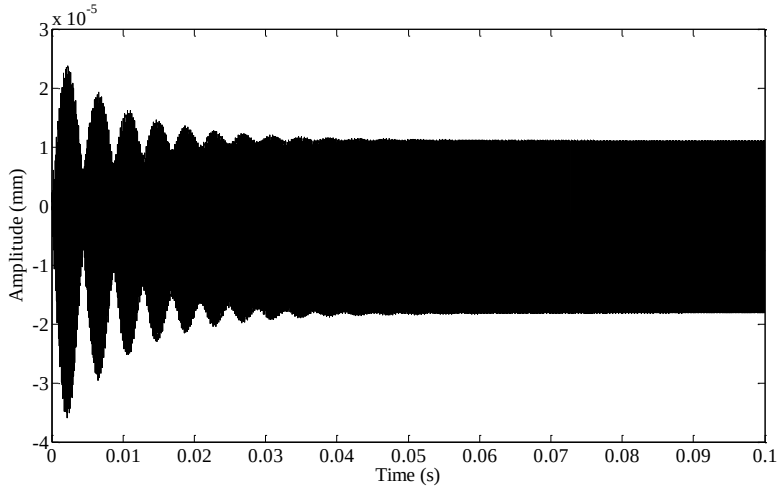

(a) Time response

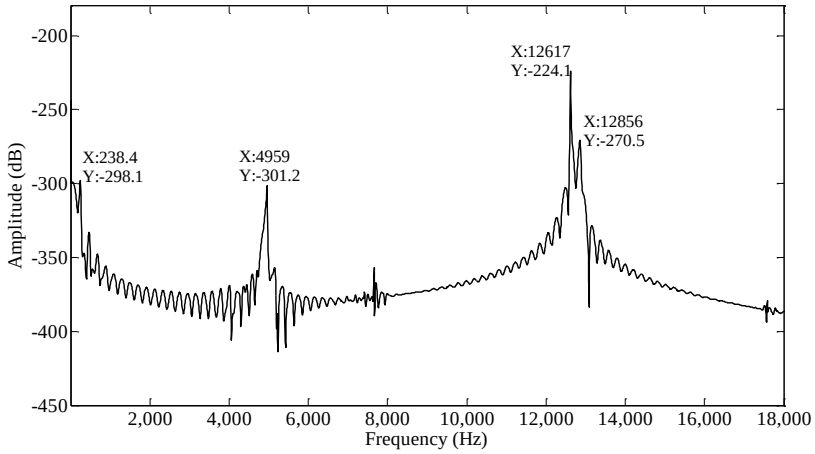

(b) Frequency response

Figure 3.27 Response at second linear resonance frequency of excitation

3.8.5.3 Effect of Third Linear Resonance Frequency of Excitation

The cracked bar was excited at the third linear resonance frequency 21029 Hz to obtain the time response. The result in Fig. 3.28 (a) showed that there was a modulation of the time response indicating the presence of some additional frequency. The FFT of time response was taken at the sampling frequency of 10 MHz. From frequency response (Fig. 3.28(b)) obtained it was clear that along with the frequency of excitation there was an additional frequency component coupled with it. This additional frequency

component was due to the free vibration taking place during the process of forced excitation, i.e. the interaction between cantilever bar and limiter.

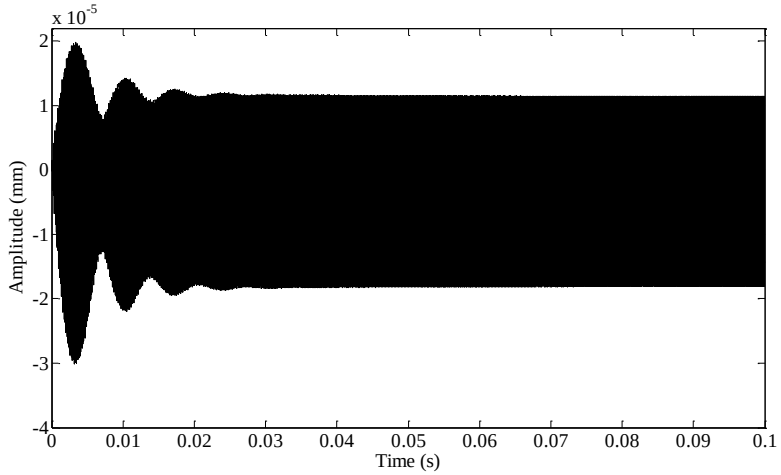

(a) Time response

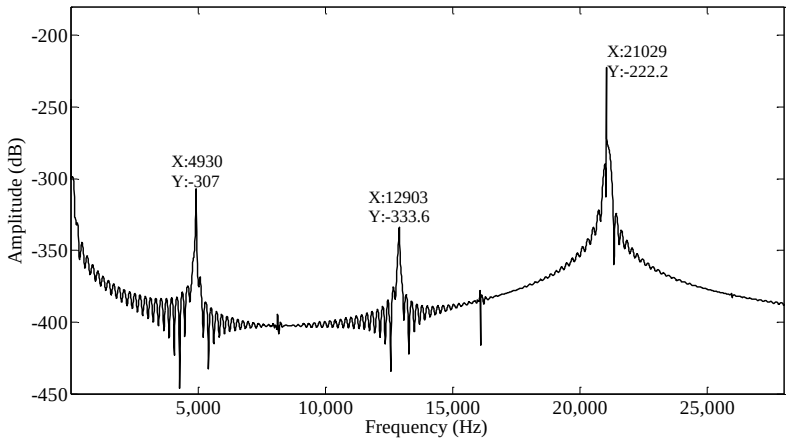

(b) Frequency response

Figure 3.28 Response at third linear resonance frequency of excitation

3.8.6 Effect of Nonlinear Resonance Frequencies of Excitation

3.8.6.1 Effect of First Nonlinear Resonance Frequency of Excitation

When the cracked cantilever bar was excited at the first nonlinear resonant frequency 4807 Hz the time response (Fig. 3.29 (a)) obtained showed no modulation of the time indicating only the presence of one frequency at the steady-state vibration. The FFT of time response was taken at the sampling frequency of 10 MHz. It was also observed from the frequency response (Fig. 3.29 (b)) that there was nonlinear coupling between the nonlinear resonance frequencies of excitation with the other nonlinear resonance frequencies of vibration indicating the sharing of energy between them.

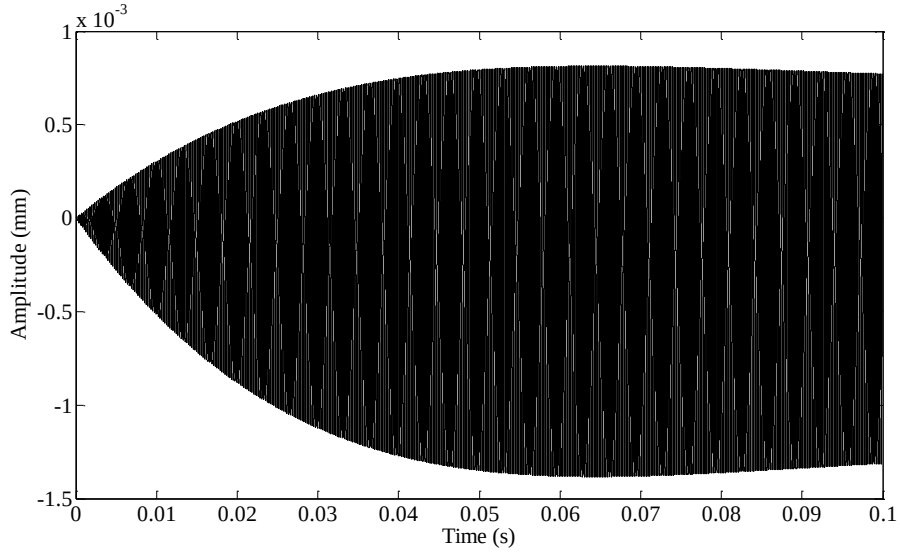

(a) Time response

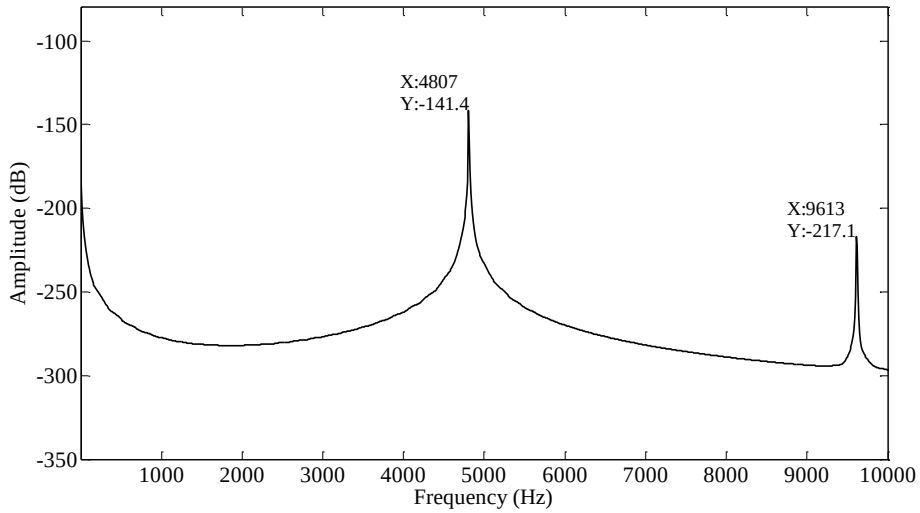

(b) Frequency response

Figure 3.29 Response at first nonlinear resonance frequency of excitation

3.8.6.2 Effect of Second Nonlinear Resonance Frequency of Excitation

When the cracked cantilever bar was excited at the second nonlinear resonant frequency12846 Hz the time response (Fig.3.30 (a)) obtained showed no modulation of the signal indicating only the presence of one frequency at the steady-state vibration. The FFT of time response was taken at the sampling frequency of 10 MHz. It was also observed from the frequency response (Fig.3.30 (b)) that there was the nonlinear coupling between the nonlinear resonance frequencies of excitation with the other nonlinear resonance frequencies of vibration indicating the sharing of energy between them.

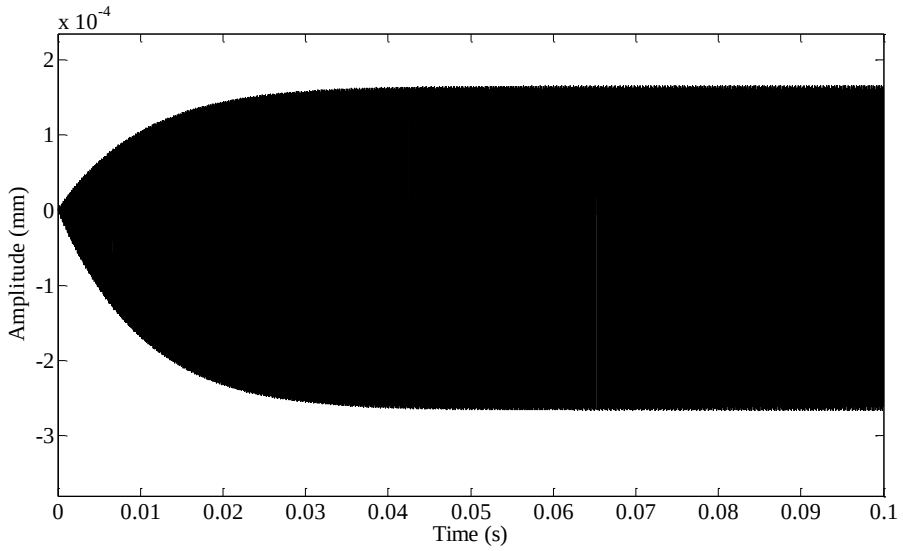

(a) Time response

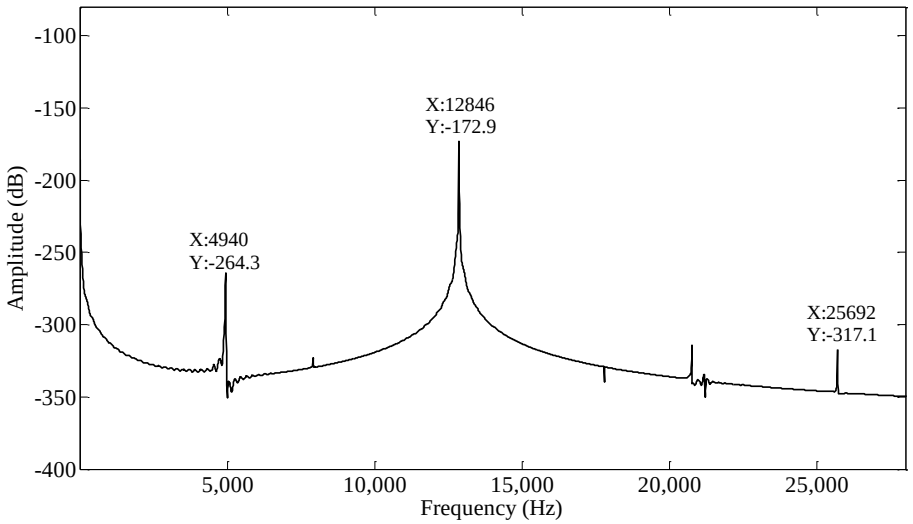

(b) Frequecny response

Figure 3.30 Response at second nonlinear resonance frequency of excitation

3.8.6.3 Effect of Third Nonlinear Resonance Frequency of Excitation

When the cracked cantilever bar was excited at the third nonlinear resonant frequency 21152 Hz the time response (Fig.3.31 (a)) obtained showed no modulation of the signal indicating only the presence of one frequency at the steady-state vibration. The FFT of time response was taken at the sampling frequency of 10 MHz. It was observed from the frequency response (Fig.3.31 (b)) that there was the nonlinear coupling between the nonlinear resonance frequencies of excitation with the other nonlinear resonance frequencies of vibration indicating the sharing of energy between them.

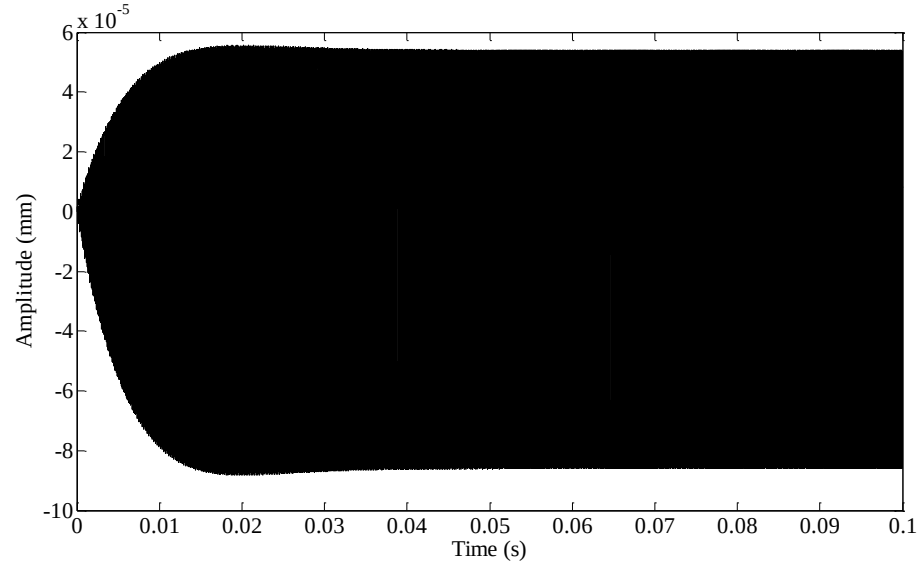

(a) Time response

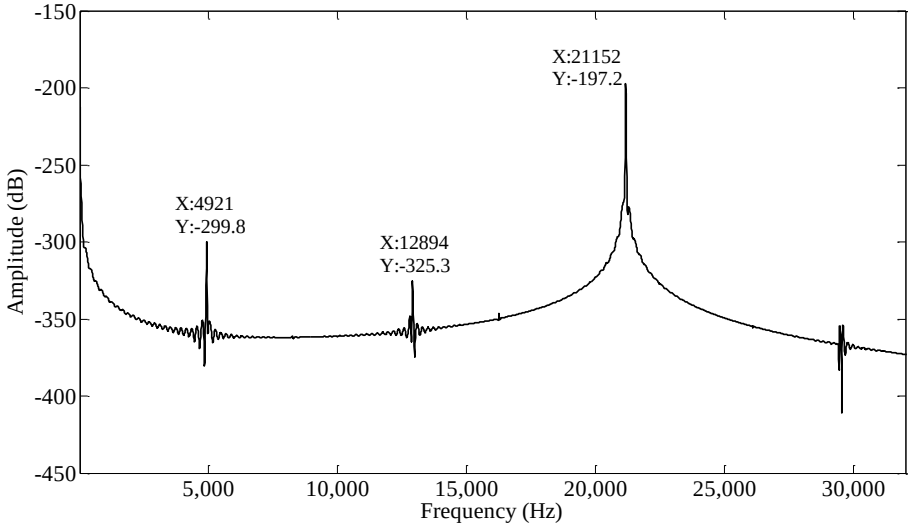

(b) Frequency response

Figure 3.31 Response at third nonlinear resonance frequency of excitation

3.8.7 Influence of Crack on the Intensity of Higher Harmonics along the Bar

The cracked bar was excited at first, second and third resonant frequencies of uncracked bar occurring at 4206 Hz, 12620 Hz and 21029 Hz, respectively, to obtain the steady-state response at each of this frequencies. The measurement of the response was taken at the different points on the bar, i.e. changing the distance from the crack. It was observed that as one moved away from the crack for the measurement of frequency response, the effect of nonlinearity decreased (Fig.3.32) indicating that it was more localised and can be used for detecting the location of the crack in the bar.

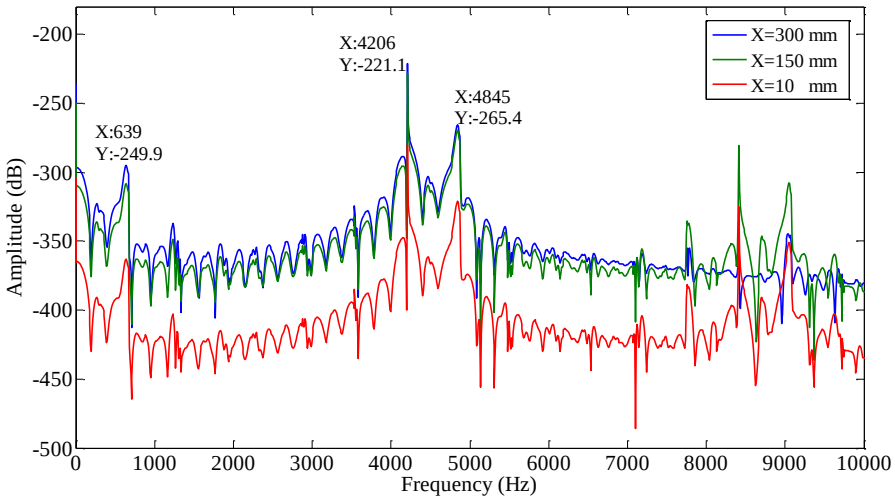

(a) First resonant frequency

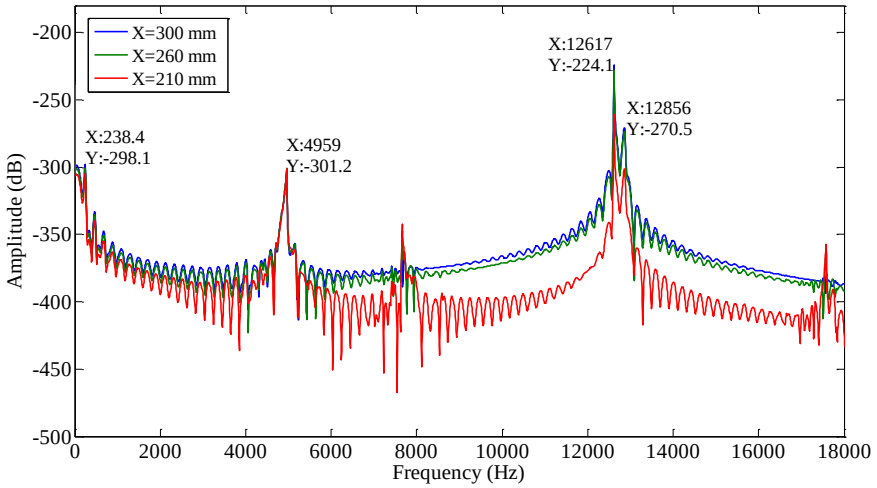

(b) Second resonant frequency

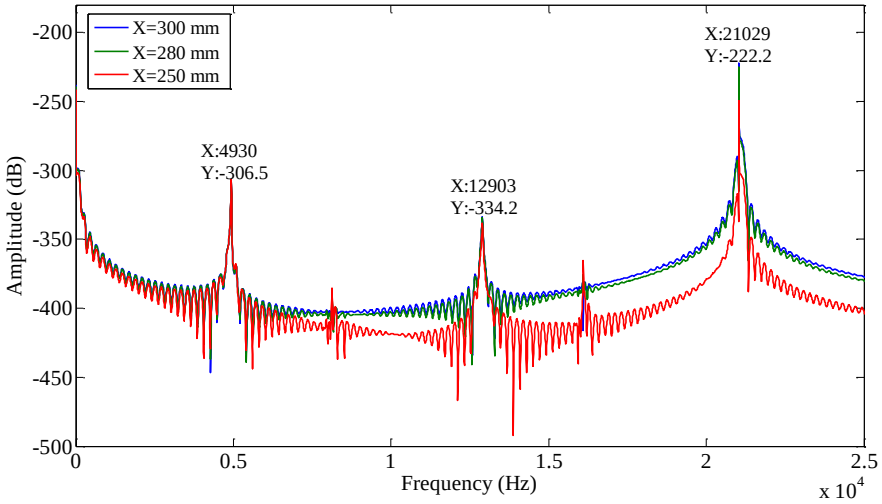

(c) Third resonant frequency

Figure 3.32 Influence of measurement point from the crack on higher harmonics

3.9 Summary

In this chapter the new procedure was developed using numerical approximation for the dynamic compliance operator and the nonlinear model of contact forces interaction implanted numerically as a nonlinear feedback. Nonlinear resonant phenomena due to vibro-impact interaction within cracked bar were obtained and analysed. This was implemented in the Matlab-Simulink software. It was found that there was significant frequency shift for the first mode of the vibration which varies from 9% to 22 % as the contact stiffness was increased. Similarly there was a frequency shift for the second and third mode for different contact stiffness but it was not that significant when compared with the frequency shift of the first mode. It was also found that the crack-induced nonlinearity has localized effect on the dynamics of the cracked bar, which leads to the generation of higher harmonics as a function of distance from the crack.

Chapter 4 Damage Assessment of a Cracked Bar: Effect of Material Nonlinearity on Vibro-Impact Response

4.1 Introduction

Finite Element Analysis (FEA) is used for the numerical solution of field problems. A field problem is solved by determining a spatial distribution of one or more dependent variables. Mathematically, a field problem is described by differential equations or by an integral expression. An Individual finite element can be visualized as a part of a structure. The word ‘finite’ distinguishes these parts from infinitesimal elements used in calculus. In each ‘finite' element a field quantity is allowed to have only a simple spatial variation; the actual variation in the region spanned by an element is more complicated. Hence FEA provides an approximate solution. Elements are connected with each other at points called nodes. The assemblage of elements is called ‘finite-element structure’. A particular arrangement of elements is called mesh. Numerically, a finite element model is represented by a system of algebraic equations to be solved for unknown magnitudes at nodes. Nodal unknowns are values of the field quantity. The solution for nodal quantities, when combined with the assumed field in any given element, completely determines a spatial variation of the field in that element. Thus the field quantity over the entire structure is approximated element by element, in a piecewise fashion [Cook *et al.*, 2002].

This chapter deals with damage assessment for a component using an example of a crack in a cantilever bar under longitudinal harmonic loading. The finite-element simulation is used to perform this analysis. The nonlinear material properties are introduced in terms of their plasticity. The effect of a crack size and position along the beam length is studied. An observed change in a frequency response is used to characterize the damage state of the component.

4.2 Procedure for Solving a Problem by FEA

Solving a problem with FEA involves formulating the problem, preparing a mathematical model, discretizing it, implementing calculations with a computer and checking the results. In many cases, more than one cycle through these steps is required.

The steps involved in solving the finite element analysis problem is shown in Fig. 4.1[Cook *et al.*, 2002]

Step 1*: Classification of Problem*

This step involves identifying important physical phenomena involved, establishing whether the problem is time-dependent or not, checking for nonlinearity involved so that an iterative solution can be used, deciding on results sought from analysis and checking for the accuracy required. In this way a proper model can be developed and can be used for the calculation.

Step 2*: Mathematical Modelling*

In this step, a mathematical model has to be developed after the physical nature of the problem has been understood. A mathematical model is an idealization, in which geometry, material properties and boundary conditions are simplified based on the analyst's understanding of what features are important or unimportant in obtaining the results required. A geometric model becomes a mathematical model when its behaviour is described by selected constitutive equations and boundary conditions. FEA is applied to this mathematical model. Thus, a fully continuous field is represented by a piecewise continuous field defined by a finite number of nodal quantities and a simple interpolation within each element.

Step 3*: Preliminary Analysis*

Preliminary analysis can involve analytical calculations or a use of existing handbook formulas, trusted previous solutions, or an experimental study. Subsequently it will be used to check the computed results.

Step 4*: Finite Element Analysis*

This step involves three sub-steps such as pre-processing, numerical analysis, and post-processing. In pre-processing input data such as geometry parameters, material properties and so on should be transferred into a mesh of respective elements with the requested density. Numerical analysis involves the generation of matrices describing the behaviour of each element, combining these matrices for the entire problem and formulating a matrix equation and solving this equation to determine values of field

quantities at nodes. In post-processing, FEA solution and quantities derived from it can be listed or displayed graphically.

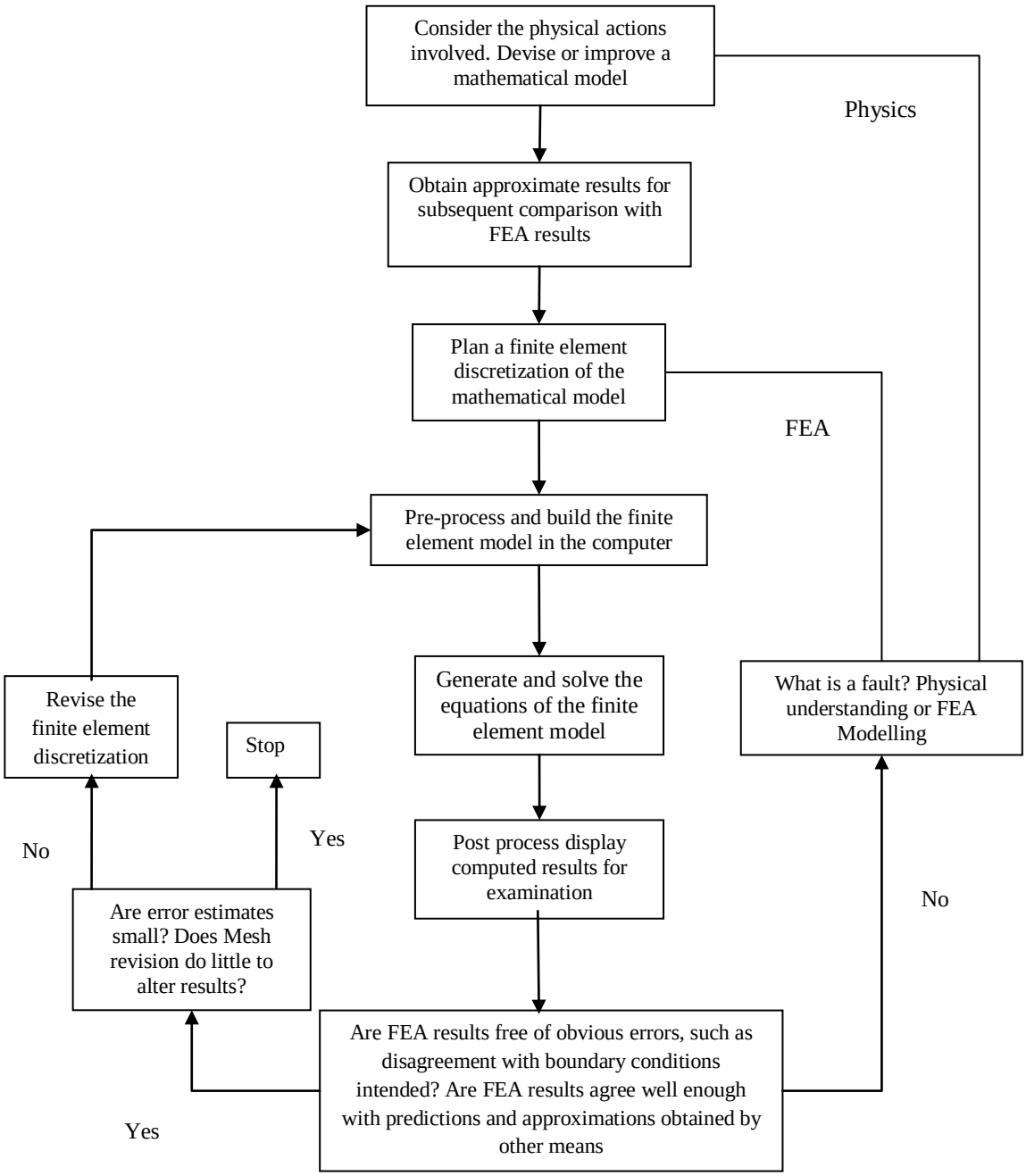

Figure 4.1 Outline of finite element analysis
Modified,after [Cook, 2002]

Step 5: *Result Checking*

FEA results obtained are compared with solutions from preliminary analysis and with any other useful information that may be available.

Step 6: *Revision*

FEA results obtained are not always satisfactory, as there may be large discrepancies with physical observation/experiment due to a lack of physical understanding or deficiencies of the FEA model or both. Hence, revision can help an analyst to learn more which results in a more appropriate solution.

4.3 Introduction to Package MSC. Marc Mentat

MSC.Marc Mentat is an interactive computer program that prepares and processes data implementing the finite element method. It is a powerful tool for performing linear and nonlinear stress analyses in the static and dynamic regimes, as well as heat transfer analysis and electromagnetic analysis. The nonlinearities that can be treated may be due to material behaviour, large deformations and/or boundary conditions.

Marc also enables researchers to assess the structural integrity and performance of parts undergoing large permanent deformations as a result of thermal and/or structural loads. Marc can also simulate deformable, part-to-part contact under varying conditions that include the effects of friction critical for analyzing a nonlinear behaviour. The software package offers an extensive library of metallic and non-metallic material models, along with a library of 175 elements for structural, thermal, and fluid analysis. It works with two pre- and post processors and also provides unique ability to process large problems in parallel using domain decomposition technique.

MSC Marc.Mentat is used for the purpose of simulation as it can solve nonlinear problem and it has robust capabilities for contact, large strain, and multi-physics analysis to solve static and quasi-static nonlinear problems [MSc Marc. 2007 r1 Volume. A].

4.4 Problem Formulation

The analysed problem physically represents a straight bar of length L, which has a single crack of depth a and has a uniform rectangular cross-section of height h and width b. The cantilever bar is clamped at the left end and is free at its right end. The crack is located at the upper edge of the bar and is at the distance d from the fixed end, with d/L being a dimensionless crack position. a/h is the dimensionless ratio between

the depth of crack to the depth of the cross-sectional area. The longitudinal harmonic force is acting at the free end of the bar. Fig. 4.2 shows the schematic of the system model for three different cases. The dimensions and the mechanical properties for the straight bar are given in Table 4.1 and Table 4.2 respectively.

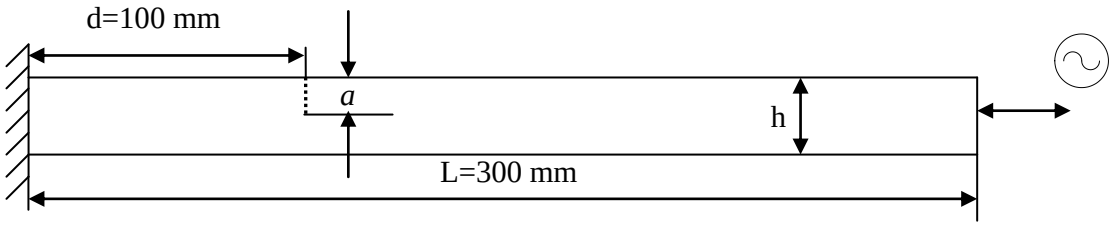

(a) Crack near the fixed end of the bar

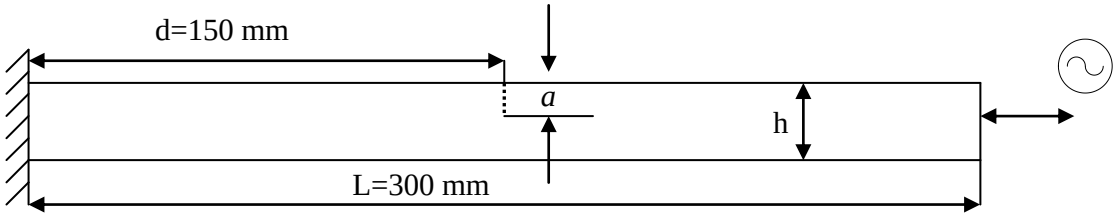

(b) Crack at the centre of the bar

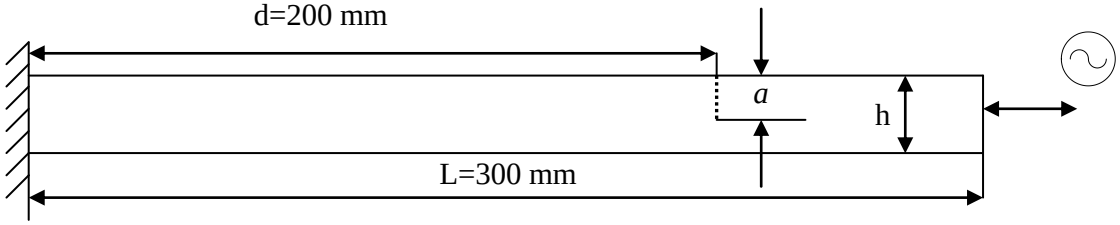

(c) Crack near the free end of the bar

Figure 4.2 Crack configurations

Parameters	**Dimensions in mm**
Length(L)	300
Width(b)	10
Height(h)	25
Depth of crack (a)	2, 4, 6, 8 and 10
Distance of crack from fixed end (d)	100, 150, 250

Table 4.1 Dimensions of cracked bar

Material	Aluminium (Grade 6082T6)
Density [kg/mm^3]	2.70 x 10^{-6}
Modulus of elasticity [N/mm^2]	7 x 10^4
Yield strength [N/mm^2]	2.514 x 10^2
Ultimate tensile strength [N/mm^2]	3.434 x 10^5

Table 4.2 Mechanical properties

4.5 Stress-Strain Curve

A representation of relationship between a stress generated due to the application of force to a specimen and a strain obtained from measuring its induced deformation is called *stress-strain curve*. It varies from material to material. In Fig. 4.3 the engineering stress-strain curve shown demonstrates mechanical behaviour of metals as the loading in the specimen gradually increased. From O to A stress is proportional to strain. Beyond point A, the deviation from the Hooke's law can be observed; hence, the stress at A represents the proportionality limit. At B, elongation of specimen begins without any appreciable increase in the load and the material is said to become plastic. This phenomenon is called *yielding*, continues until the test bar is stretched plastically as much as ten to fifteen times the elastic stretch up to the proportional limit. The stretch at which this yielding takes place is called *yield point*. At point C the material begins to

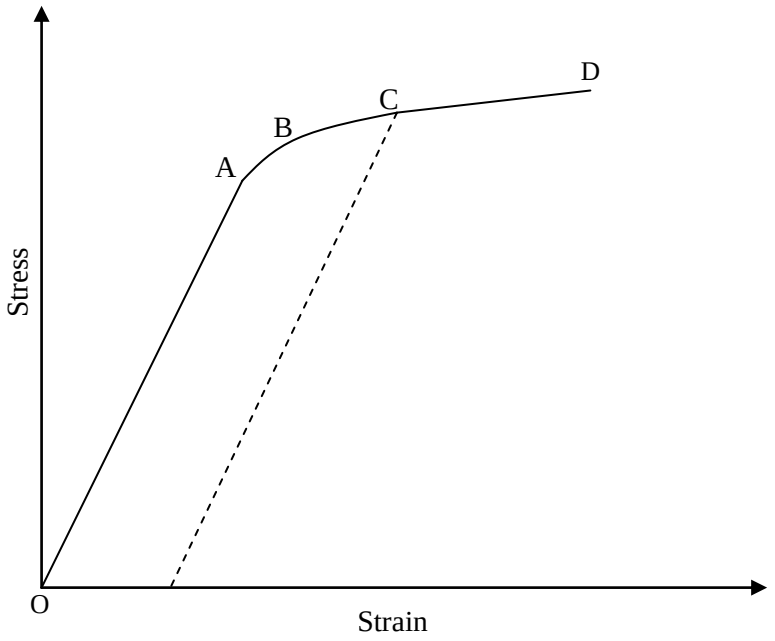

Figure 4.3 Stages of stress-strain curve

strain-harden, recovers some of its elastic properties, and with further elongation the stress-strain curve reaches point D, representing the maximum tensile strength or ultimate tensile strength. Beyond point D, further stretching of the bar is accompanied by a decrease in the load and fracture takes place [Timoshenko, 2002].

The engineering stress-strain curve does not give a true indication of deformation characteristics of a metal because it is based entirely on original dimensions of the specimen and these dimensions change continuously during the test. Actually, the metal continues to strain-harden all the way up to fracture, so that the stress required to produce further deformation should also increase. If the true stress based on the current cross-sectional area of the specimen and the strain measurement based on instantaneous measurements is used then the curve obtained is known as a *true stress-true strain curve* [Timoshenko,2002].

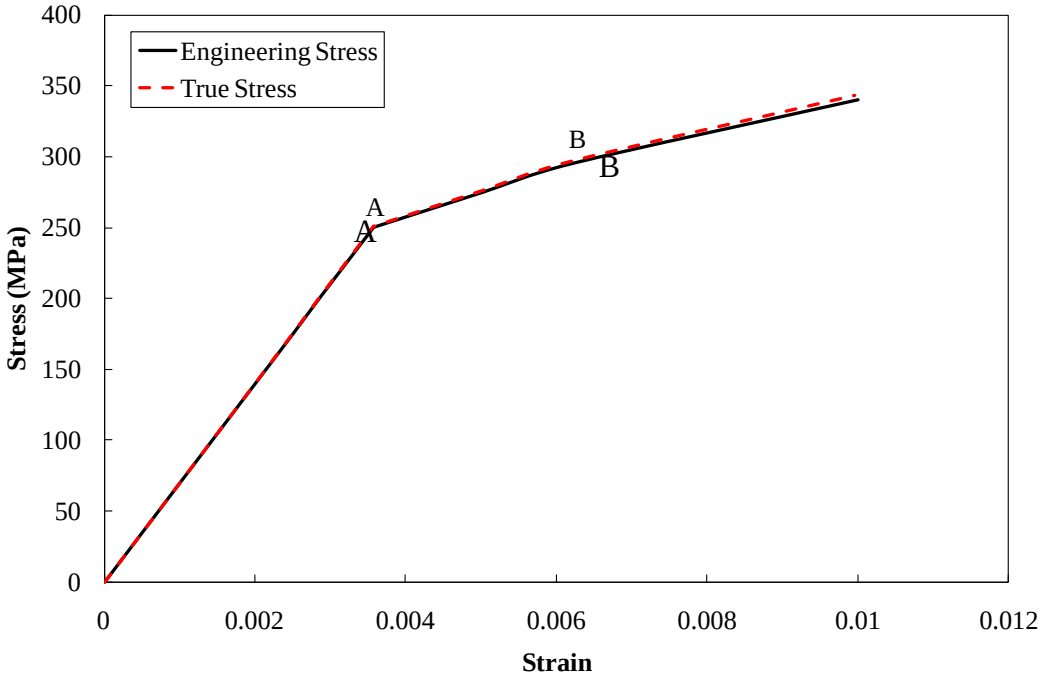

Figure.4.4 Stress-Strain curve of Aluminium (Grade 6082T6)

The true stress is given by

$$\sigma = \frac{P}{A} = \frac{P}{A_0(1+\epsilon)}\ , \tag{4.1}$$

where

A= Actual area of specimen;

A_0= Original area of specimen;

P = Applied load;

ϵ = strain.

The true strain is determined by

$$\epsilon = \ln(e + 1) \ , \tag{4.2}$$

where e = Elongation of specimen.

Fig. 4.4 shows the comparison between the engineering stress-strain curve and the true stress-strain curve for aluminium. In the Fig. 4.4 true stress-strain curve is shown in dotted line and engineering stress-strain curve in solid line.

4.6 Strain Additivity

The total strain can be presented as a sum of elastic and plastic components [Meyers *et al.*, 2009]

$$\epsilon = \epsilon^e + \epsilon^p \ . \tag{4.3}$$

The bilinear model combining elasticity with linear strain-hardening plasticity can be used for low-level plastic strains. It can be expressed as follows:

elastic part:

$$\epsilon^e = \frac{\sigma}{E^e} , \tag{4.4}$$

plastic part:

$$\epsilon^p = \frac{\sigma - \sigma_y}{E^p} , \tag{4.5}$$

where E^p is the slope of the true stress-plastic strain curve

Using Eq. 4.1 and Eq. 4.5 we can obtain the graph (Fig 4.5) for true stress-plastic strain relationship used for the FEA simulations

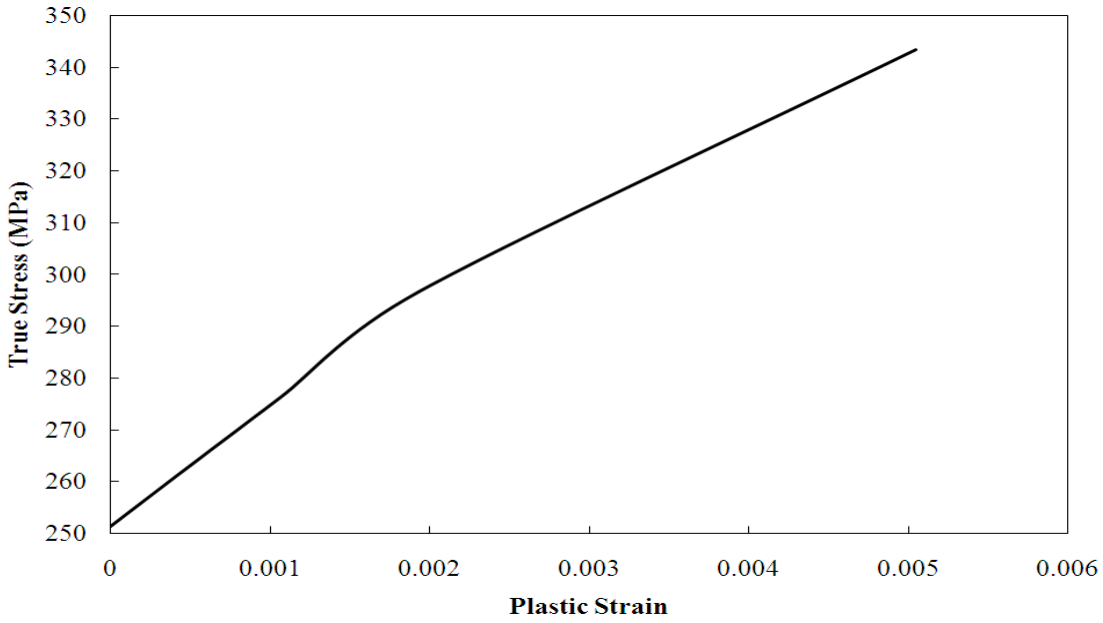

Figure. 4.5 True stress vs. Plastic strain for Aluminium (Grade 6082T6)

4.7 Methodology of Simulation

Fig. 4.6 shows the flow chart of the simulation process for the cantilever bar. It can be seen from it that the harmonic analysis is performed on the cracked bar and uncracked bar with linear and nonlinear material properties. The static analysis is performed on the

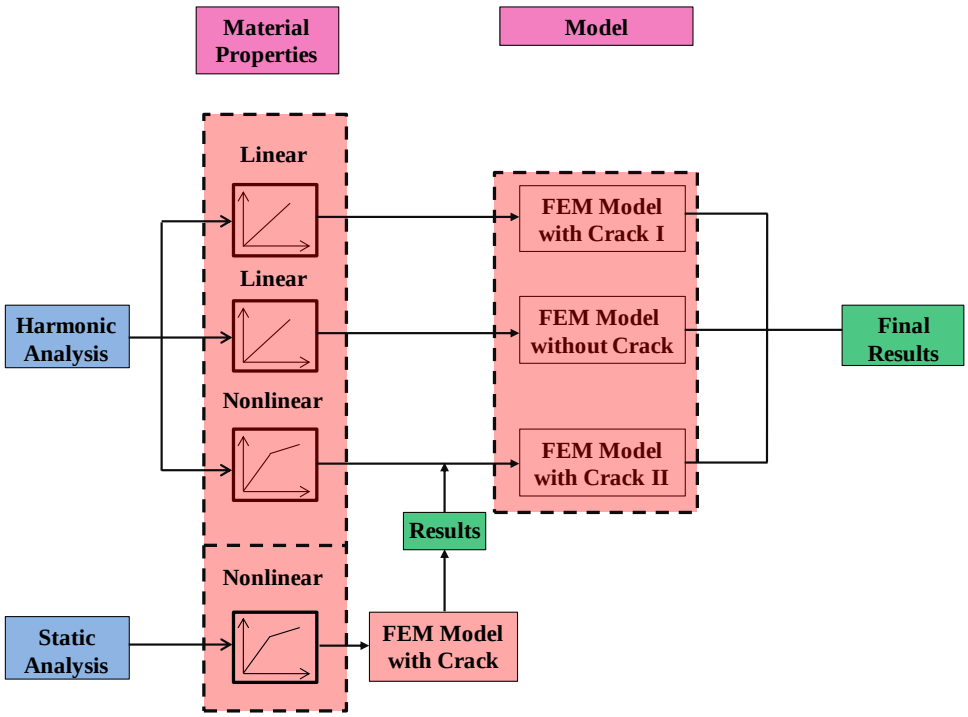

Figure.4.6 Flow chart for simulation

cracked cantilever bar with nonlinear material properties. The results obtained from this static analysis are used as an initial condition for the FEM model with the crack II. Using this initial condition, harmonic analysis is performed for the FEM Model II. The results obtained from this analysis are compared for those of FEM model without a crack. Similarly, the harmonic analysis is performed on the FEM model I with crack having linear material properties. The results obtained are also compared with those of the FEM model without a crack. Further the final results are obtained from the comparison between FEM model I and FEM model II. In all this analysis friction between the cracks faces is neglected.

4.8 Finite Element Model of Cracked Cantilever Bar

The 2D finite-element model of the cracked cantilever bar was modelled with MSC Marc commercial software. The finite element model of the cracked cantilever bar is modeled using element type 3. Element type 3(Fig 4.7) is a four-node, isoparametric, arbitrary quadrilateral element used for plane stress applications. This element uses bilinear interpolation functions; the strain is constant throughout the element. The stiffness of this element is formed using four point Gaussian integration. The crack is introduced in the cantilever bar by drawing the geometry of bar with a crack as a notch and meshing with the quad element. Fig 4.8(a) shows the finite element model of a cantilever bar fixed at the left end and harmonic loading applied at the free end for

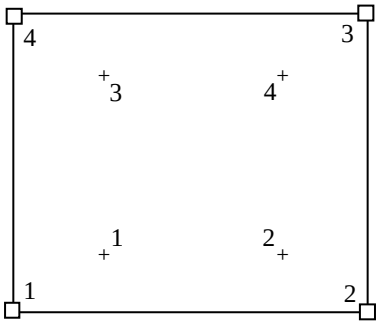

Figure 4.7 Quad element

performing harmonic analysis. In all total 7500 elements are used. The simulation is performed on the cracked cantilever bar with and without account for crack-tip plasticity. Fig. 4.8(c) presents results for the former case while Fig. 4.8(b) for a latter

one. The first three natural frequencies are obtained for both cases and are compared to estimate the effect of crack-tip plasticity on them.

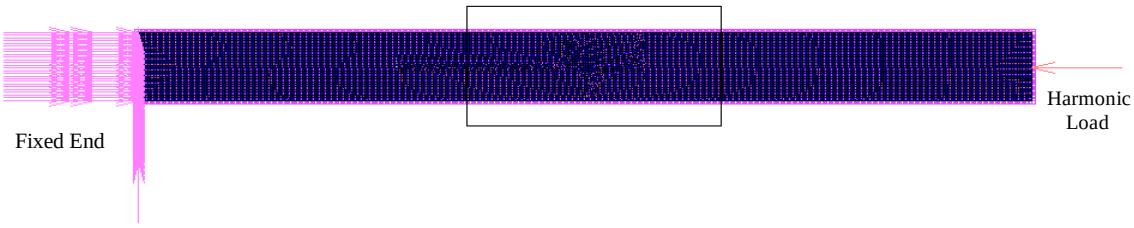

(a) Entire bar with boundary conditions

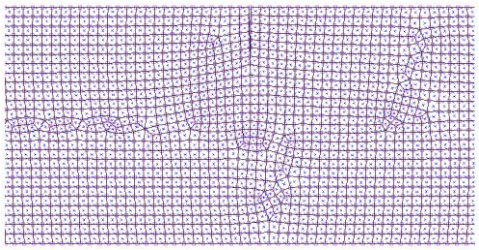

(b) Meshing near crack tip

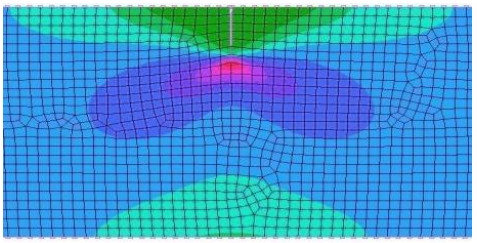

(c) Stress concentration near crack tip

Figure.4.8 FEA model of a cracked cantilever bar

4.9 Irwin's Approach

According to the Irwin's approach linear elastic stress analysis of sharp cracks predicts infinite stresses at the crack tip. In real materials, however, stresses at the crack tip are finite because the crack tip radius is finite. Inelastic material deformation, such as plasticity in metals leads to the relaxation of crack-tip stress. The elastic stress analysis becomes increasingly inaccurate in the inelastic region as the crack tip grows. Simple corrections to linear elastic fracture mechanics are available when moderate crack-tip yielding occurs. The size of crack tip yielding zone can be estimated by this approach

Consider the crack plane on which the normal stress σ_{yy} , in a linear elastic material is given by Eq. (4.6) as an approximation. We assume that the boundary between elastic and plastic behaviours occurs when the stresses given by Eq. (4.6) satisfy the yield criterion. For plane-stress conditions, yielding occurs when $\sigma_{yy} = \sigma_{YS}$, the uniaxial yield strength of material [Anderson, 2005].

$$\sigma_{yy} = \frac{K_I}{\sqrt{2\pi r}} \tag{4.6}$$

Where

K_I is stress intensity factor

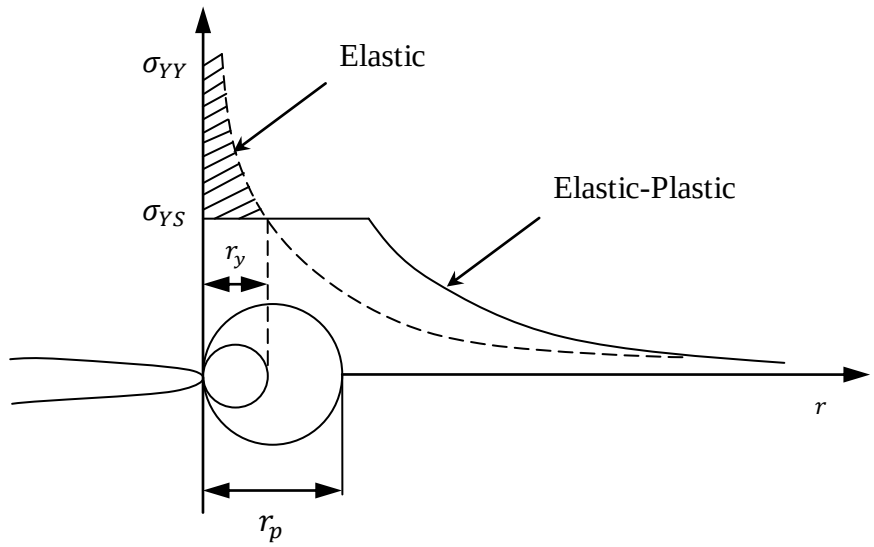

Figure.4.9 First-order and second-order estimates of plastic zone
Modified,after [Anderson, 2005]

For plane stress the size of the crack-tip plastic zone is given by

$$r_y = \frac{1}{2\pi}\left(\frac{K_I}{\sigma_{YS}}\right)^2 \tag{4.7}$$

Following the yielding (Fig. 4.9) there will be redistribution in the crack tip stress to make up for the load carrying capacity lost due to yielding.

According to the Irwin's analysis, we have

$$\sigma_{YS} r_p = \int_0^{r_y} \sigma_{yy} dr \tag{4.8}$$

Substituting Eq. (4.6) in Eq. (4.8) we have

$$\sigma_{YS} r_p = \int_0^{r_y} \frac{K_I}{\sqrt{2\pi r}} dr \tag{4.9}$$

Solving Eq. (4.9) one gets the second estimate for the size of a plastic zone

$$r_p = \frac{1}{\pi}\left(\frac{K_I}{\sigma_{YS}}\right)^2 \tag{4.10}$$

Comparing Eq. (4.7) and Eq.(4.10) we obtain

$$r_p = 2r_y \tag{4.11}$$

Hence Eq. (4.11) can be used to validate the number of elements defined in the Finite element analysis of the cracked cantilever bar. From the finite element analysis it is found that for elasto-plastic crack number of elements defined for FEA simulation satisfies the criteria of Eq. (4.11). Table 4.3 shows the results for FEA simulation performed for calculating K_I and corresponding values of r_y and r_p .

Crack Depth (mm)	$\mathbf{K_I}\left(\frac{Kg}{\sqrt{mm}\,s^2}\right)$	$\mathbf{r_y}$ (mm)	$\mathbf{r_p}$ (mm)
2	661180	0.7994	1.599
4	705300	1.0295	2.059
6	679850	0.845	1.6905
8	698940	0.8934	1.786
10	434650	0.345	0.6910

Table 4.3 Calculation of plastic zone size

4.10 Simulation Results

The force longitudinal vibration analysis was performed to obtain the natural frequencies of the cantilever bar. The first, second and third natural frequencies of the uncracked aluminum cantilever bar of chosen dimensions are 4242.12 Hz, 12729.37 Hz and 21215.62 Hz respectively. The first three natural frequencies of the cracked aluminum bar with and without plasticity at the crack tip are compared below for several cases.

4.10.1 Case (A) Crack near the Fixed End of the Bar

It was found that in Case (A) there was no change in the first natural frequency (Fig. 4.10) and there was only a marginal change in the third natural frequency initially but as

the crack-to-depth ratio was increased the change in frequency with and without plasticity almost remained the same (Fig. 4.12). Contrary to that there was a constant change in the second natural frequency as shown in Fig. 4.11. The bar chart (Fig. 4.13) shows that the first natural frequency was not affected by crack-tip plasticity whereas the second frequency and third natural frequencies showed some change due to it. This change in frequencies was due to the crack-induced plasticity which affected the overall stiffness of the cracked cantilever bar.

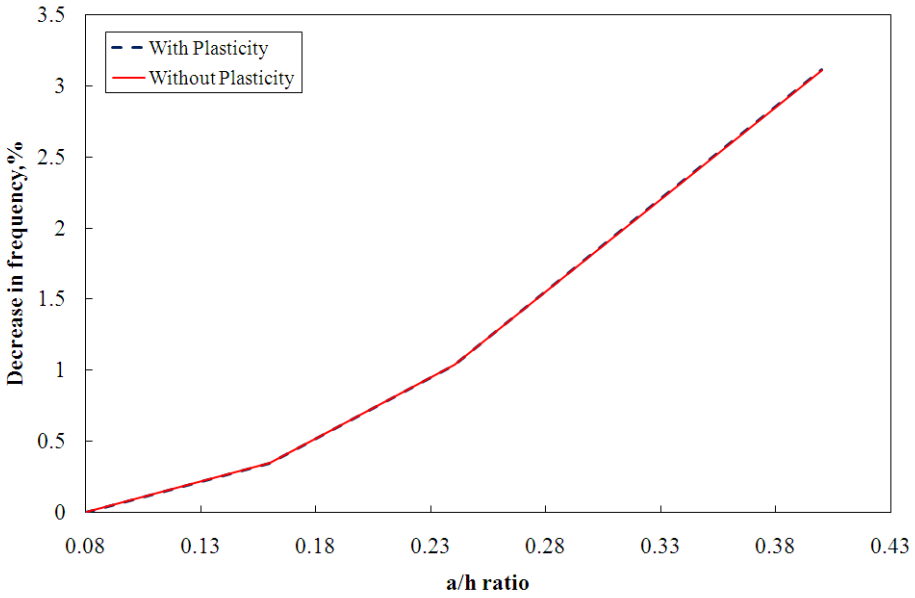

Figure.4.10 Effect of a/h ratio on first natural frequency for d/L =0.33

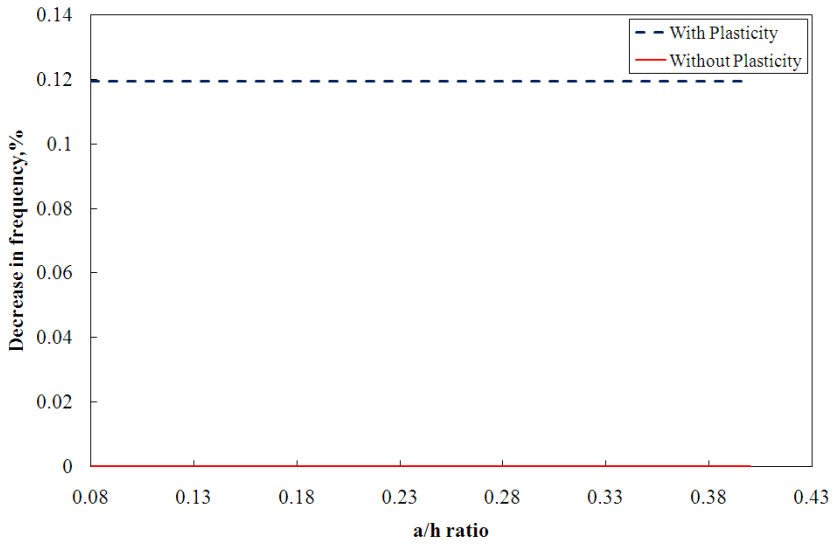

Figure.4.11 Effect of a/h ratio on second natural frequency for d/L =0.33

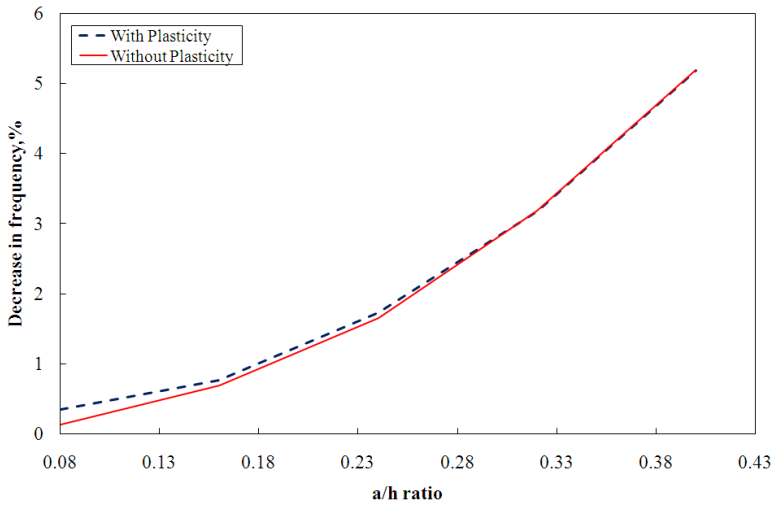

Figure.4.12 Effect of a/h ratio on third natural frequency for d/L =0.33

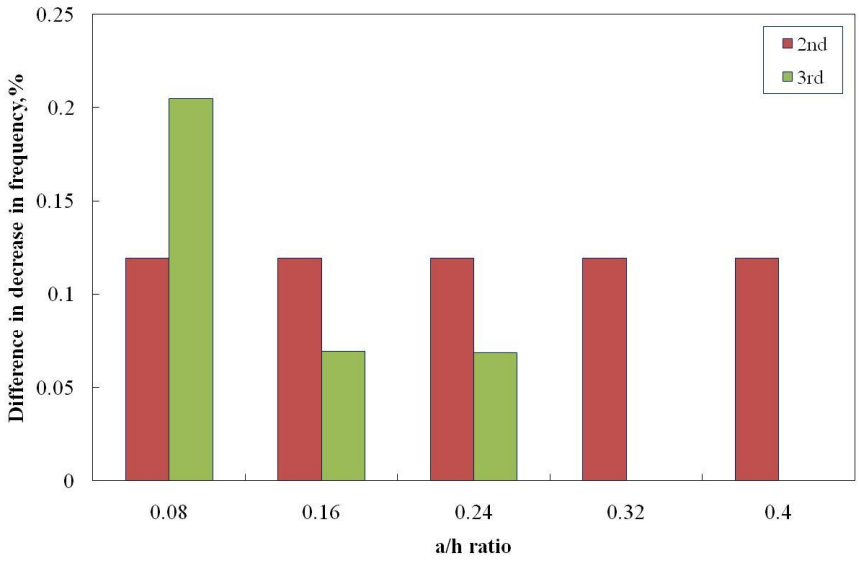

Figure.4.13 Effect of a/h ratio on natural frequencies d/L=0.33

4.10.2 Case (B) Crack at the Centre of Bar

It was found that in Case (B) there was no change in the first natural frequency (Fig 4.14) and there was a small change in the second and third natural frequencies initially due to the effect of plasticity that for all a/h ratios remains the same (Fig. 4.15 and Fig. 4.16). The first natural frequency shows no effect due to crack tip plasticity, where as the second and third natural frequencies change with it as presented in Fig. 4.17. This change in frequencies was due to the crack-induced plasticity which affected the overall stiffness of the cracked cantilever bar.

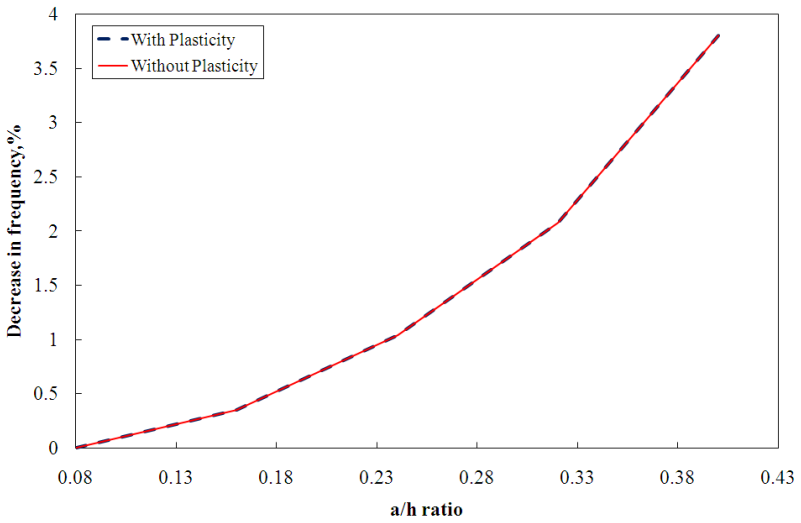

Figure.4.14 Effect of a/h ratio on first natural frequency for d/L =0.5

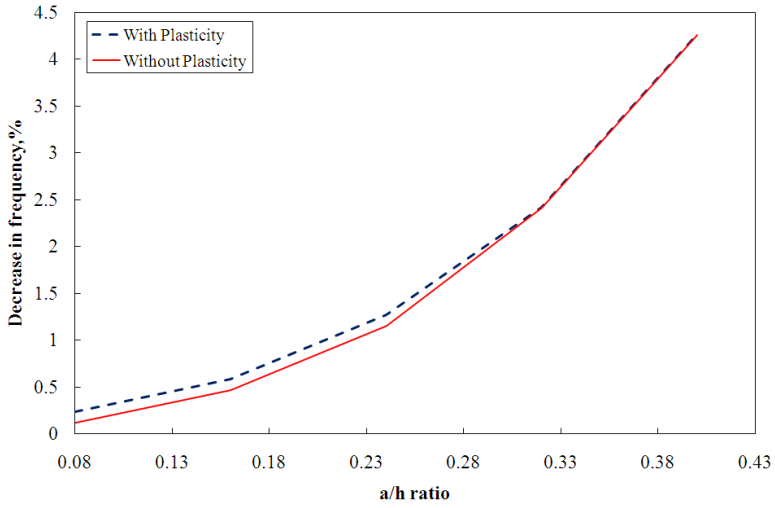

Figure.4.15 Effect of a/h ratio on second natural frequency for d/L =0.5

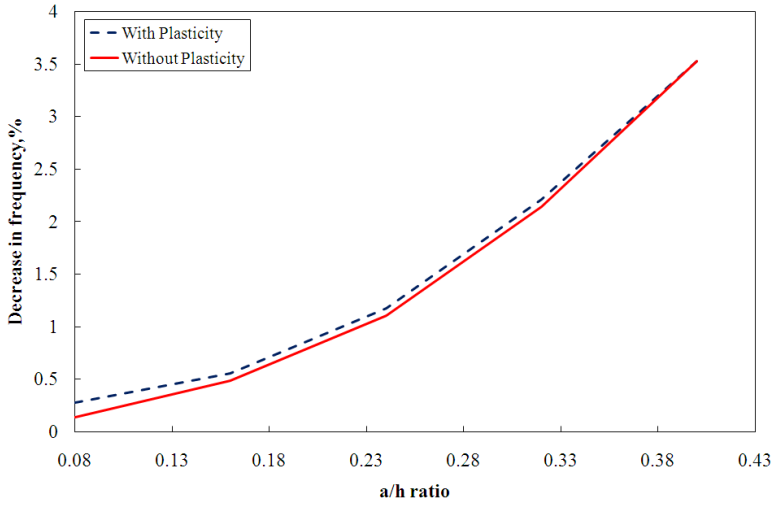

Figure 4.16 Effect of a/h ratio on third natural frequency for d/L =0.5

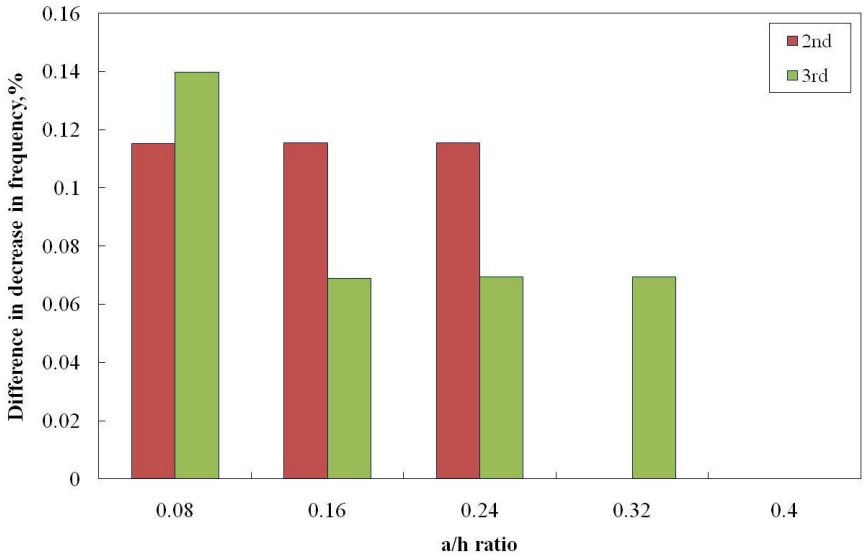

Figure.4.17 Effect of a/h ratio on natural frequencies d/L=0.5

4.10.3 Case (C) Crack near the Free End of the Bar

It was found that in this case the crack near the free end of the bar caused no change in the level of the first natural frequency (Fig 4.18) and there was a marginal change in the second natural frequency (Fig.4.19) whereas third natural frequency showed significant change (Fig. 4.20). This change in third natural frequency was due to the crack-induced plasticity near the crack tip which overall affected the stiffness of the cracked cantilever bar.

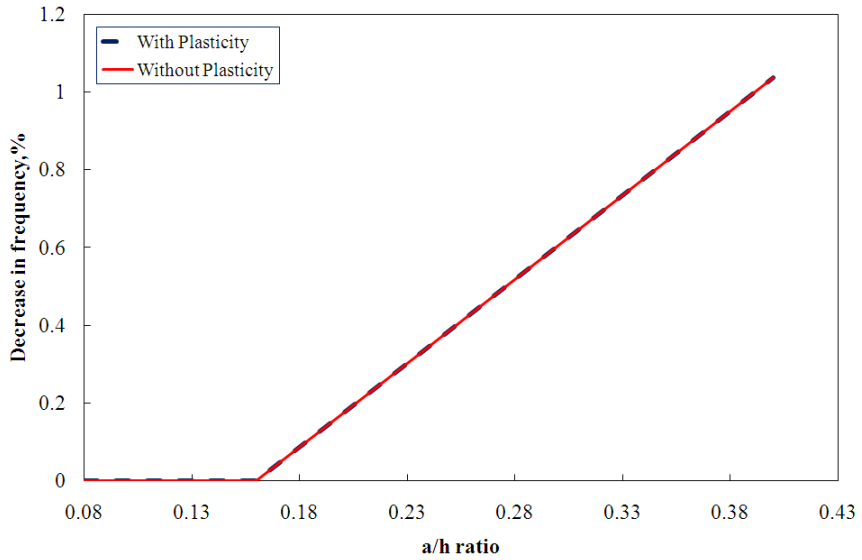

Figure 4.18 Effect of a/h ratio on first natural frequency for d/L =0.66

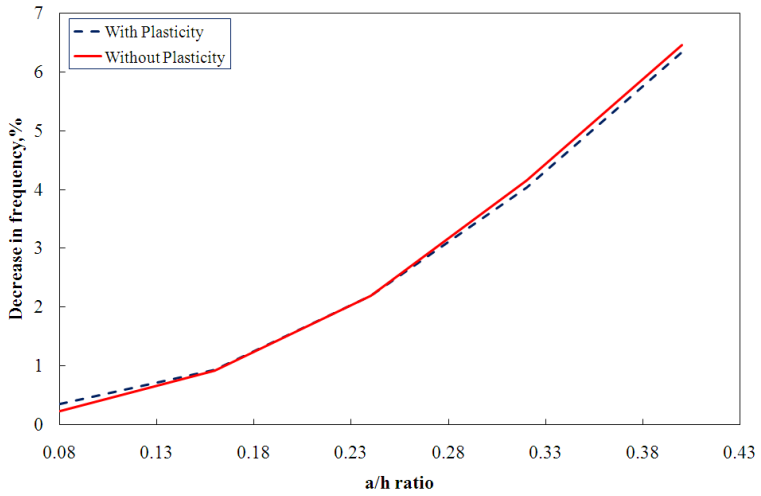

Figure 4.19 Effect of a/h ratio on second natural frequency for d/L =0.66

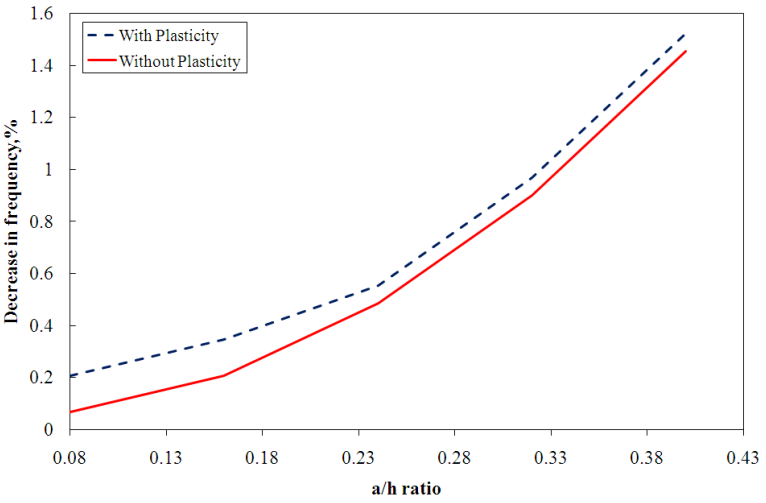

Figure.4.20 Effect of a/h ratio on third natural frequency for d/L =0.66

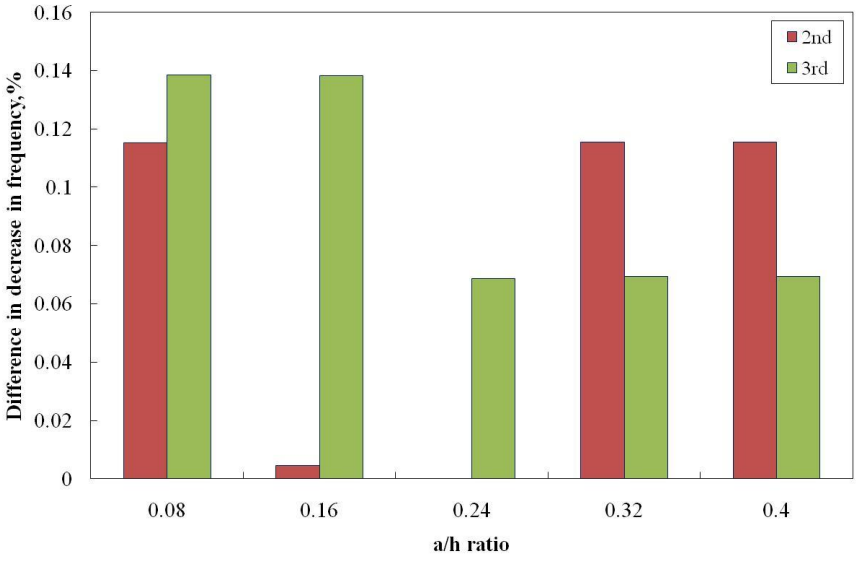

Figure.4.21 Effect of a/h ratio on natural frequencies d/L=0.66

4.10.4 Effect of Crack Location on the Natural Frequency

Figures 4.22, 4.23 and 4.24 shows a comparison between the cases with (dashed line) and without (solid line) plasticity at the crack tip for the first, second and third natural frequency for different d/L ratio at the given crack depth (2mm, 4mm, 6mm, 8mm and 10mm). It was observed that there was no change in first natural frequency (Fig. 4.22) where as there was small change in the second and third natural frequencies as the d/L ratio increased (Fig. 4.23 and Fig. 4.24). This was due to the crack-induced plasticity near the crack tip.

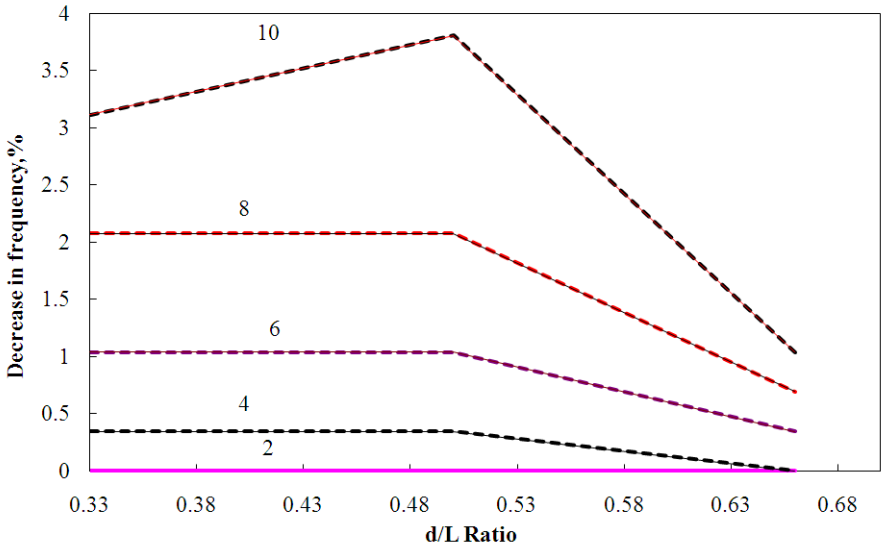

Figure.4.22 First natural frequency

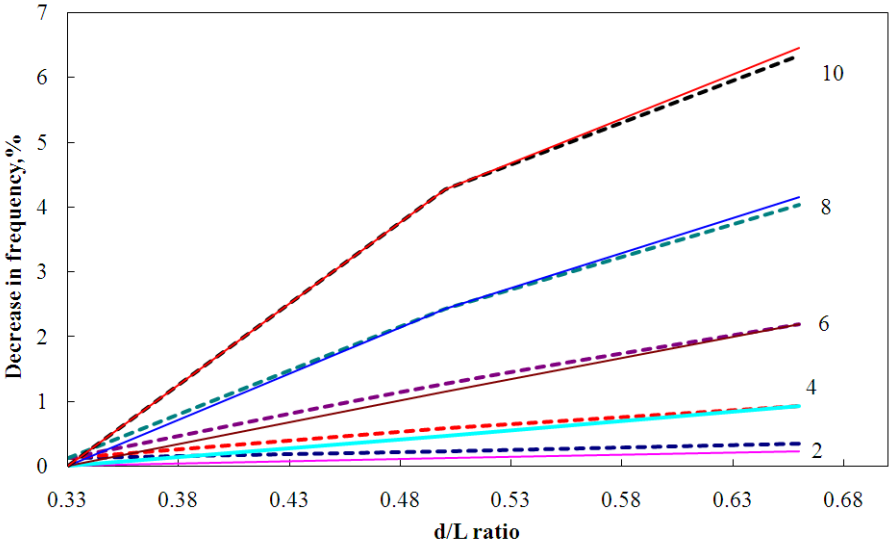

Figure.4.23 Second natural frequency

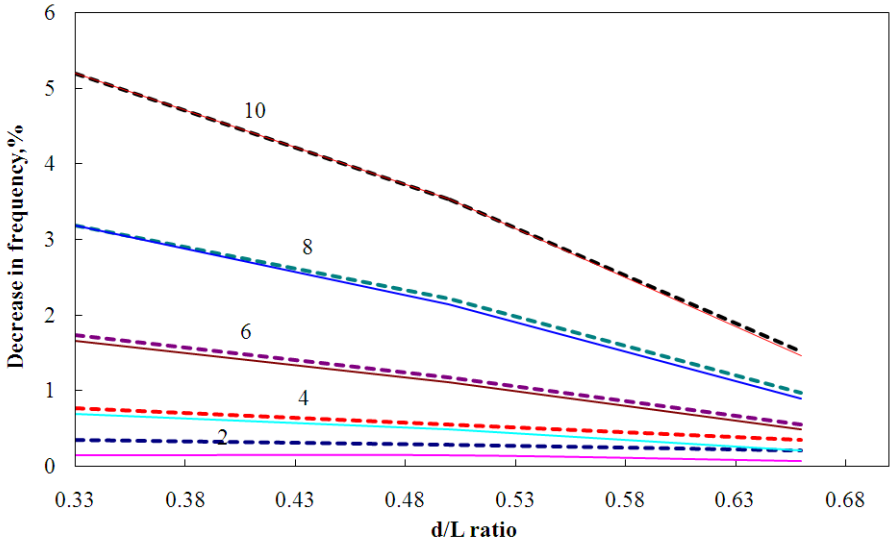

Figure.4.24 Third natural frequency

4.11 Summary

This chapter was devoted to the characterization of the effect of material nonlinearity on the natural frequencies. The 2D finite element model of the cracked cantilever bar was modelled with the commercial software MSC.Marc to study the effect of crack-tip plasticity on the first three natural frequencies. It was found that the presence of plasticity at the crack tip has no effect on the first natural frequency whereas there was a low-level influence on the second and third natural frequencies as the a/h ratio increased. In addition to that there was no effect on the first natural frequency as the d/L ratio increased for different crack depths. On the contrary, as the d/L ratio increased the second and third natural frequencies were affected for different crack depth. This effect of change in the second and third natural frequency for different a/h and d/L ratios was attributed to the change in stiffness due to the crack-tip plasticity. Hence, it can be concluded that crack-induced plasticity can affect the natural frequency. This change depends on the mode shape, a/h ratio and d/L ratio.

Chapter 5 Experiments

5.1 Introduction

The experiments are performed to compare the theoretical and simulation results. Experiments are planned in three stages. In the first stage material is selected after careful consideration of its properties and availability. In the second stage, the fatigue crack is generated in the specimens of Aluminium and PMMA. In the third stage of the experiment ,the specimen with fatigue crack is used for studying the dynamics of the cracked bar having a boundary condition fixed at one end and forced longitudinal harmonic excitation at the other end. Fig.5.1 shows the experimental plan.

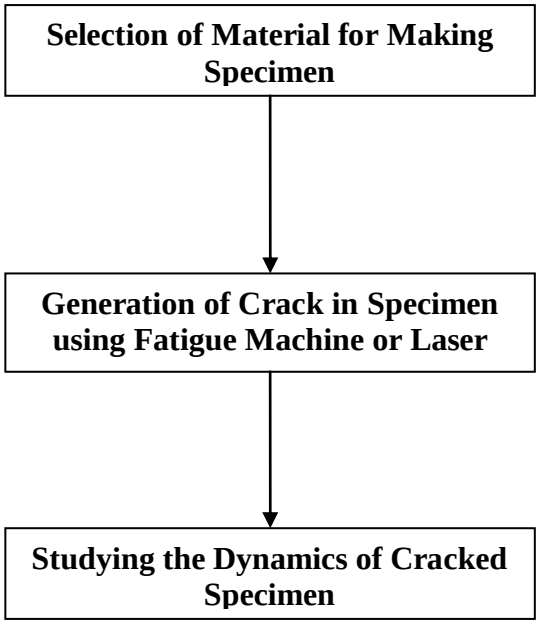

Figure 5.1. Experimental Plan

5.2 Selection of Specimen

The selection of the specimen is based on the availability of the material in the workshop and depending upon the mechanical properties of the materials. The material selected for making the specimen are Aluminium and PMMA. The dimension of the specimen is 420mm x 25mm x 10mm each. The mechanical properties of the materials are given in Table 5.1.

Material	Modulus of Elasticity (N/mm^2)	Density (Kg/mm^3)	Ultimate Tensile Strength (σ_{ut}) (N/mm^2)	Poisson's Ratio
Aluminium	70×10^3	2.70×10^{-6}	340	0.33
PMMA	3000	1.18×10^{-6}	60	0.35-0.4

Table 5.1 Mechanical properties of material

5.3 Fatigue

A periodic stress oscillating between maximum stress (σ_{max}) and minimum stress σ_{min} levels applied to a machine member is called repeated, alternating or fluctuating. The machine members failing under the action of these stresses is called fatigue failure. Generally a small crack is enough to initiate fatigue failure since the stress concentration effect becomes greater around it and the crack progresses rapidly. The components of stresses are depicted in Fig. 5.2 where σ_{min} is minimum stress, σ_{max} is maximum stress, σ_a the stress amplitude or the alternating stress, σ_m the mid range or mean stress ,σ_r the stress range and σ_s the steady or static stress. The steady stress can have any value between σ_{min} and σ_{max} and exists for a fixed load. It is usually independent of the varying portion of the load. The relation between the stress components are as follows.

$$\sigma_m = \frac{\sigma_{max} + \sigma_{min}}{2}$$

$$\sigma_a = \frac{\sigma_{max} - \sigma_{min}}{2}$$

The stress ratios

$$R = \frac{\sigma_{min}}{\sigma_{max}}$$

are used to describe the fluctuating stresses. Table 5.2 shows the calculation of fatigue load.

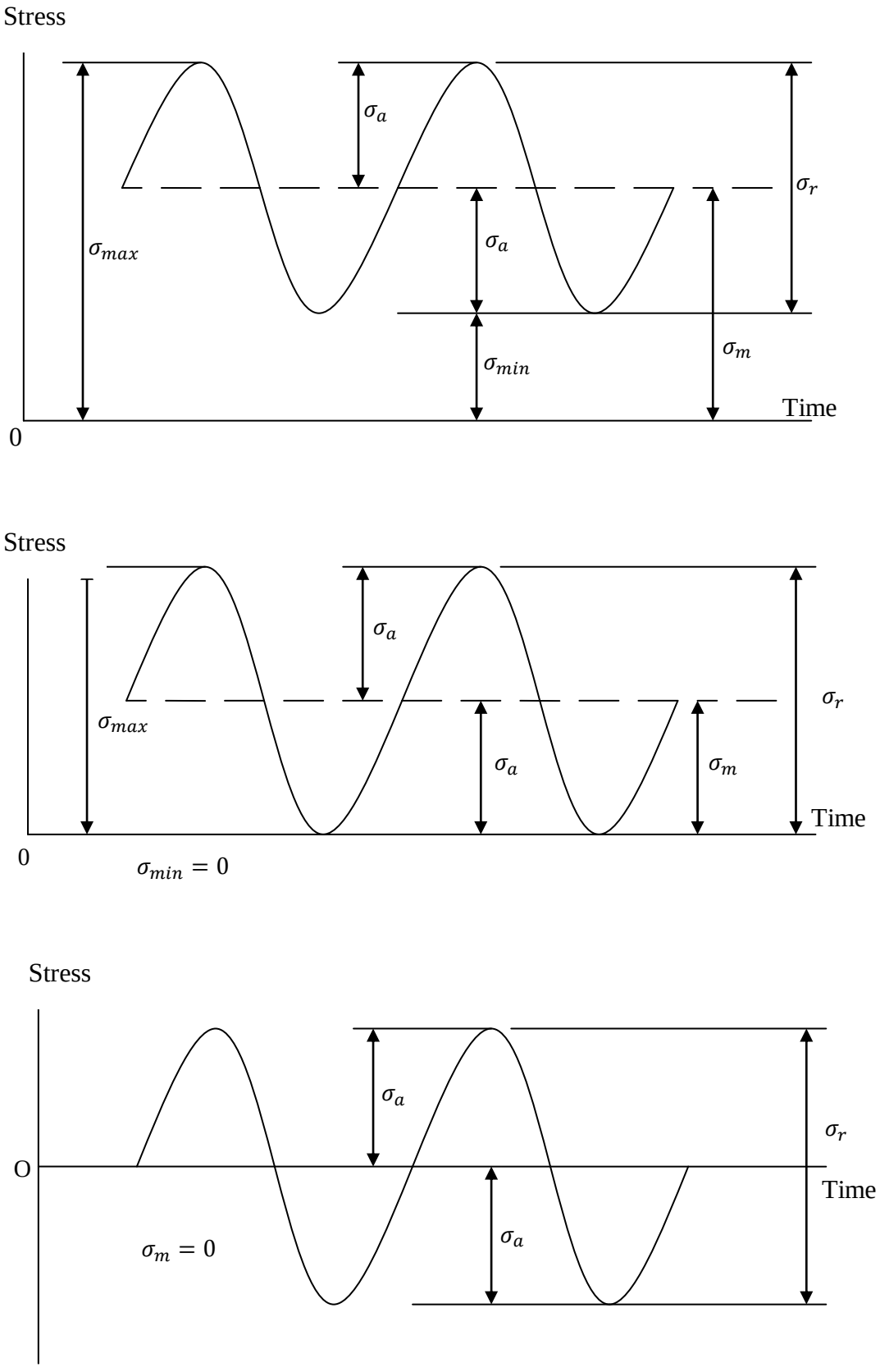

Figure 5.2 Sinusoidal fluctuating stresses

	Aluminium	**PMMA**
Ultimate Tensile Strength (σ_{ut})	340 N/mm^2	60 N/mm^2
Modulus of Elasticity (E)	70 x 10^3 N/mm^2	3000 N/mm^2
Stress ratio (R)	0.1	0.1
Area	250 mm^2	250 mm^2
Force=σ_{ut} x Area	85KN	15K N
Fmax= 0.7x Force	52.5KN	10.5 KN
Fmin	5.525 KN	1.05 KN

Table 5.2 Calculation of fatigue load

5.4 Crack Generation using Fatigue Machine

The Fig. 5.3 shows the Instron hydraulic fatigue testing machine. The load cell capacity used in fatigue machine is 200 KN for quasi static load and 100KN for dynamic load. The hydraulic grips in the machine are used for firmly gripping material specimen so

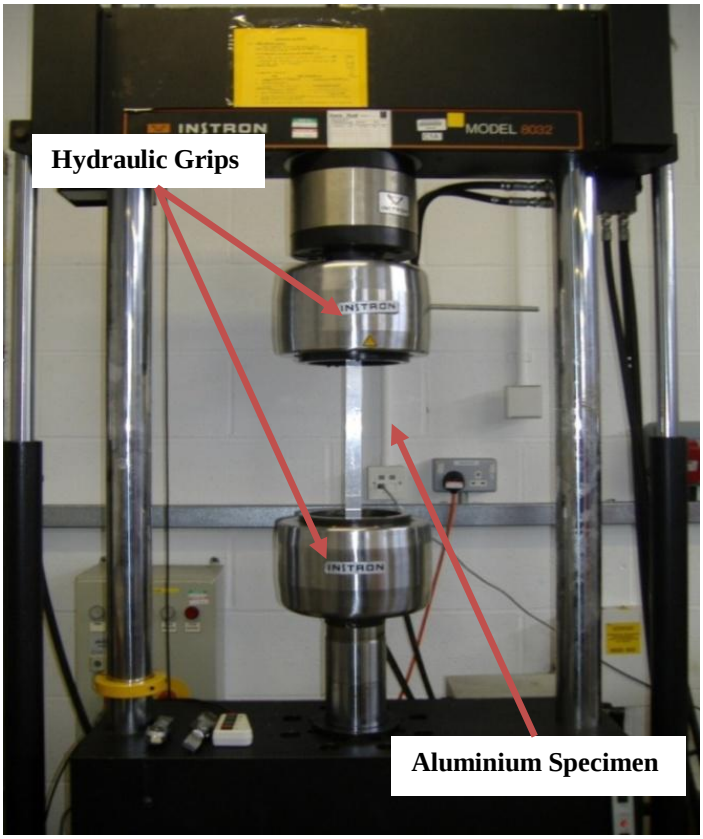

Figure 5.3 Instron testing machine

that while testing specimen slip does not occur. The fatigue machine is controlled by the 9600 controller box and multi-channel transducer box. The fatigue machine can be used for both constant fatigue loading and complex loading. The Fig. 5.3 shows that the aluminium specimen is fixed in the hydraulic grip and the dynamic loading is applied for generating the crack in specimen at the notch of the specimen. The cyclic load is applied having a stress ratio of R=0.1. It is applied for 1900 cycles and then the specimen is removed once the crack is seen on the surface. Fig. 5.4 shows the microscopic view of the crack generated in the aluminium specimen

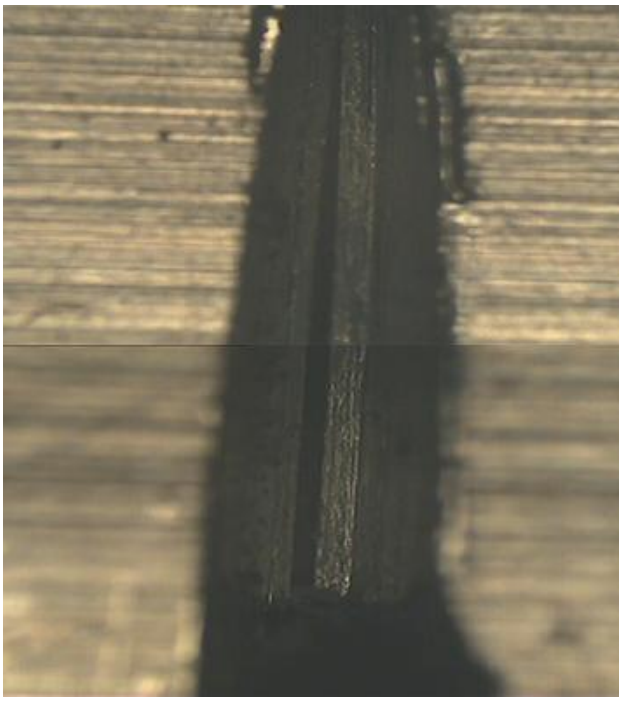

Figure 5.4 Microscopic view of the crack generated in the aluminium specimen

Similarly, when the cyclic load is applied for the PMMA specimen it breaks of all of a sudden without any sign of initial crack. Fig.5.5 shows the failure of the PMMA specimen under the fatigue loading. So it becomes very difficult to generate a crack in PMMA specimen using the fatigue machine. So the crack in the PMMA specimen is generated using the laser cutting which can generate a cut of 300 microns thickness. The Fig.5.6 shows the crack generated in the PMMA specimen using laser cutting. The crack generated using laser is just like an open notch. So it will always remain open while performing the experiment .As the experiment is supposed to study the effect of the vibro-impact response due to the breathing crack it is not feasible to perform the

experiment using PMMA so the experiments are performed only on the aluminium specimen.

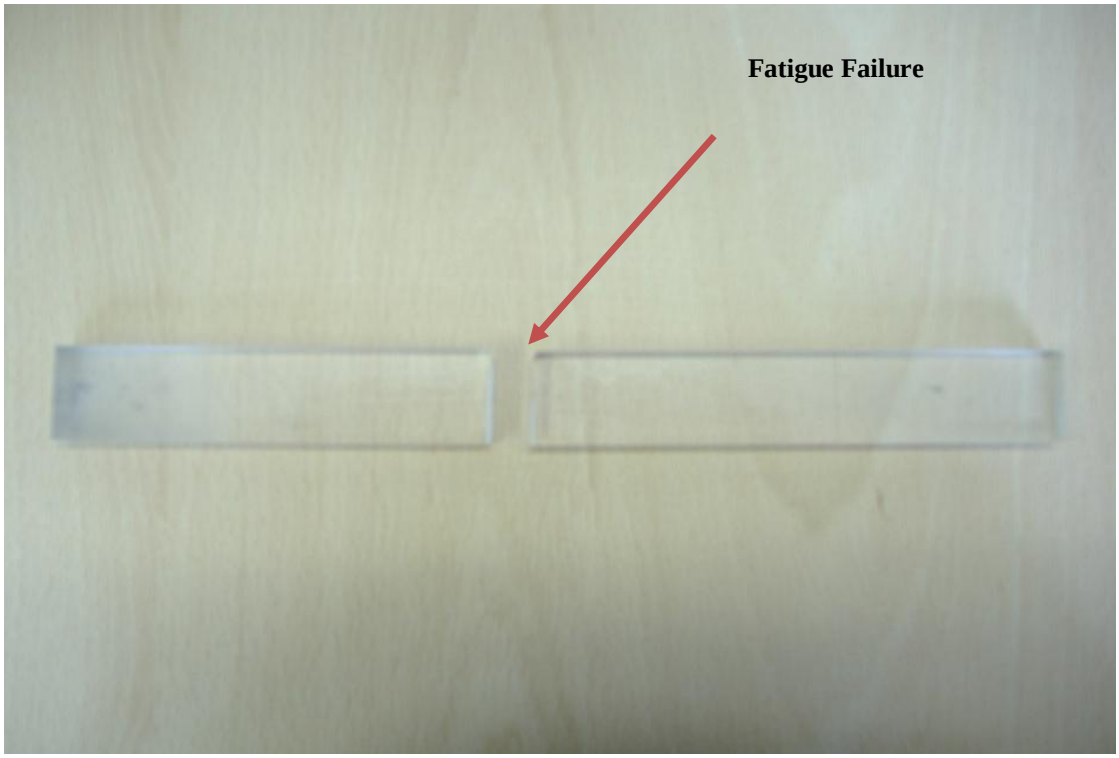

Figure 5.5 Failure of the PMMA specimen using fatigue machine

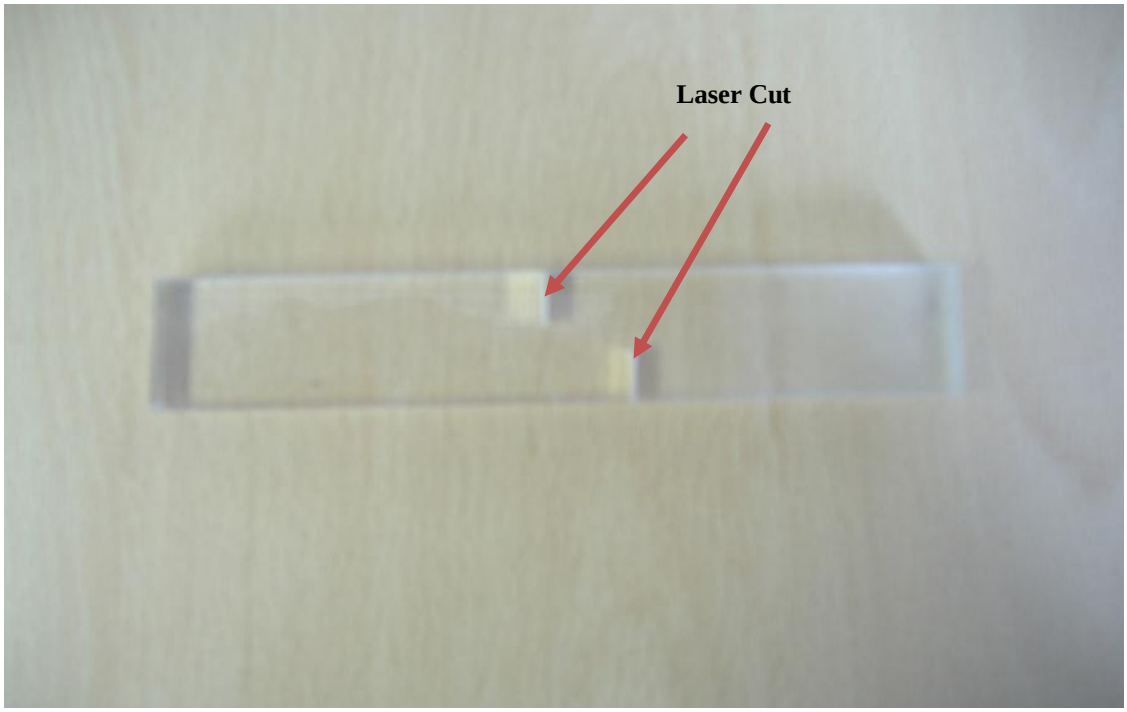

Figure 5.6 Laser cutting in the PMMA specimen of 300 microns

5.5 Experimental Setup

The experimental setup consists of the Shaker, Signal generator, Aluminium bar (cracked and uncracked specimen), Piezo-electric strain gauges and Picoscope. Each of the components used in the experimental set up is described below:

Shaker: Ling Dynamic Systems 200 series vibrators are miniature units for use in small scale vibration testing or as non-seismic pick-ups. The 200 series Vibrators can be driven by a TPO 20 oscillator of the Ling Dynamic Systems. A light weight armature construction, top and bottom laminated spiders, vibrator body and trunnion mounting where required, form the main parts of the Model 200 series vibrator. Being permanent magnet design the 200 series vibrators do not require a field power supply. Cooling is not required although the provision is made for the easy connection of a forced air supply (Fig. 5.7).

Figure 5.7 Shaker

Oscillator/Amplifier: The model TPO 20 power amplifier has been designed as a drive source for the Ling Dynamic Systems 100 and 200 series vibrators. The equipment is completely self contained and in addition to the built in oscillator, the unit has protection circuits to prevent damage to the equipment in the event of excessive output current. The TPO 20 is a quasi complementary class B amplifier. It uses an silicon transistor driver board which drives two NPN power output transistors connected in a half bridge configuration. The oscillator section is of the Wien-bridge type and module also incorporates a delay and interlock protection circuits (Fig. 5.8).

Figure 5.8 Oscillator

Piezo Strain Gauges: The piezo-electric strain gauge (Fig.5.9) consists of a strip of piezoelectric ceramic , silvered and polarized across the thickness dimension, with the lower silvering carried round to the top to facilitate electrical connection. These strain gauges have extremely high sensitivities of the order of several hundred times that obtainable with wire strain gauges. Output for an expansion of 10^{-6} cm is in the order of 200 mV for 0.5 mm thick. Approximate capacity is 1000pF having low frequency limit 150 c/s. The dimension of this strain gauge is 20mm x 3 mm x 0.5 mm. For the lower

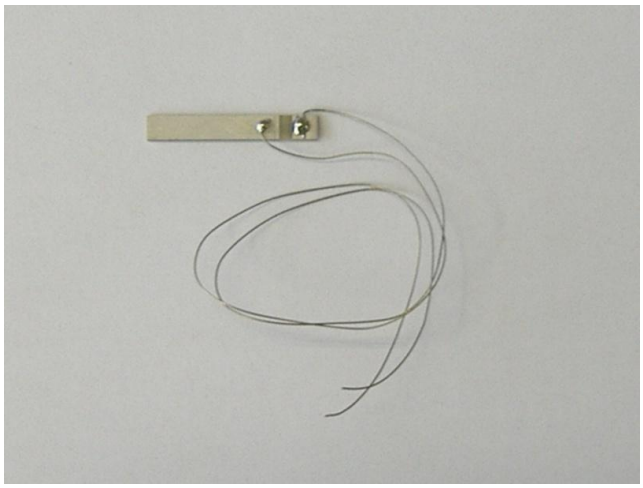

Figure 5.9 Piezo-strain gauges

frequencies a voltage follower or charge amplifier unit may be used. At resonance a considerable displacement of the structures is obtained with a very low power input to

the element The transducers are so small that they do not materially affect the vibrational characteristics of the structure.

Picoscope: Picoscope 2202 (Figure 5.10) is a dual channel USB oscilloscope. It is suitable for use on any laptop or desktop PC, with a USB port, running Microsoft Windows XP or Vista. PicoScope oscilloscopes works with PicoScope software that provides oscilloscope, spectrum analyzer and multimeter functions. It also has the capabilities to view real-time signals, zoom in on your signal, and save and print captured waveforms. It also has a Picolog data acquisition software that transforms PC into a high-speed data logger.

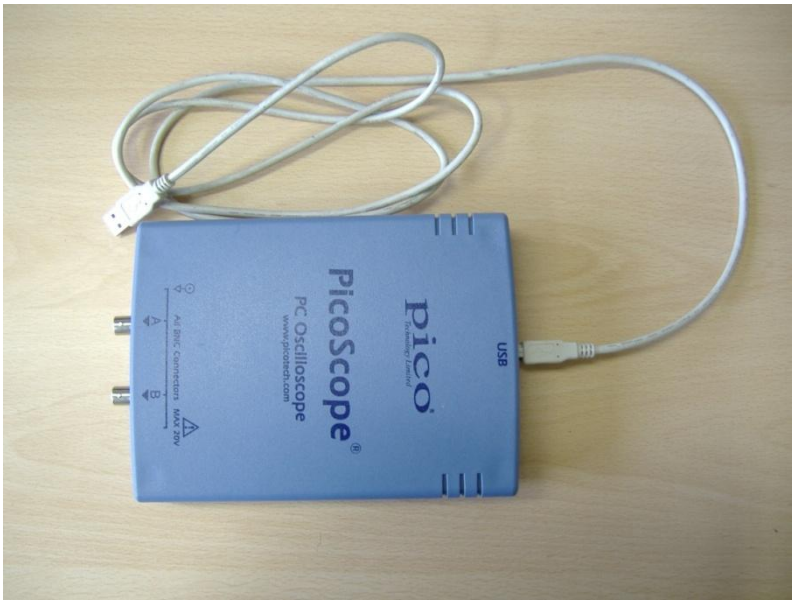

Figure 5.10 Picoscope

5.6 Experimental Procedure

Before performing the experiment all the components of the setup were assembled as shown in Fig. 5.11 and Fig. 5.12 for the uncracked bar and the cracked bar. The piezo strain gauges (sensors) for the cracked bar were fixed at the four different locations. One strain gauge was fixed near the fixed end of the bar and one strain gauge was fixed near the free end. Other two strain gauges were fixed near the crack. The frequency sweep was performed on the cracked bar to find the resonances. After the resonant frequency was obtained, the cracked bar was excited at each of these resonant frequencies and the response was obtained at each of the strain gauge fixed on the

cracked bar. The signal from each of the piezo-strain gauge was acquired using the Picoscope and it was processed in the picoscope software. The proper sampling rate for signal was maintained taking in to consideration of Nyquist criteria throughout the experiments to avoid aliasing error. Hanning window was used; while processing the signal so that leakage error is minimized.

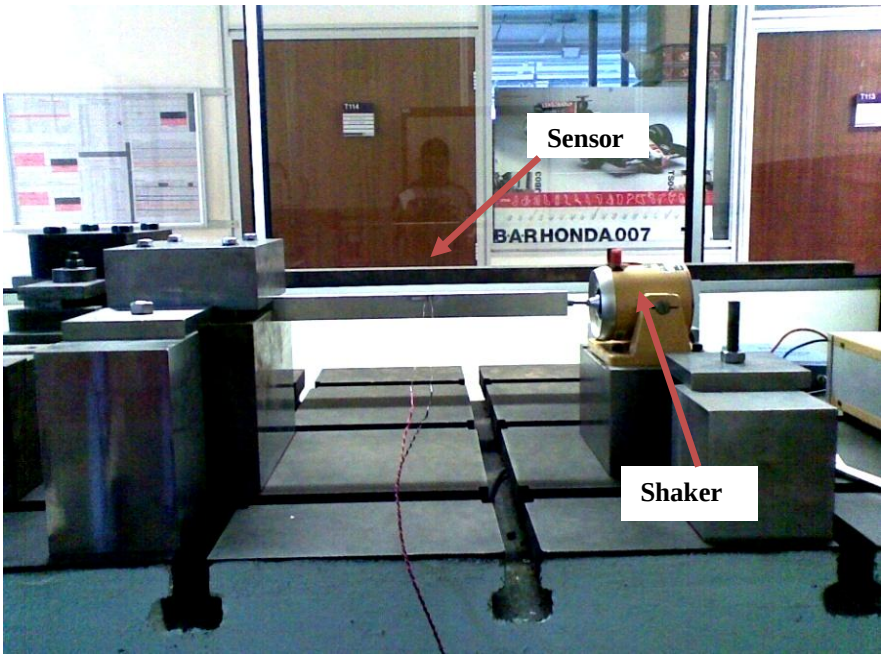

Figure 5.11 Experimental setup for uncracked bar

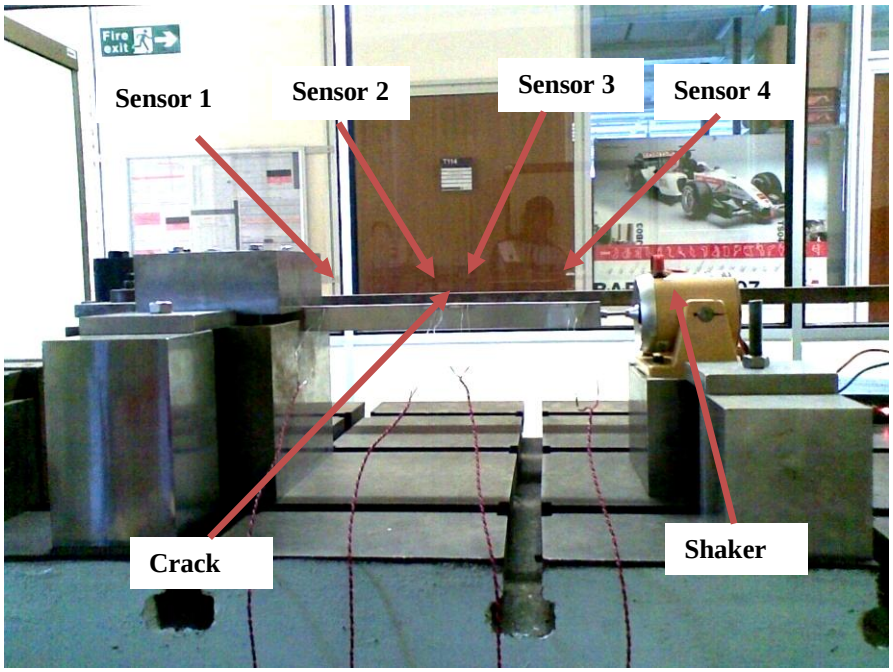

Figure 5.12 Experimental setup for cracked bar

5.7 Experimental Results

5.7.1 Uncracked Bar

The frequency sweep was performed on the uncracked aluminum bar. The signal was acquired at the centre of the bar in the form of time and frequency response. During frequency sweep, it was found that the resonances occurred at the frequencies of 2844 Hz, 3650 Hz, 4504 Hz, 5996 Hz and 6445 Hz. The frequency responses were obtained at each of these frequencies for lower and higher excitation amplitude. The magnitude of lower and higher vibration amplitude was approximately 2.8 N and 16 N respectively.

5.7.1.1 Excitation at frequency of 2844 Hz

The uncracked bar was excited at the lower and the higher vibration amplitude at resonant frequency of 2844 Hz. For lower vibration amplitude, resonant frequency was observed in frequency response (Fig.5.13). For higher vibration amplitude, along with the resonant frequency one can observe the harmonics of resonant frequency at 5689 Hz and 8513 Hz (Fig.5.14).

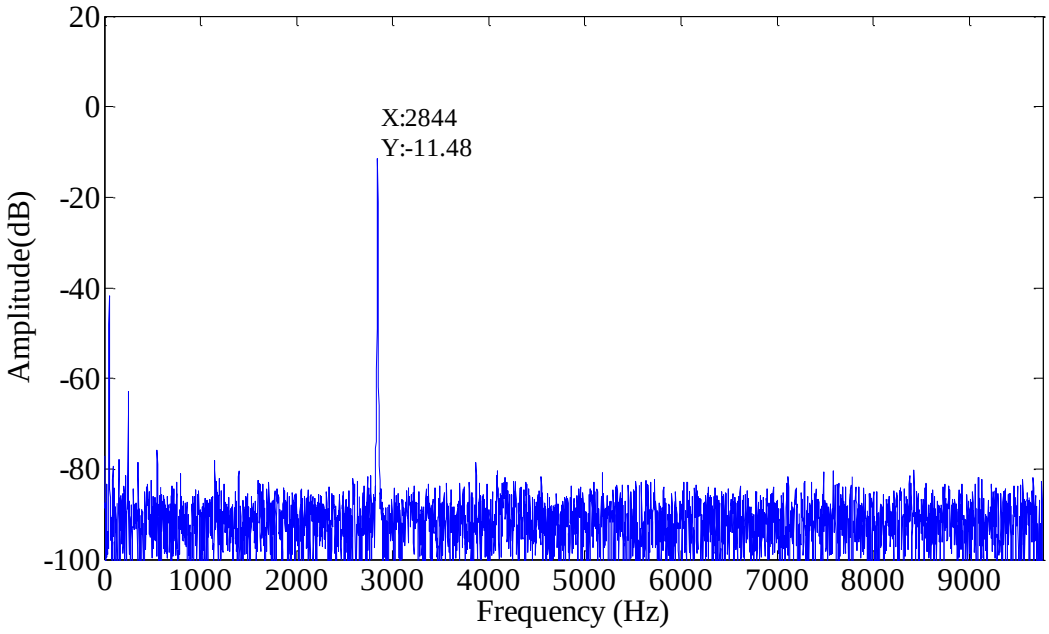

Figure 5.13 Measurement of response at the centre of bar

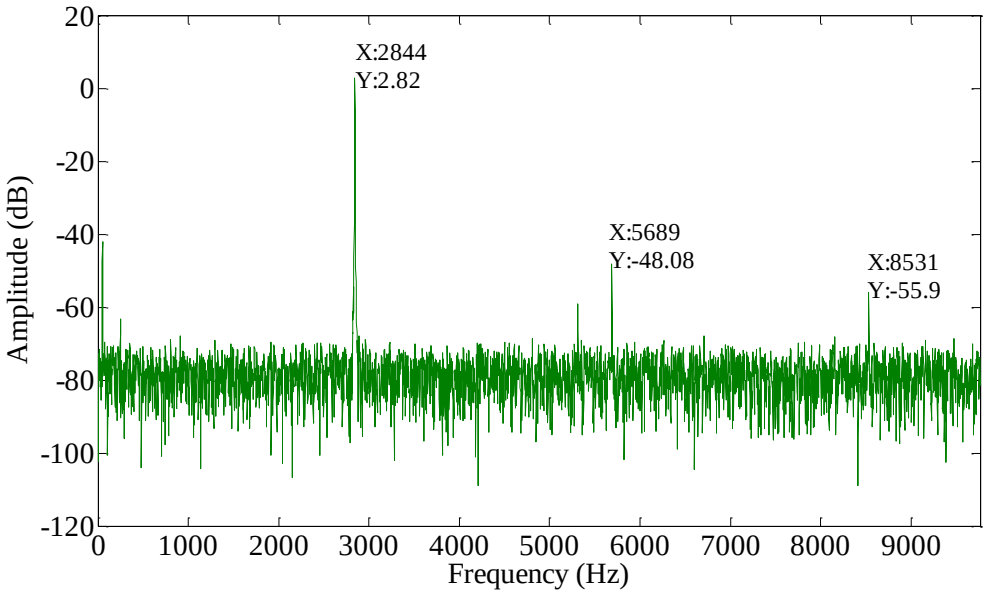

Figure 5.14 Measurement of response at the centre of bar

5.7.1.2 Excitation at frequency of 3650 Hz

The uncracked bar was excited at the lower and the higher vibration amplitude at resonant frequency of 3650 Hz. For lower vibration amplitude, resonant frequency was observed in frequency response (Fig.5.15). For higher vibration amplitude, along with the resonant frequency one can observe the harmonic of resonant frequency at 7303 Hz and lower frequency component at 1273 (Fig.5.16). This lower frequency caused

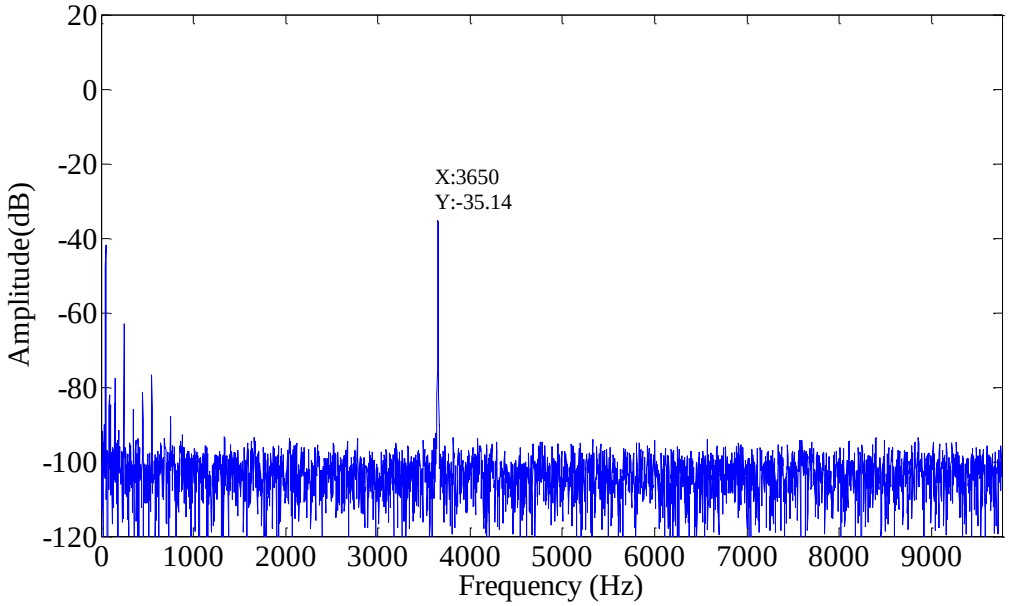

Figure 5.15 Measurement of response at the centre of bar

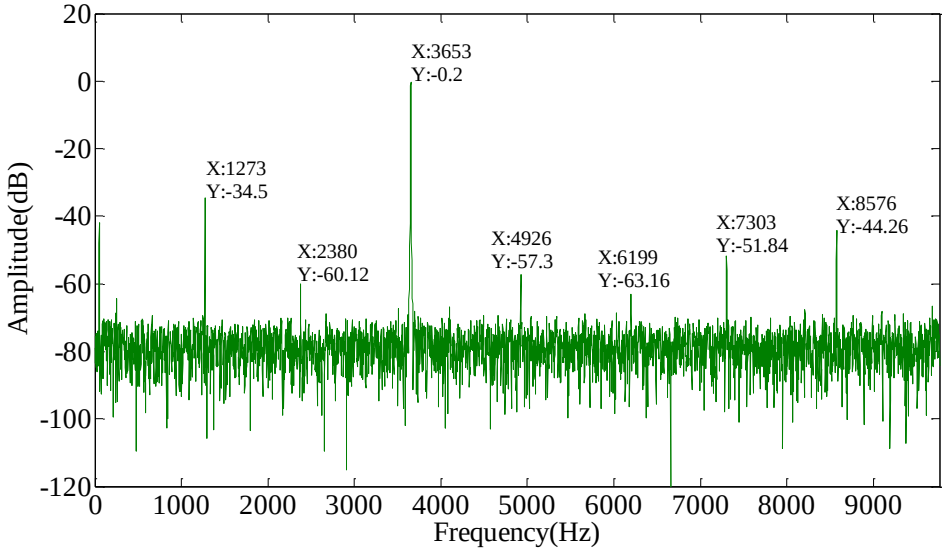

Figure 5.16 Measurement of response at the centre of bar

modulation of signal which led to the generation of side band frequencies near the resonant frequency at 2380 Hz, 4926 Hz, 6199 Hz and 8576 Hz. This might be due to the coupling of modes of vibration.

5.7.1.3 Excitation at frequency of 4504 Hz

The uncracked bar was excited at the lower and the higher vibration amplitude at resonant frequency of 4504 Hz. For lower vibration amplitude, resonant frequency was observed in the frequency response (Fig.5.17). For higher vibration amplitude, along

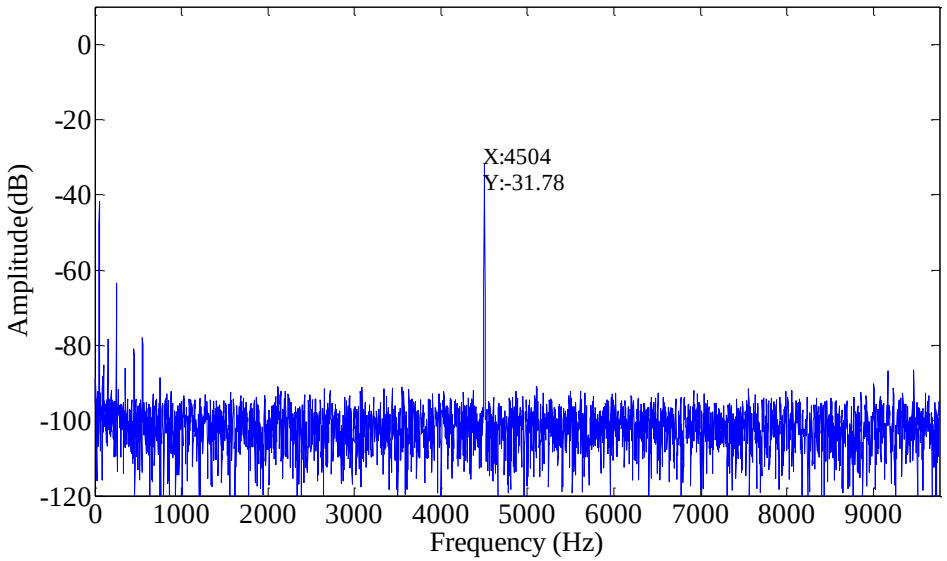

Figure 5.17 Measurement of response at the centre of bar

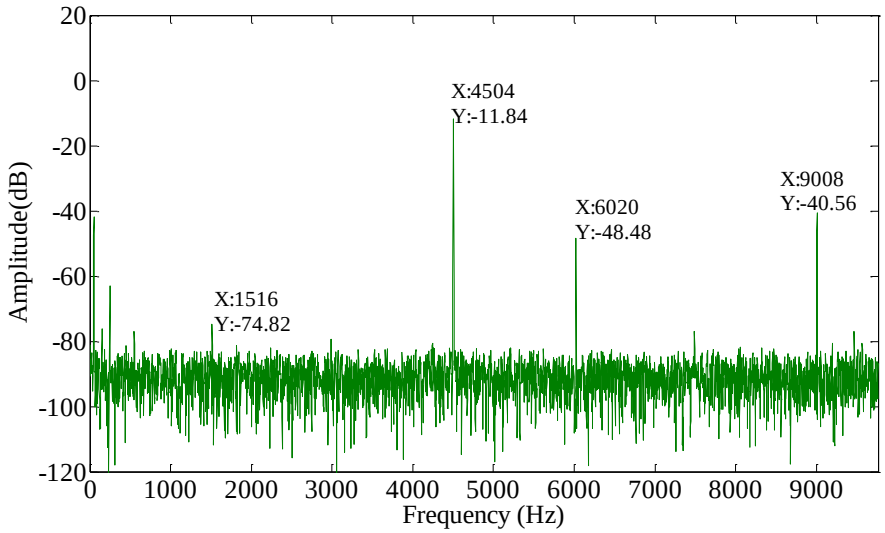

Figure 5.18 Measurement of response at the centre of bar

with the resonant frequency one can observe the harmonic of resonant frequency at 9008 Hz and lower frequency component at 1516 Hz (Fig.5.18). This lower frequency caused modulation of the signal which led to the generation of side band frequency near the resonant frequency at 6020 Hz. This might be due to the coupling of modes of vibration.

5.7.1.4 Excitation at frequency of 5996 Hz

The uncracked bar was excited at the lower and the higher vibration amplitude at resonant frequency of 5996 Hz. For lower vibration amplitude, resonant frequency was observed in the frequency response (Fig.5.19). For higher vibration amplitude, along

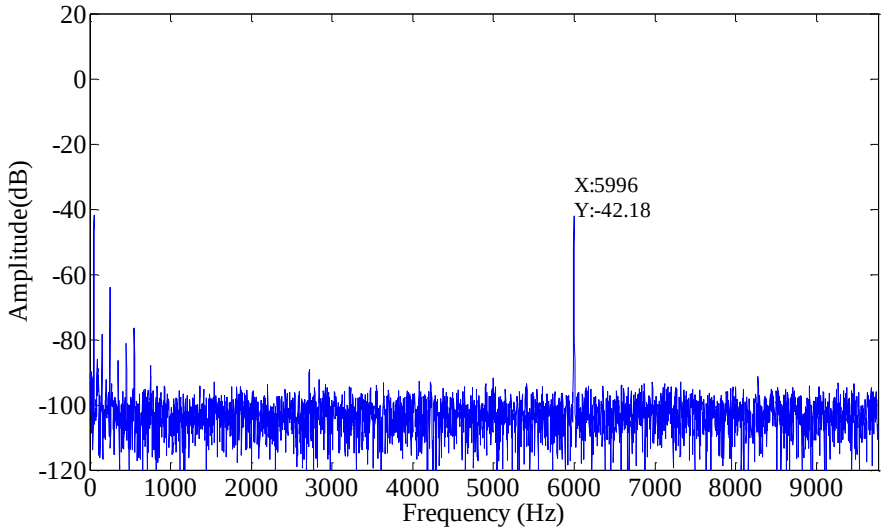

Figure 5.19 Measurement of response at the centre of bar

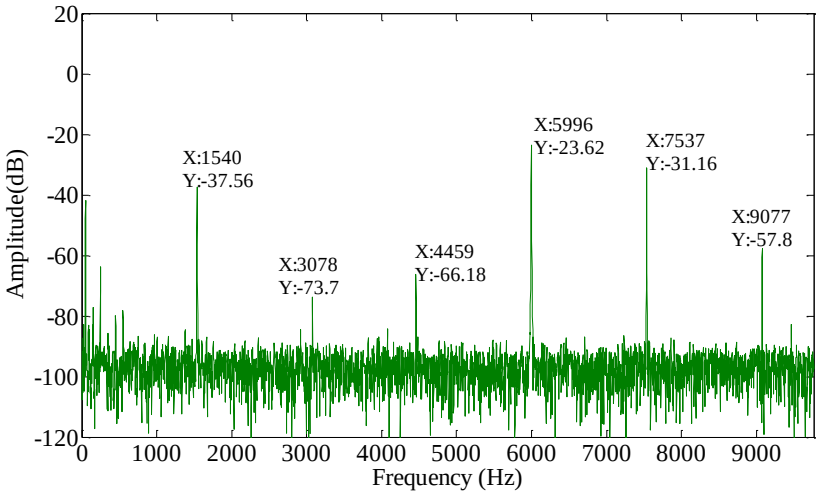

Figure 5.20 Measurement of response at the centre of bar

with the resonant frequency one can observe lower frequency component at 1540 Hz (Fig.5.20). This lower frequency caused modulation of the signal which led to the generation of side band frequencies near the resonant frequency at 3078 Hz, 4459 Hz, 7537 Hz and 9077 Hz. This might be due to the coupling of modes of vibration.

5.7.1.5 Excitation at frequency of 6454 Hz

The uncracked bar was excited at the lower and the higher vibration amplitude at resonant frequency of 6454 Hz. For lower vibration amplitude, resonant frequency was observed in the frequency response (Fig.5.21). For higher vibration amplitude, along

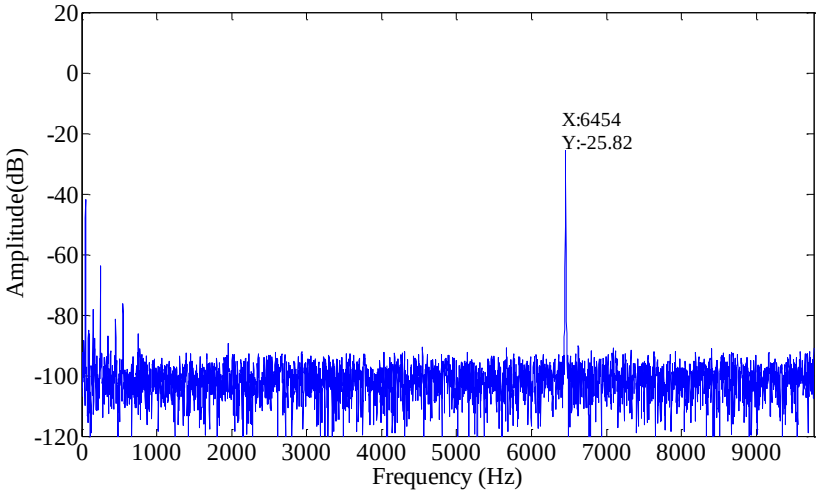

Figure 5.21 Measurement of response at the centre of bar

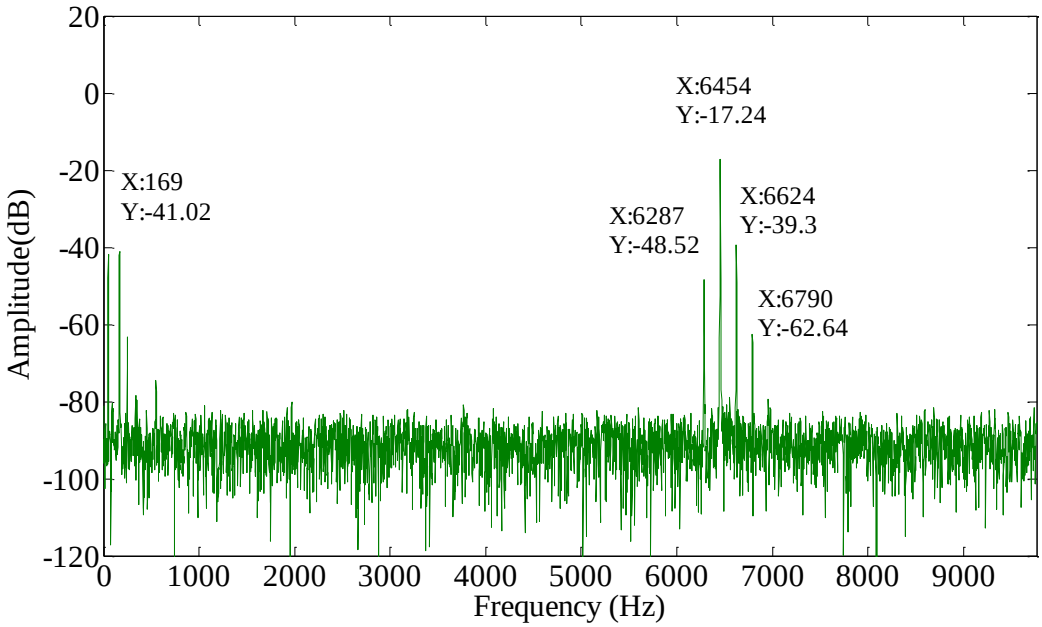

Figure 5.22 Measurement of response at the centre of bar

with the resonant frequency one can observe lower frequency component at 169 Hz (Fig.5.22). This lower frequency caused modulation of the signal which led to the generation of side band frequencies near the resonant frequency at 6287 Hz, 6624 Hz and 6790 Hz. This might be due to the coupling of modes of vibration.

5.7.2 Cracked Bar

The frequency sweep was performed on the cracked aluminium bar. During frequency sweep it was found that the resonances occurred at the frequencies of 2821 Hz, 3634 Hz, 4499 Hz 6008 Hz and 6445 Hz like the bar without crack with slight difference in resonant frequencies. At each of these resonant frequencies, frequency response was obtained for lower and higher vibration amplitude. The magnitude of lower and higher vibration amplitude was approximately 2.8 N and 16 N respectively. These frequency responses were acquired at the four different points on the cracked aluminium bar.

5.7.2.1 Case (A): Excitation at Frequency of 2821 Hz (Low Vibration Level)

The cracked bar was excited at lower vibration amplitude at resonant frequency of 2821 Hz. The response acquired at sensor 1 (Fig.5.23) and at sensor 4 (Fig.5.26) of the bar showed only resonant frequency. It was also found that response acquired near the crack from sensor 2 (Fig.5.24) and sensor 3 (Fig.5.25) showed the resonant frequency along

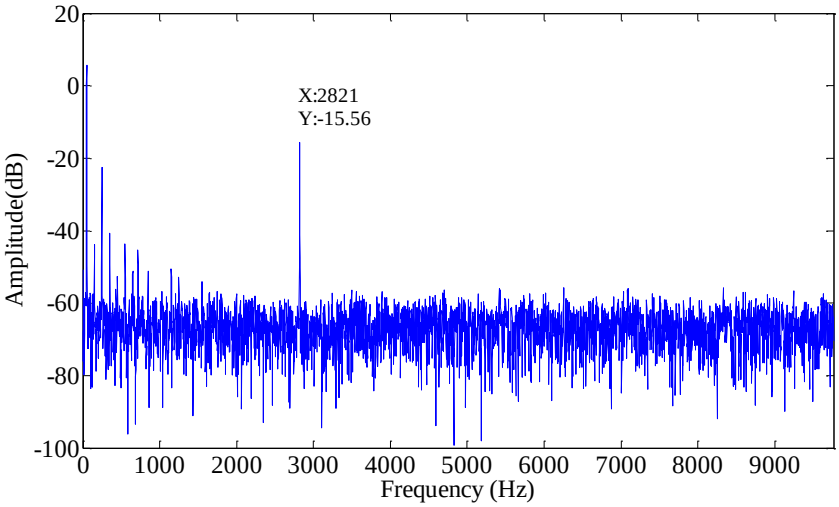

Figure 5.23 Measurement of frequency response at sensor 1

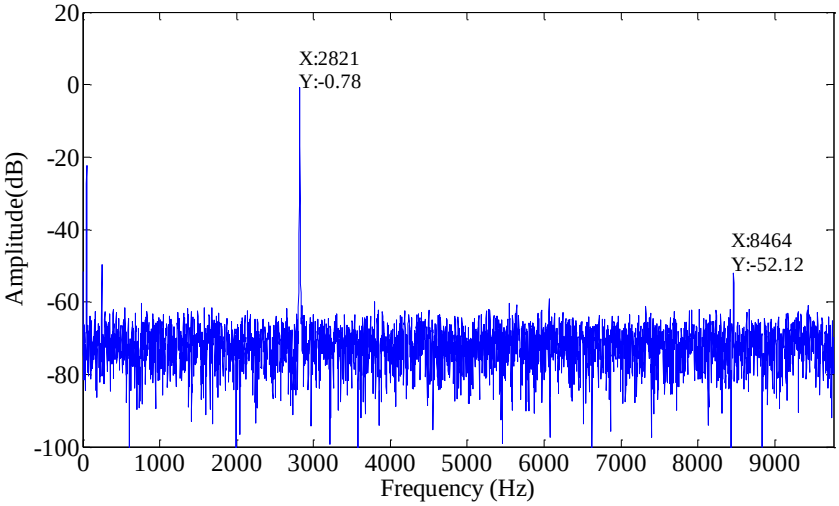

Figure 5.24 Measurement of frequency response at sensor 2

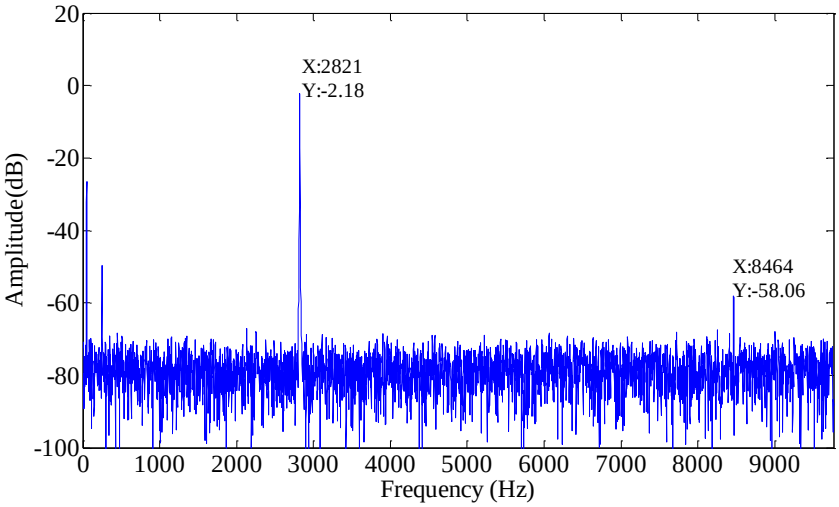

Figure 5.25 Measurement of frequency response at sensor 3

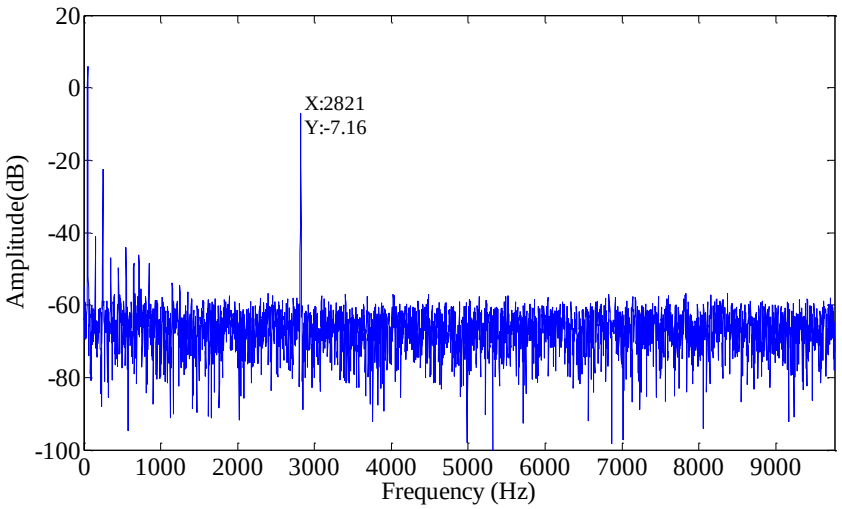

Figure 5.26 Measurement of frequency response at sensor 4

with the third harmonic of the resonant frequency. This third harmonic of the resonant frequency occurred due to the crack which induced additional perturbations in the cracked bar. When comparison was made between the frequency response (Fig. 5.13) of uncracked bar and frequency response (Fig. 5.24 and Fig 5.25) of cracked bar it was observed that presence of crack in a bar led to generation of higher harmonic.

5.7.2.2 Case (B): Excitation at Frequency of 2821 Hz (High Vibration Level)

The cracked bar was excited at the higher vibration amplitude at resonant frequency of 2821 Hz. The response acquired at sensor 1(Fig. 5.27) and sensor 4 (Fig. 5.30) indicated the presence of the low frequency component at 517 Hz which resulted in modulation showing the presence of side band frequencies near the resonant frequency. It also showed the second and third harmonics of resonant frequency at 5644 Hz and 8464 Hz respectively. Similarly, the response acquired at sensor 2 (Fig. 5.28(a)) indicated the presence of low frequency components at 219 Hz and 515 Hz (Fig.5.28 (b)) these low frequency components occurred due to the presence of crack in a bar which resulted in modulation showing the additional side band frequencies (2306 Hz and 3338 Hz) near the resonant frequency and along with the higher harmonics (5644 Hz and 8464 Hz) of resonant frequency. On similar grounds when the response was acquired at the sensor 3 (Fig. 5.29) it showed the presence of low frequency components at 222 Hz and 513 Hz which resulted in modulation showing the presence of additional side band frequencies (2308 Hz, 2601Hz, 3042 Hz and 3336 Hz) near the resonant frequency along with the higher harmonics (5644 Hz and 8464 Hz) of resonant frequency. When the comparison

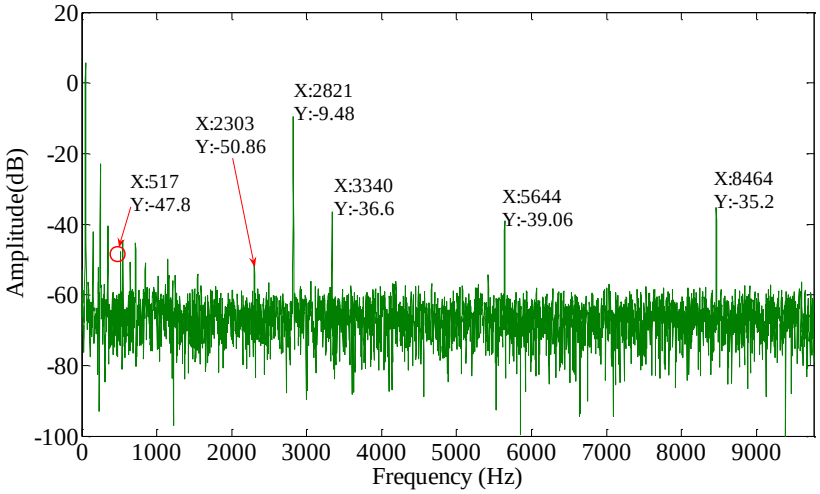

Figure 5.27 Measurement of frequency response at sensor 1

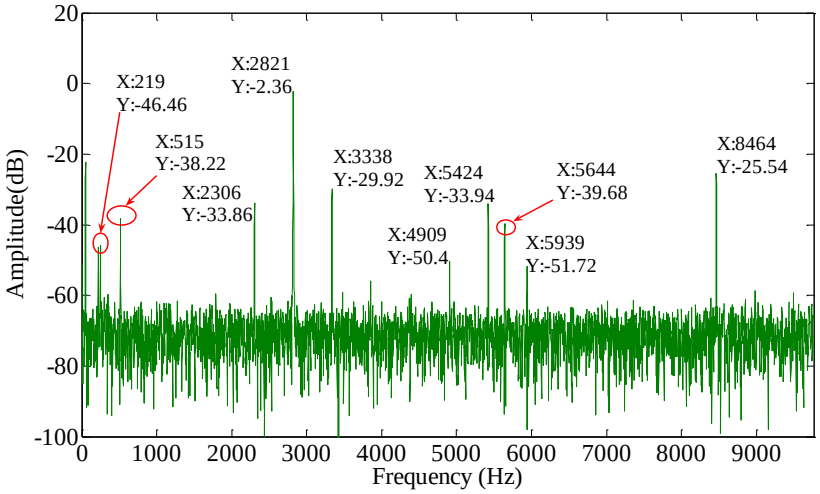

(a) Frequency Response

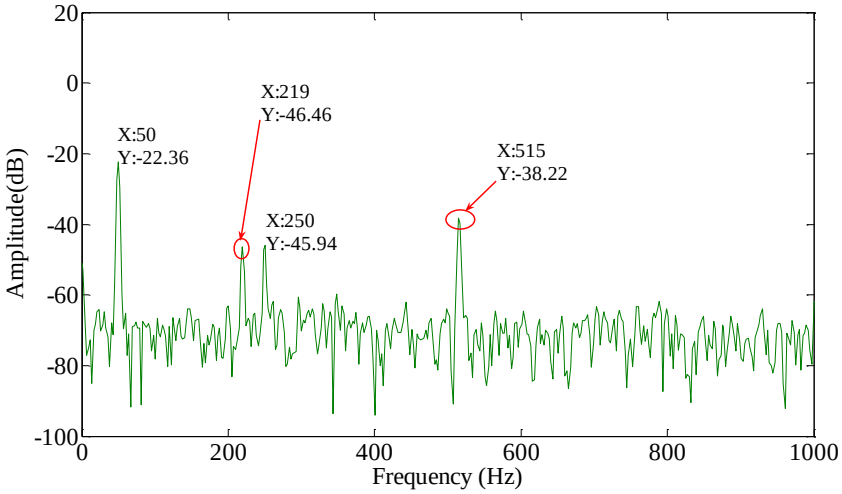

(b) Frequency Response (Zoomed1 to 1000 Hz)

Figure 5.28 Measurement of frequency response at Sensor 2

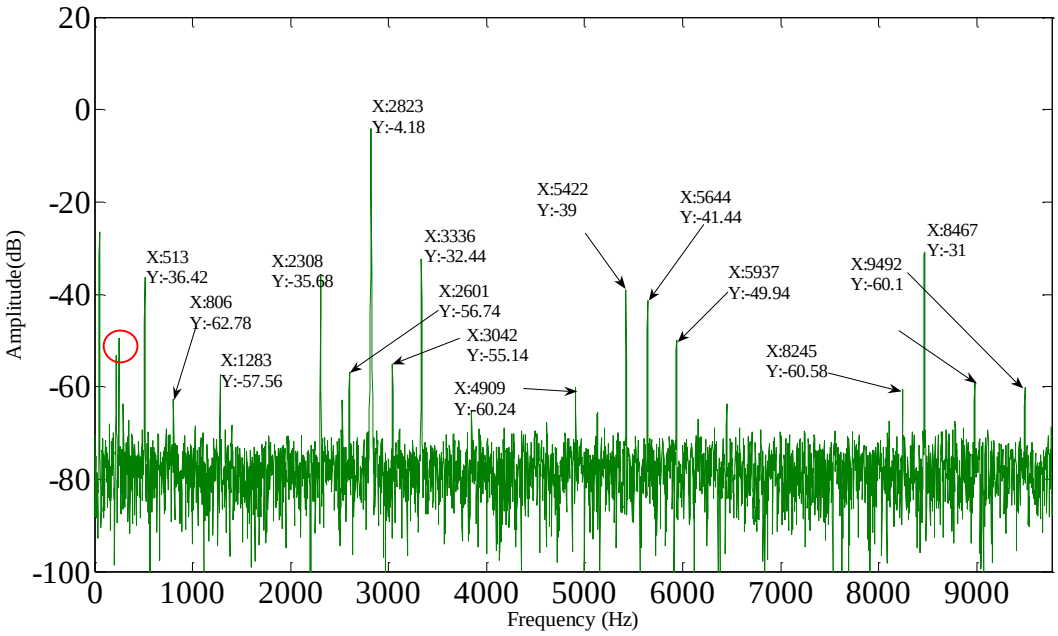

(a) Frequency Response

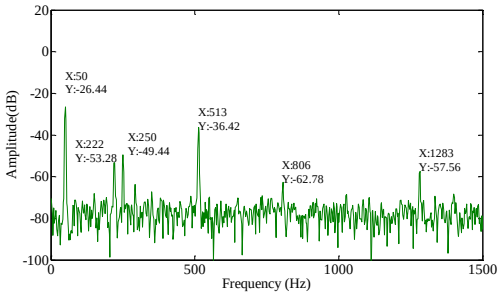

(b) Frequency Response (1-1500 Hz)

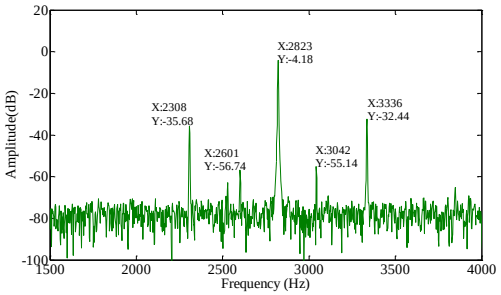

(c)Frequency Response (1500-4000 Hz)

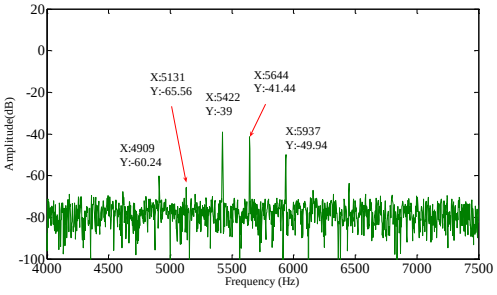

(d)Frequency Response (4000-7500 Hz)

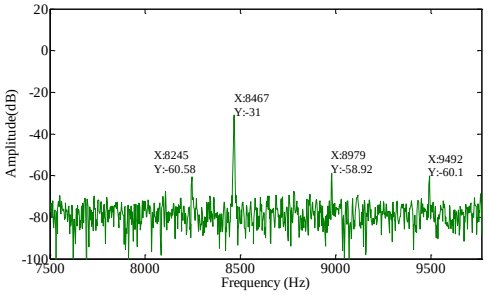

(e)Frequency Response (7500- 9677 Hz)

Figure 5.29 Measurement of frequency response at Sensor 3

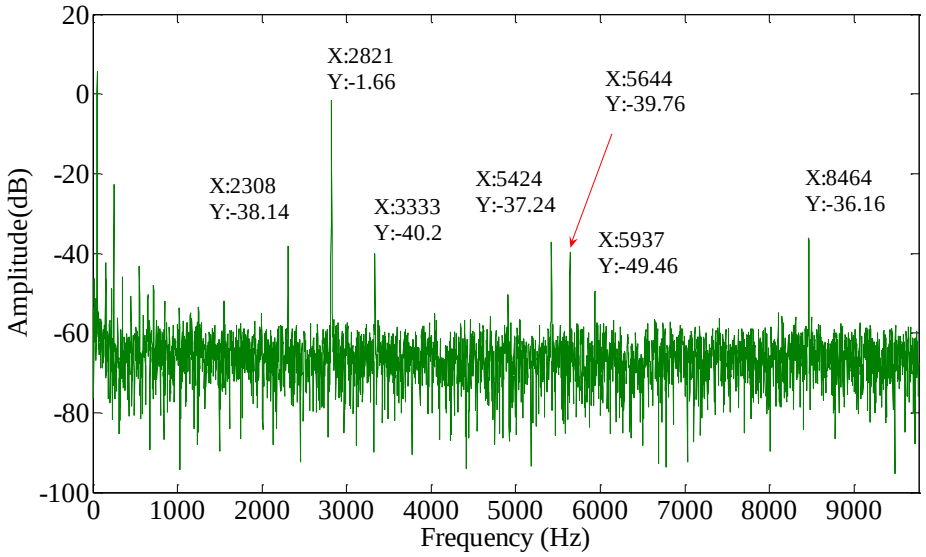

Figure 5.30 Measurement of frequency response at sensor 4

was made between the frequency responses of the uncracked bar (Fig 5.14) and cracked bar (Fig 5.27 to Fig 5.30) it was observed that there was no lower frequency component in the frequency response of the uncracked bar. But for the cracked bar it was observed from the frequency response (Fig 5.27 to Fig 5.30) that along with side band frequencies near the resonant frequency, lower frequency components exist The occurrence of low frequency component and side band frequency might be attributed to the vibro-impact behaviour of crack. The magnitude of this low frequency component was proportional to the excitation frequency. This indicates that crack behaves like a signal modulator, detector of low frequency component and amplifier as the magnitude of low frequency was proportional to the magnitude of excitation frequency.

5.7.2.3 Case(C): Excitation at Frequency of 3634 Hz (Low Vibration Level)

The cracked bar was excited at lower vibration amplitude at resonant frequency of 3634 Hz. It was found that, the frequency response obtained at the sensor 1 (Fig. 5.31) and the sensor 4 (Fig. 5.34) showed only resonant frequency. It was also found that, the response acquired near the crack from sensor 2 (Fig 5.32) and sensor 3 (Fig 5.33) showed the resonant frequency along with its higher harmonics. As seen from Fig.5.32 and Fig. 5.33 higher harmonic (7270 Hz) is exactly 2 times the resonant frequency. When comparison was made between the frequency responses (Fig. 5.15) of uncracked

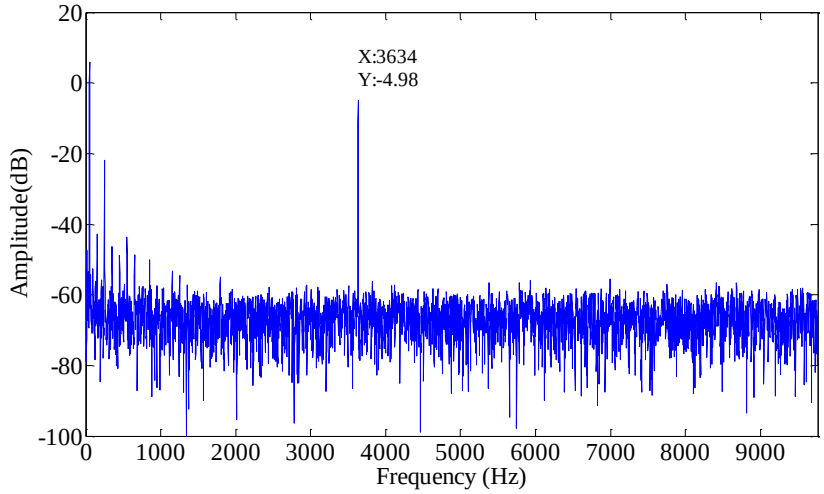

Figure 5.31 Measurement of frequency response at sensor 1

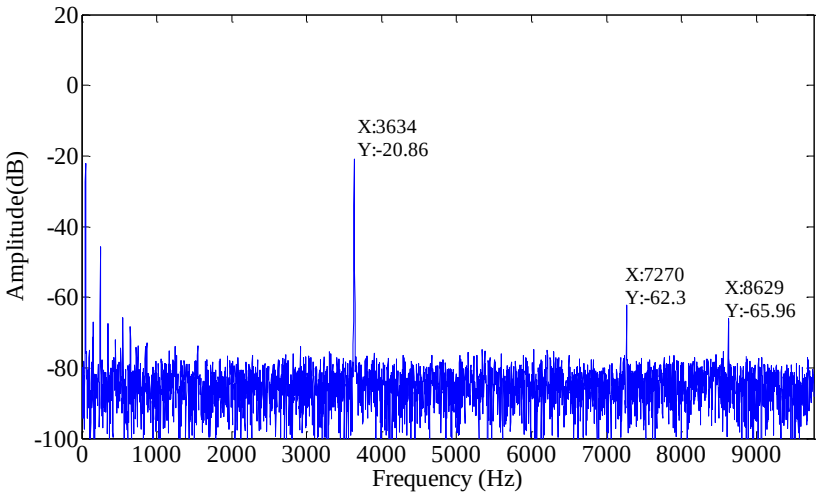

Figure 5.32 Measurement of frequency response at sensor 2

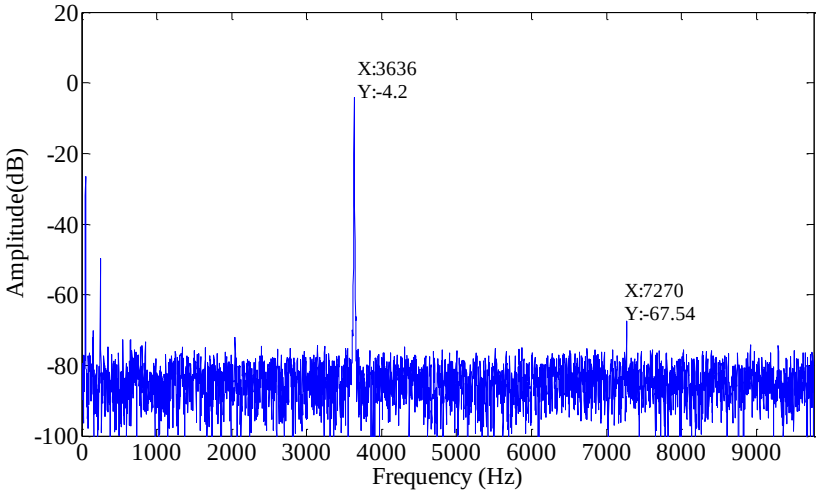

Figure 5.33 Measurement of frequency response at sensor 3

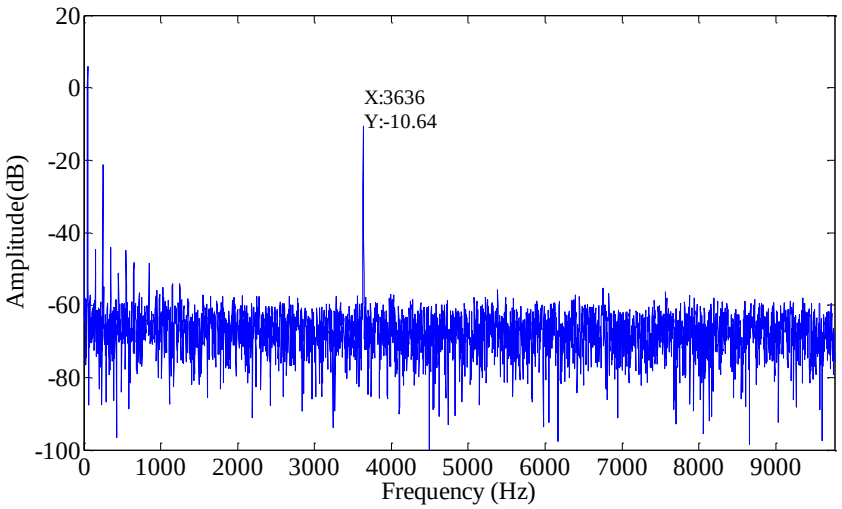

Figure 5.34 Measurement of frequency response at sensor 4

bar and frequency response (Fig. 5.32 and Fig 5.33) of cracked bar it was observed that presence of crack in a bar led to generation of higher harmonic.

5.7.2.4 Case (D): Excitation at Frequency of 3634 Hz (High Vibration Level)

The cracked bar was excited at higher vibration amplitude at frequency of 3634 Hz. The response acquired at sensor 1 (Fig. 5.35) and sensor 4 (Fig. 5.38) indicated the presence of the low frequency (1359 Hz) component which resulted in modulation showing the presence of side band frequencies near the resonant frequency at 2275 Hz and higher harmonic of resonant frequency at 7270 Hz. Similarly, the response acquired at sensor 2 (Fig. 5.36) indicated the presence of low frequency components (1359 Hz) which resulted in the modulation showing the presence of additional side band frequencies (2275 Hz and 4993 Hz) near the resonant frequency along with higher harmonic of resonant frequency at 7270 Hz. On similar grounds the response s acquired at the sensor 3 (Fig. 5.28) indicated the presence of low frequency components (1357 Hz) which resulted in modulation showing the presence additional side band frequencies (2279 Hz and 4990 Hz) near the resonant frequency along with higher harmonic of resonant frequency at 7270 Hz. When the comparison is made between the frequency responses of uncracked bar (Fig. 5.16) and cracked bar (Fig. 5.36 and Fig 5.37). It was observed that there is not much difference in the frequency responses. This might be due to the coupling between modes along with the crack. It was difficult to discriminate the frequencies due to the presence of crack and the coupling between the transverse mode and longitudinal mode. It was also observed from Fig 5.35 to Fig.5.38 that frequency

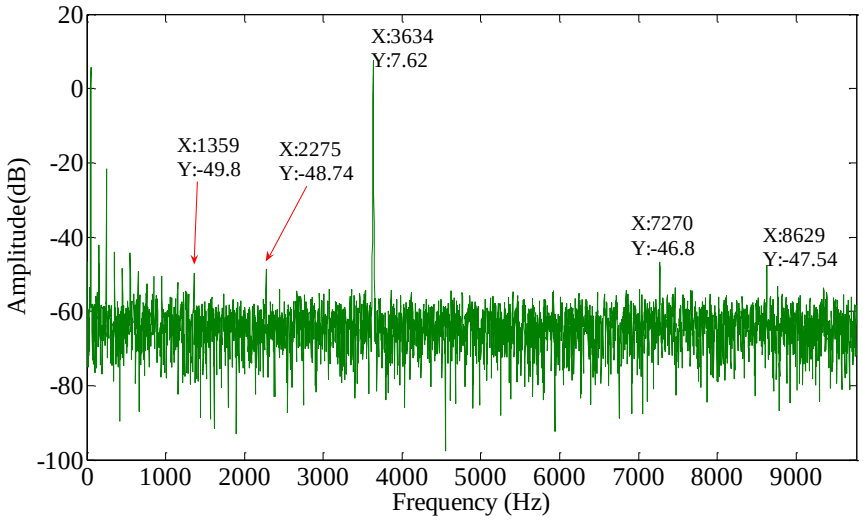

Figure 5.35 Measurement of frequency response at sensor 1

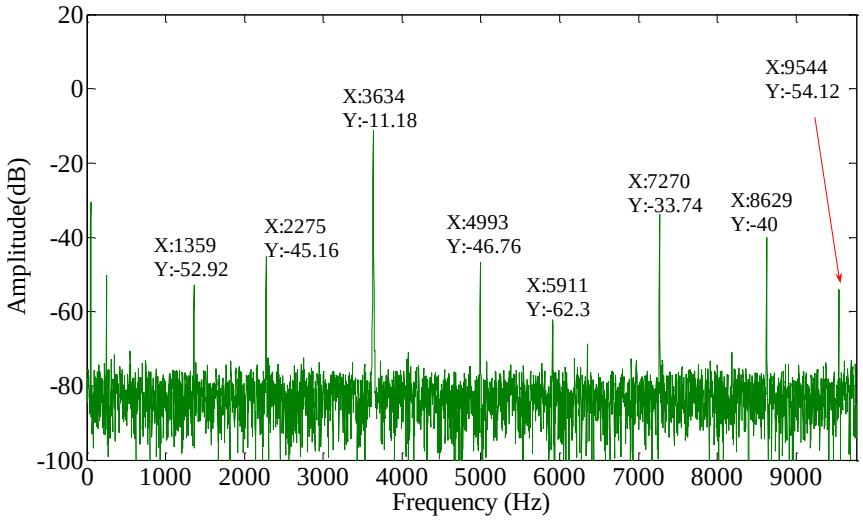

Figure 5.36 Measurement of frequency response at sensor 2

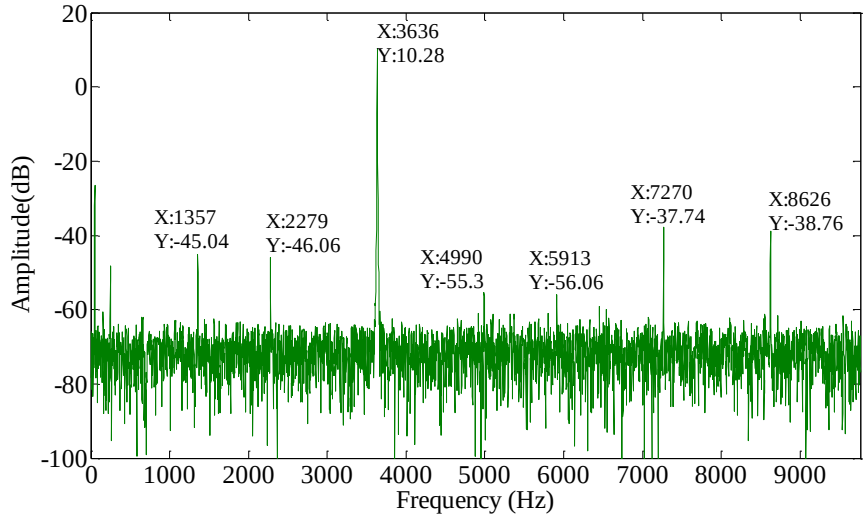

Figure 5.37 Measurement of frequency response at sensor 3

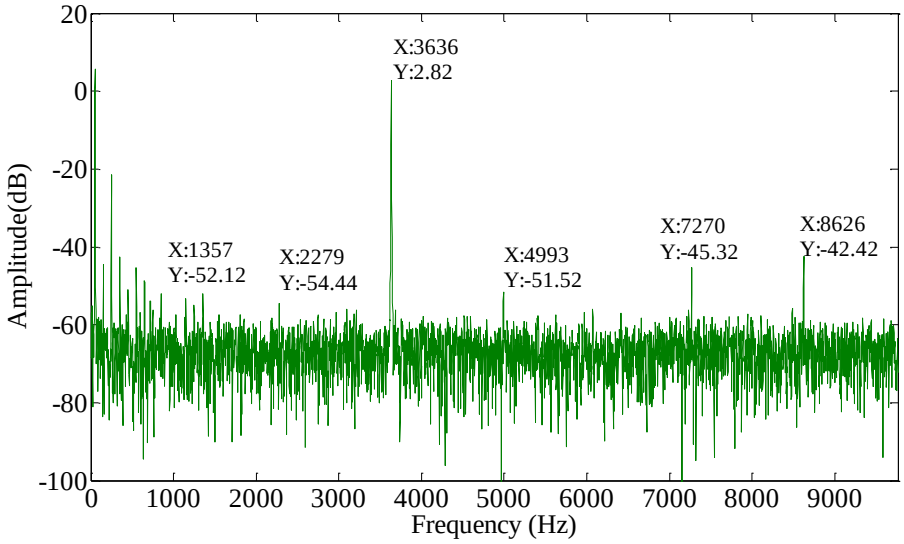

Figure 5.38 Measurement o frequency response at sensor 4

response measured at different sensor position there was change in amplitude of sideband frequency.

5.7.2.5 Case (E): Excitation at Frequency of 4499 Hz (Low Vibration Level)

The cracked bar was excited at lower vibration amplitude at frequency of 4499 Hz. It was found that, the frequency response at sensor 1 (Fig. 5.39) and at sensor 4 (Fig.5.42) showed only resonant frequency. It was also found that signal acquired near the crack from sensor 2 (Fig.5.40) and sensor 3 (Fig.5.41) showed the increase in amplitude of resonant frequency.

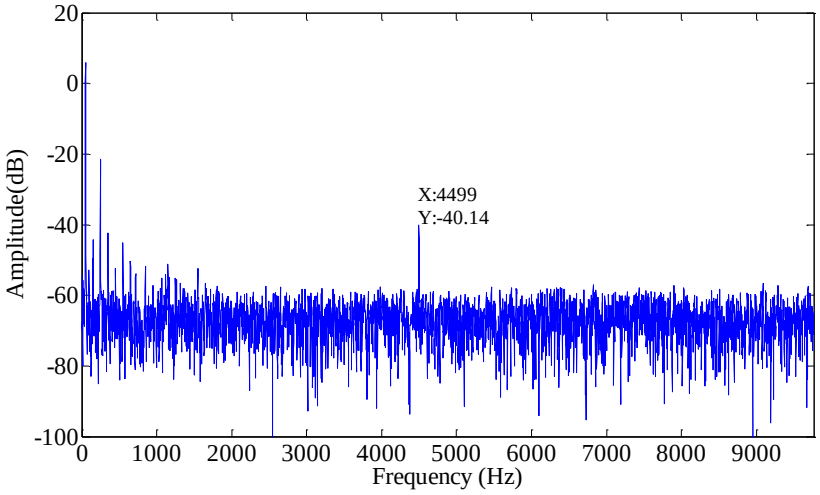

Figure 5.39 Measurement of frequency response at sensor 1

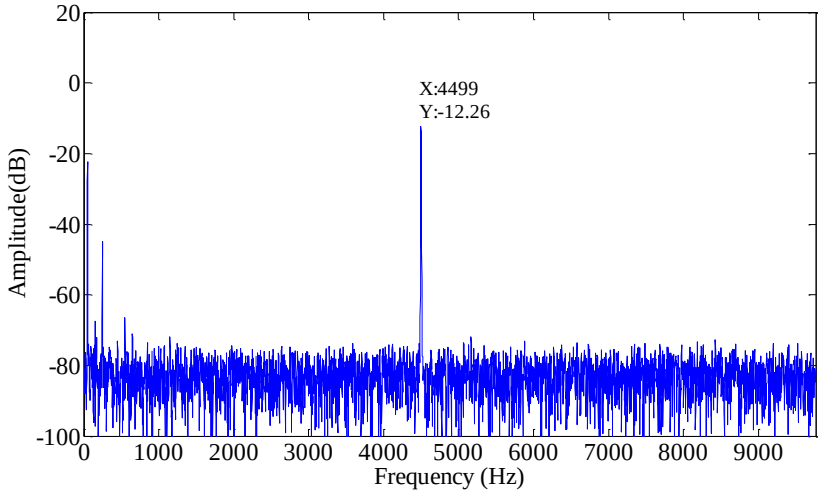

Figure 5.40 Measurement of frequency response at sensor 2

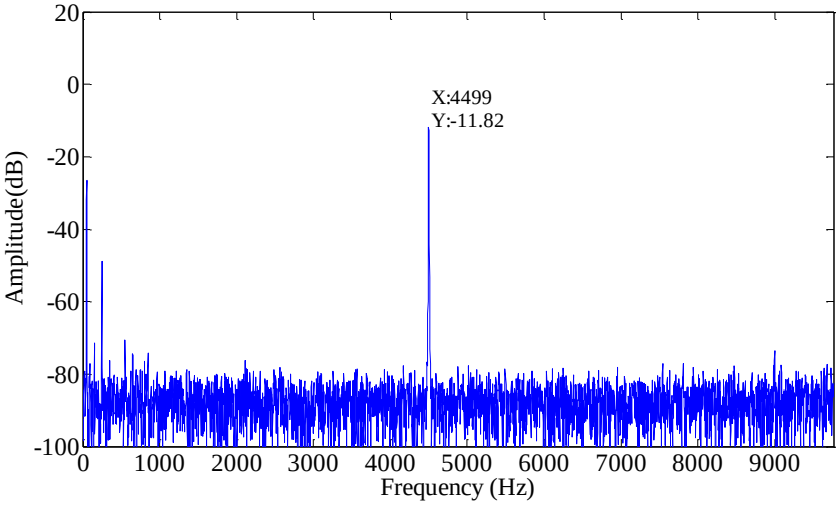

Figure 5.41 Measurement of frequency response at sensor 3

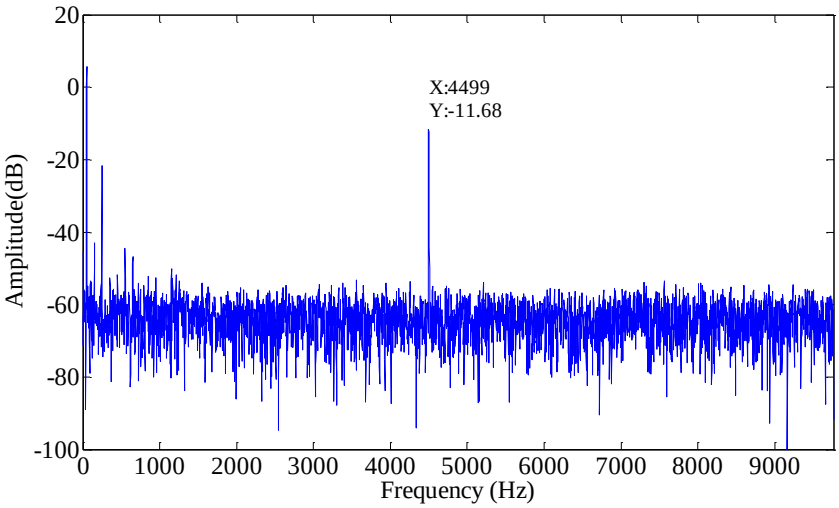

Figure 5.42 Measurement of frequency response at sensor 4

5.7.2.6 Case (F): Excitation at Frequency of 4499 Hz (High Vibration Level)

The cracked bar is excited at higher vibration amplitude at the frequency of 4499 Hz. The response acquired at each of the sensors (Figures 5.43, 5.44, 5.45 and 5.46) showed the presence of resonance frequency along with the high harmonic of resonant frequency at 9001 Hz. When comparison is made between the frequency responses of uncracked bar (Fig. 5.18) and of cracked bar (Fig 5.43 to Fig 5.46) it was observed that presence of crack in a bar led to generation of higher harmonic.

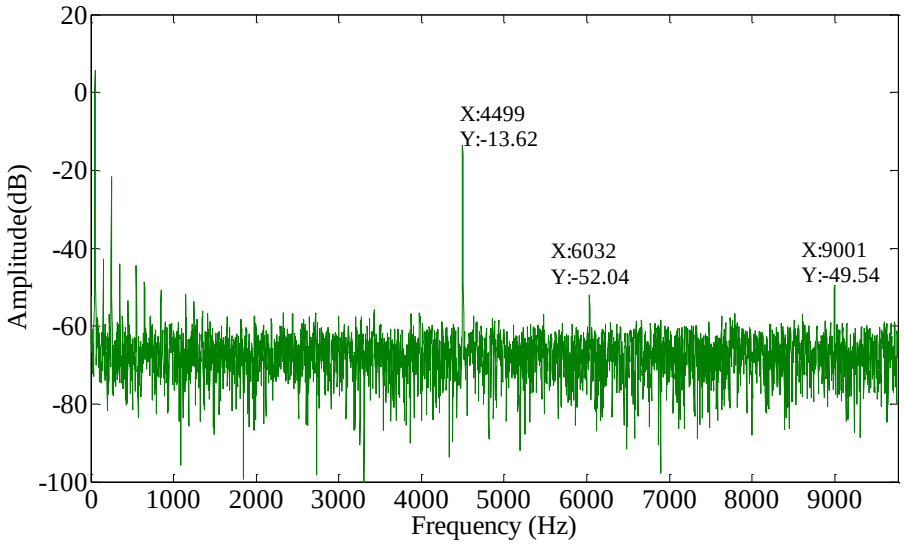

Figure 5.43 Measurement of frequency response at sensor 1

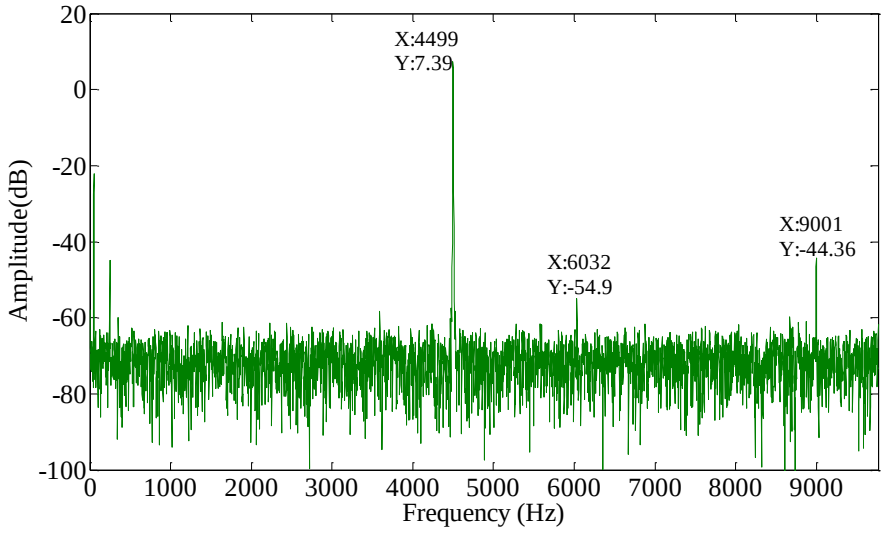

Figure 5.44 Measurement of frequency response at sensor 2

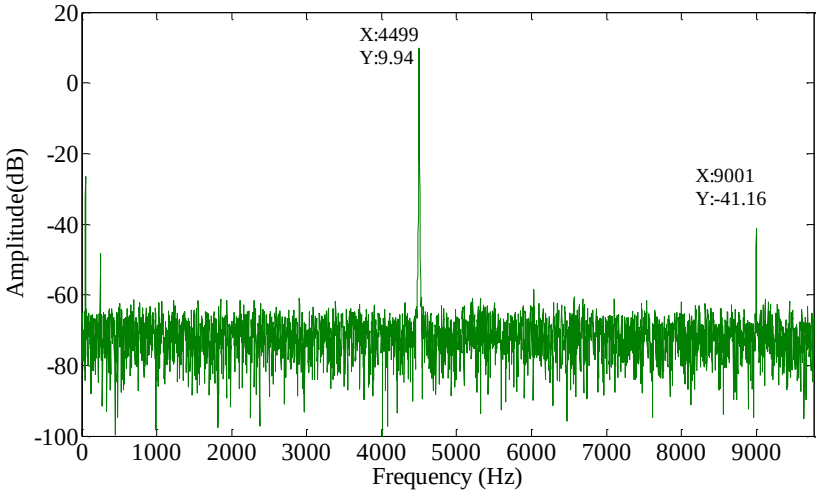

Figure 5.45 Measurement of frequency response at sensor 3

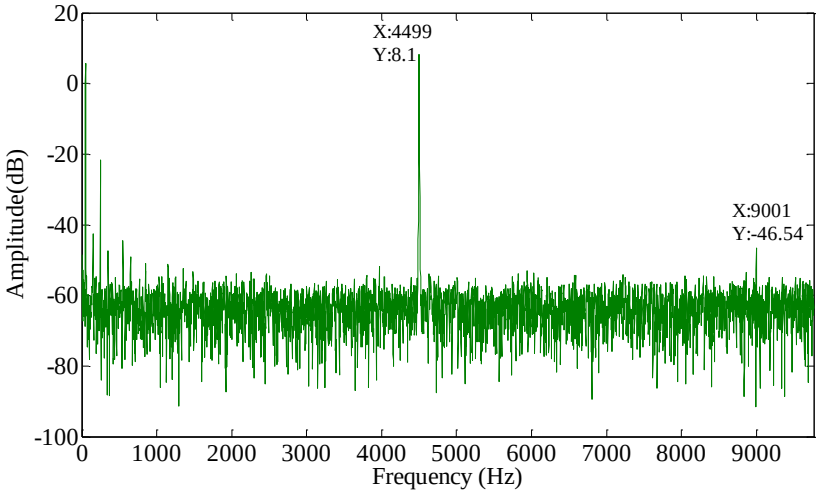

Figure 5.46Measurement of frequency response at sensor 4

5.7.2.7 Case (G): Excitation at Frequency of 6008 Hz (Low Vibration Level)

The cracked bar was excited at lower vibration amplitude at the frequency of 6008 Hz. It was found, that response obtained from the sensor near the fixed end (Fig.5.47) shows the resonance frequency along with one more frequency component. It was also found, that the frequency response obtained at the sensor near the free end (Fig.5.50) and the sensors near the crack (Fig.5.48 and Fig.5.49) showed slight shift in the resonant frequency of vibration from 6008 Hz to 6011 Hz. There was also a shift in additional frequency component from 7515 Hz to 7508 Hz. When comparison was made between the frequency responses of uncracked bar (Fig. 5.19) and of cracked bar (Fig 5.43 to Fig 5.46) it was observed that presence of crack in a bar led to generation of additional frequency component coupled with the resonant frequency. This additional frequency

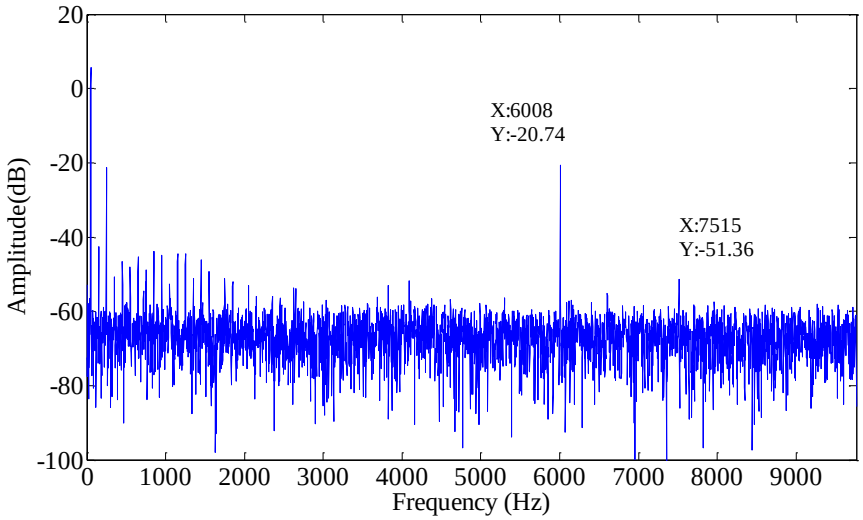

Figure 5.47 Measurement of frequency response at sensor 1

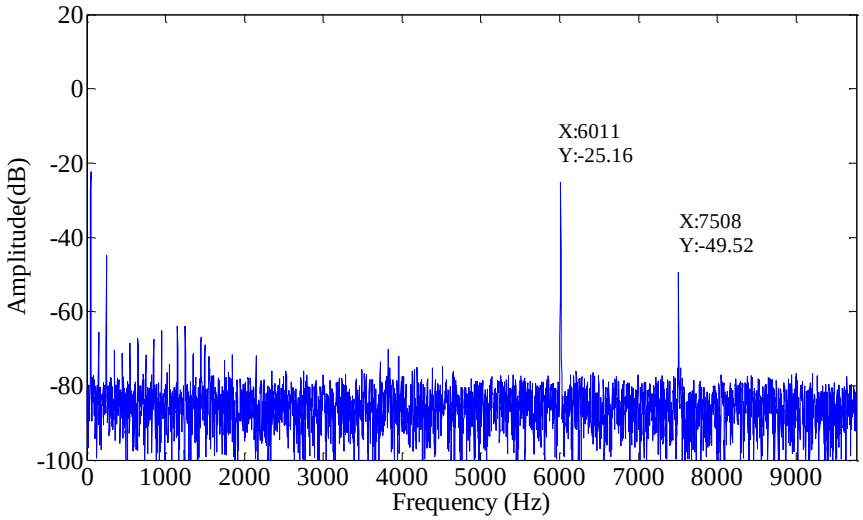

Figure 5.48 Measurement of frequency response at sensor 2

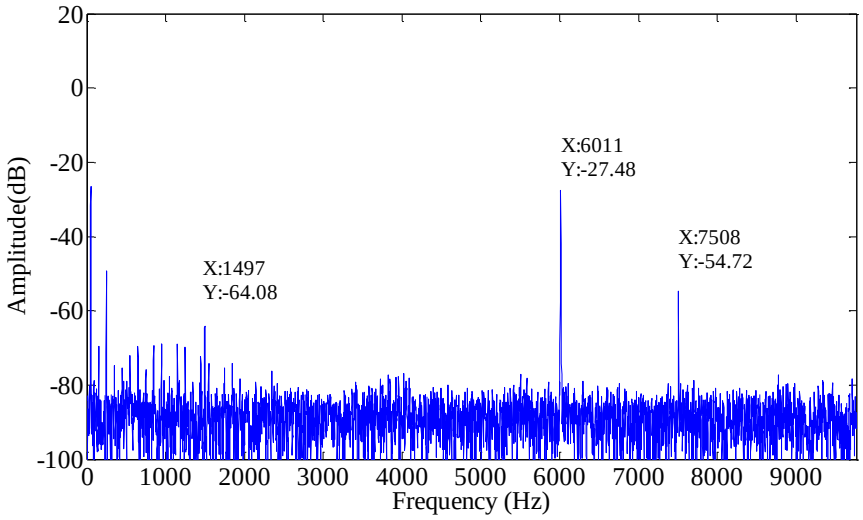

Figure 5.49 Measurement of frequency response at sensor 3

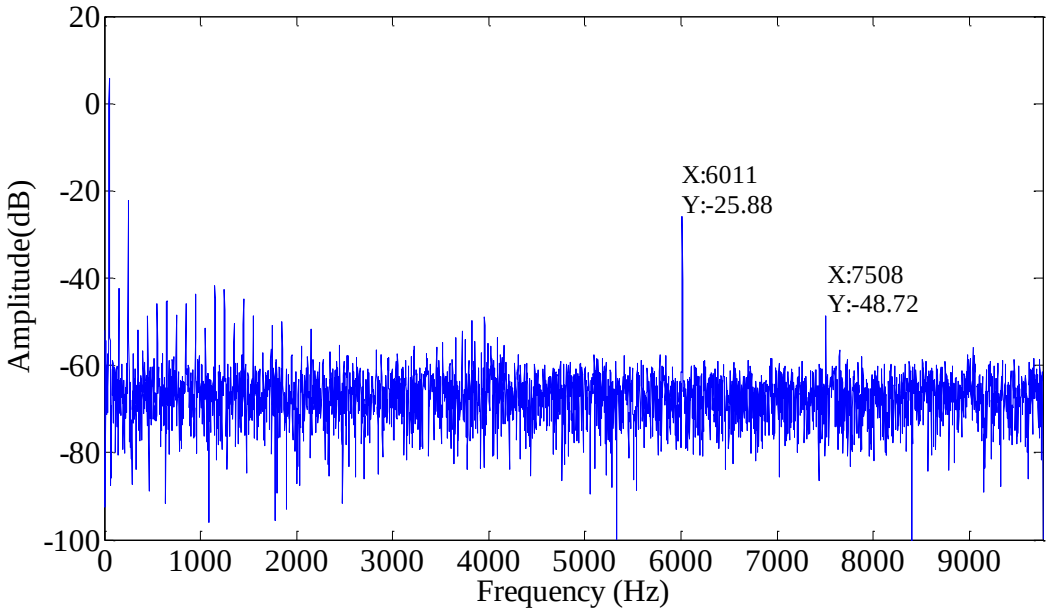

Figure 5.50 Measurement of frequency response at sensor 4

might be due to the free vibration taking place during the process of forced excitation i.e. is due to the vibro-impact behaviour of the crack.

5.7.2.8 Case (H): Excitation at Frequency of 6008 Hz (Higher Vibration Level)

The cracked bar was excited at higher vibration amplitude at the frequency of 6008 Hz. It was found that, the frequency response obtained from the sensor near the fixed end (Fig. 5.51) and the free end of the bar (Fig.5.54) showed the resonance frequency along with low frequency component at 1500 Hz. This lower resonant frequency caused modulation which led to the generation of side band frequency (7510 Hz) near the resonant frequency. It was also found that response acquired near the crack from sensor 2 (Fig. 5.52) showed the presence of side band frequencies in the multiples of 1500 Hz along with the resonant frequency. The frequency response obtained at sensor 3(Fig. 5.53) showed that there was slight shift in the resonant frequency. It also showed the presence of the side band frequencies in the multiples of 1500 Hz near the resonant frequency. When the comparison is made between the responses of uncracked bar (Fig. 5.20) and cracked bar (Fig. 5.52 and Fig 5.53) there was very little difference in the frequency response. It was also difficult to discriminate the frequencies due to the presence of crack and the coupling between the modes.

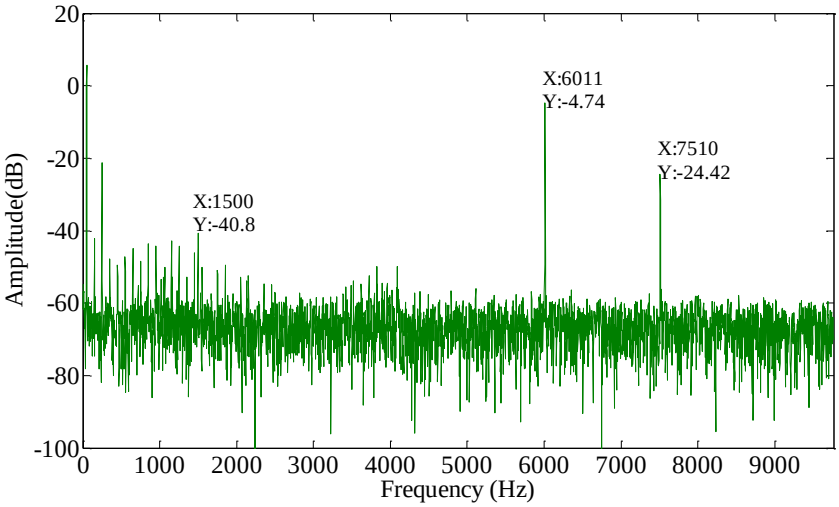

Figure 5.51 Measurement of frequency response at sensor 1

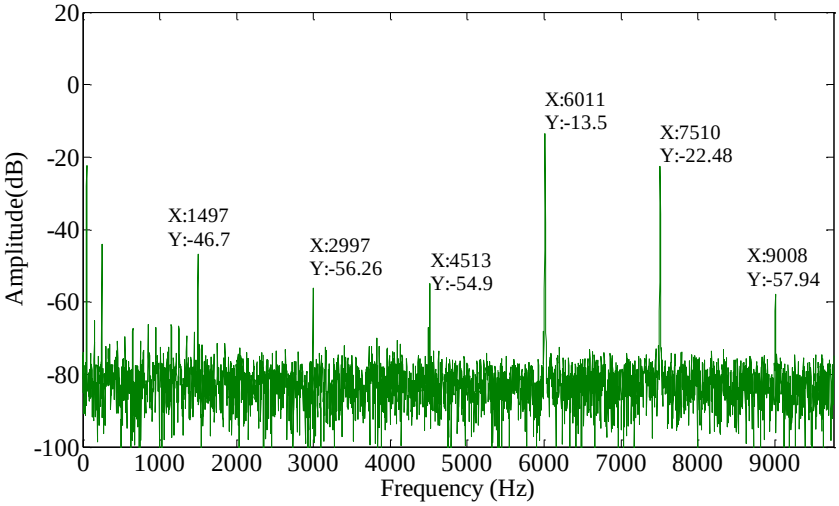

Figure 5.52 Measurement of frequency response at sensor 2

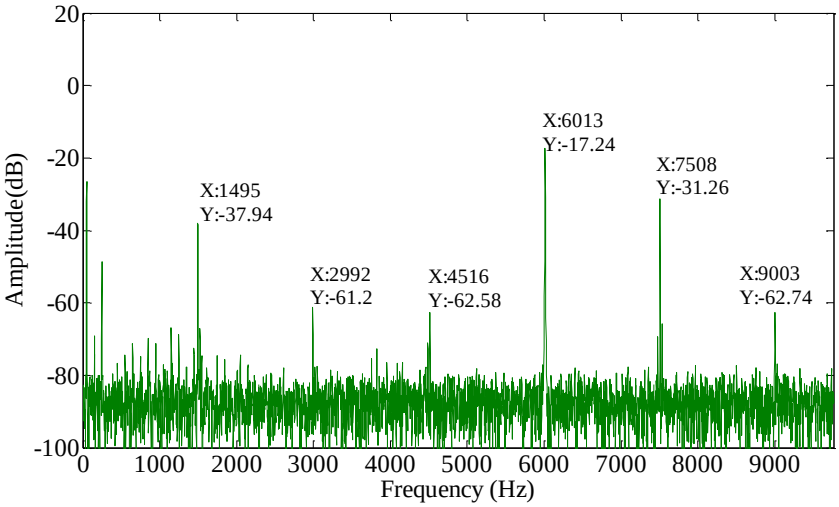

Figure 5.53Measurement of frequency response at sensor 3

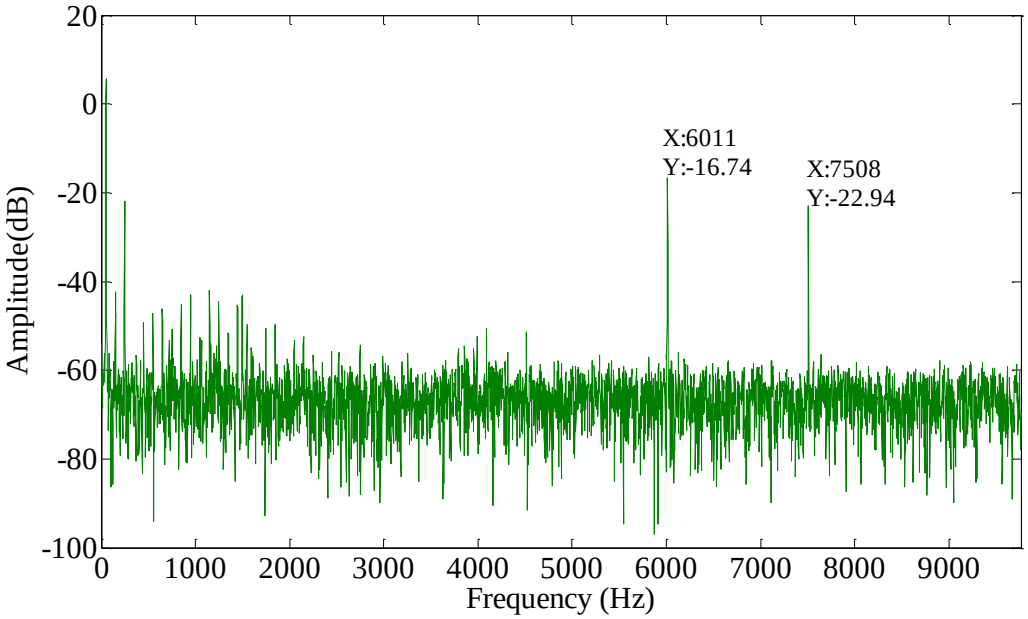

Figure 5.54 Measurement of frequency response at sensor 4

5.7.2.9 Case (I): Excitation at Frequency of 6445 Hz (Low Vibration Level)

The cracked bar was excited at lower vibration amplitude at the frequency of 6445 Hz. The response acquired at each of the sensors (Figures 5.55, 5.56, 5.57 and 5.58) showed only the resonant frequency.

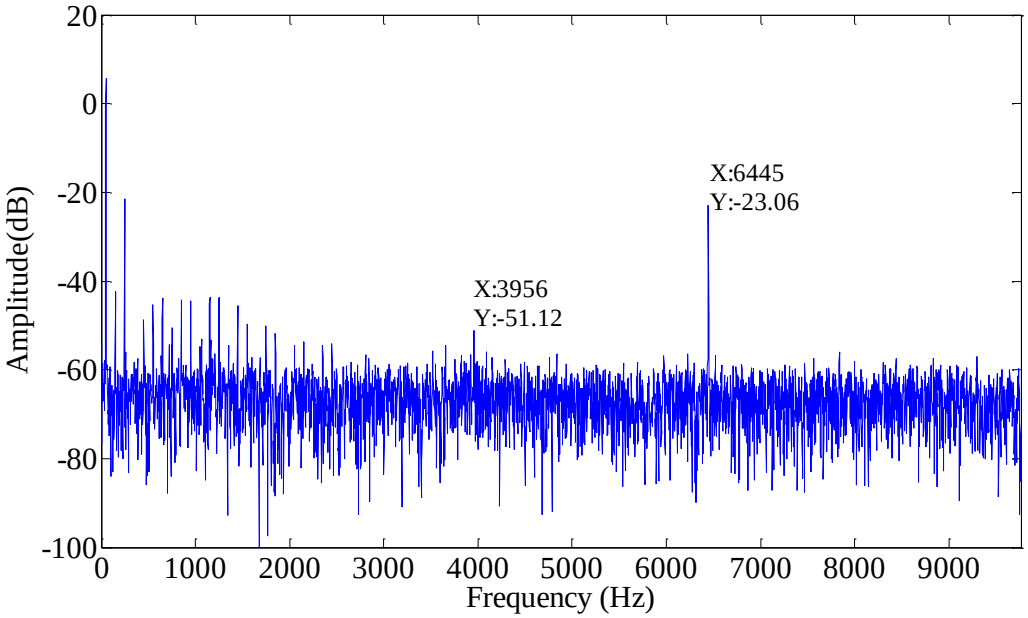

Figure 5.55Measurement of frequency response at sensor 1

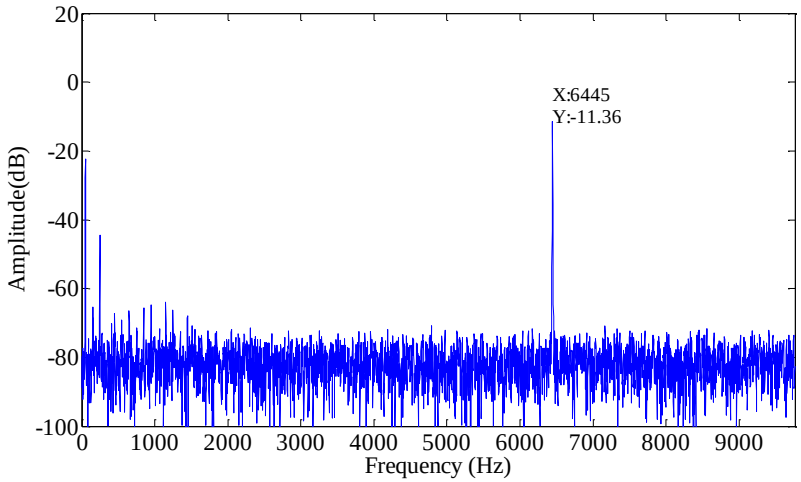

Figure 5.56 Measurement of frequency response at sensor 2

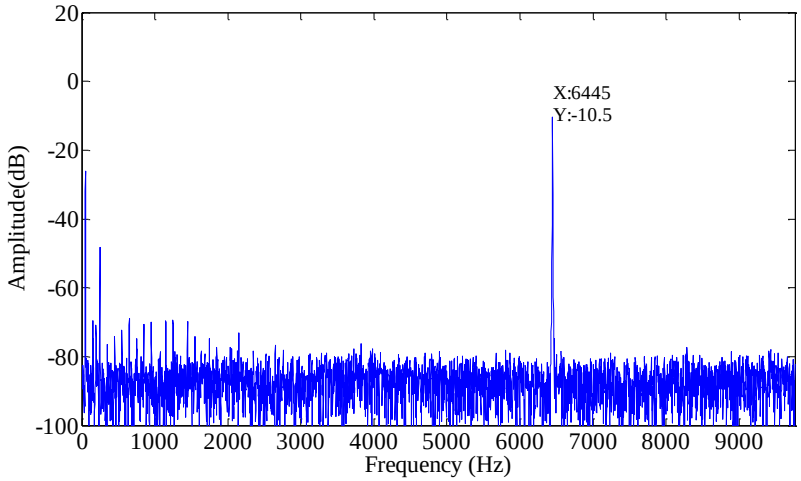

Figure 5.57 Measurement of frequency response at sensor 3

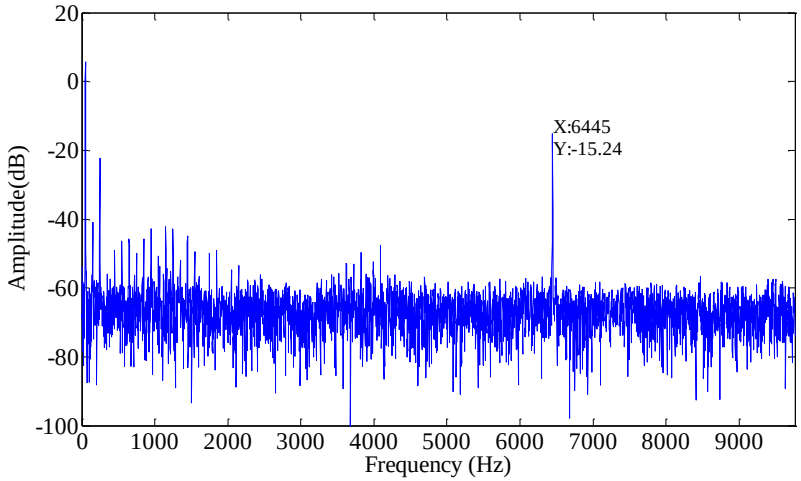

Figure 5.58 Measurement of frequency response at sensor 4

5.7.2.10 Case (J): Excitation at Frequency of 6445 Hz (High Vibration Level)

The cracked bar was excited at higher vibration amplitude at the frequency of 6445 Hz. The response acquired at sensor 1 (Fig.5.59) showed the resonant frequency. Similarly, the response acquired at sensor 2, sensor 3 and sensor 4 (Figures 5.60, 5.61 and 5.62) showed the presence of additional low frequency component at 196 Hz along with the resonant frequency. This low frequency component caused modulation which led to the generation of side band frequency near the resonant frequency at 6640 Hz. This indicated that presence of crack causes additional perturbations.

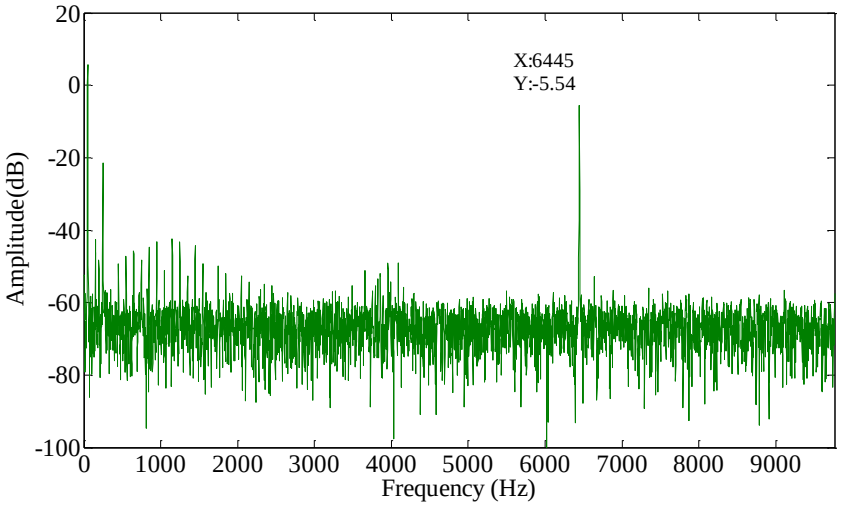

Figure 5.59 Measurement of frequency response at sensor 1

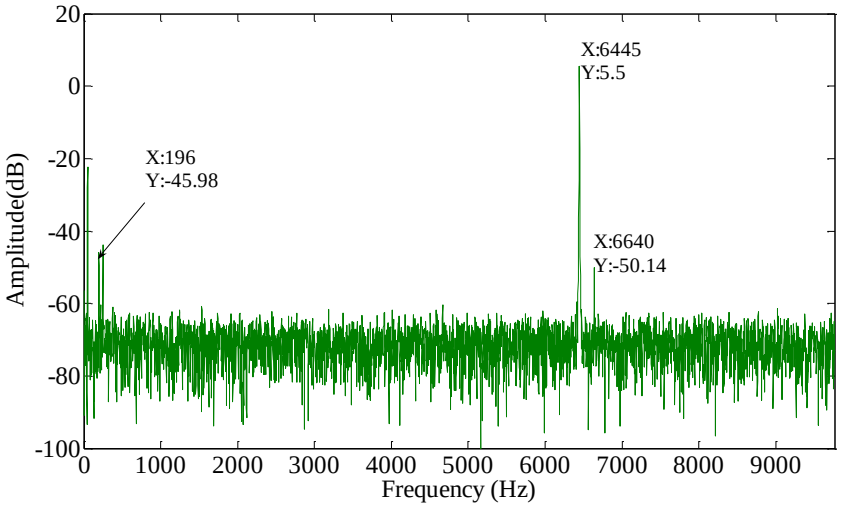

Figure 5.60 Measurement of frequency response at sensor 2

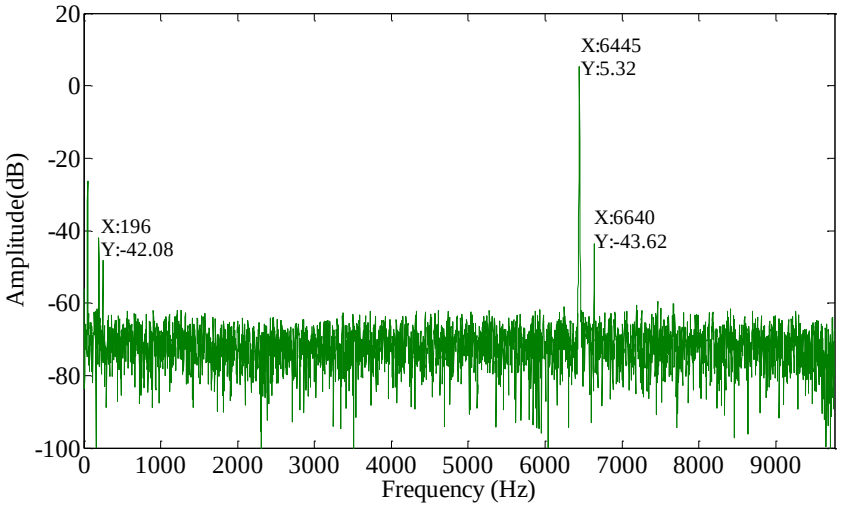

Figure 5.61 Measurement of frequency response at sensor 3

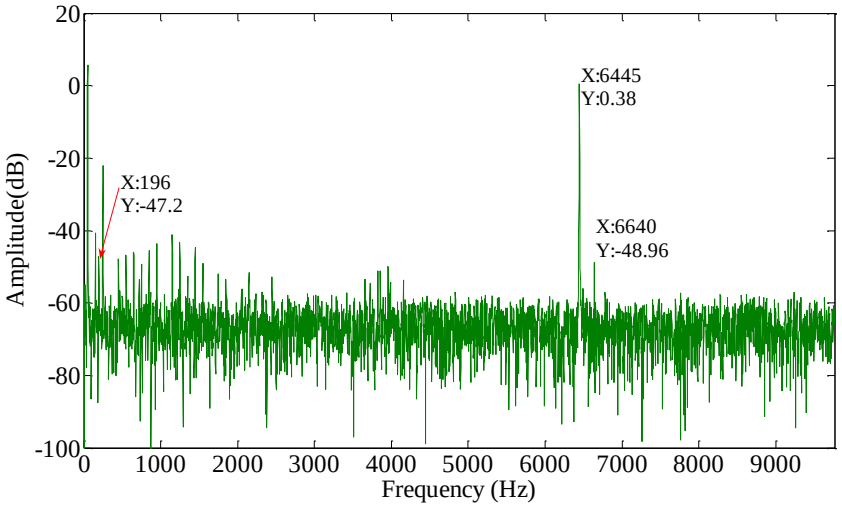

Figure 5.62 Measurement of frequency response at sensor 4

5.8 Summary

In this chapter experimental results were analyzed. It was found that the presence of crack has the significant effect on the dynamic behaviour of the cracked bar as observed from the frequency response obtained at the different locations of the bar. As seen from the frequency responses, it was observed that measurements near the crack showed that there was generation of higher harmonics at lower vibration amplitude. This generation of higher harmonics indicated that the presence of crack induces additional perturbations in the bar. When the cracked bar was excited at the higher vibration amplitude. It was observed that along with the higher harmonics of resonant frequency,

low frequency component appeared in the response. This low frequency component caused modulation which resulted in the generation of side band frequencies near the resonant frequency. The occurrence of low frequency component and side band frequency might be attributed to the vibro-impact behaviour of crack. The magnitude of this low frequency component was proportional to the magnitude of resonant frequency. This indicates that crack behaves like a signal modulator, detector of low frequency component and amplifier as the magnitude of low frequency component was proportional to the magnitude of excitation frequency. To make an analogy with the one of the communication system i.e. heterodyne receiver. It was concluded that the response obtained from bar with a crack is similar to that obtained from heterodyne receiver, which led to the generation of new frequencies by mixing of two oscillating frequency. This signature of the frequency response at lower and higher vibration amplitude was used for predicting the location of the crack by measuring the frequency response at the different location from the crack. It was found that crack-induced nonlinearity effect reduced as one moved away from the crack to measure the frequency response. Hence, measuring the frequency response at different location on the cracked bar can help to locate the crack position in the bar under consideration.

Chapter 6 Conclusions and Further Work

6.1 Conclusion

Vibration based structural health monitoring is advantageous as it doesn't require dismantling of the structure to get insight of the structural health under working condition. This technique can considerably reduce the cost of monitoring the structural health in real time. Moreover, it would also help in making the optimum utilization of the structural life. Hence, this is very promising method to monitor structural health. The thesis was aimed at exploring the nonlinear vibration based cracked monitoring techniques. In this thesis work was focussed on developing the new technique of simulation of continuous system with discontinuities such as crack, characterizing the effect of material nonlinearity on the dynamics of the cracked bar and performing the experiments to study the dynamics of bar having a fatigue crack in it.

The new technique was developed using the numerical approximation for dynamic compliance and nonlinear model of contact force generated due cracks faces interaction implanted numerically as a nonlinear feedback. This new technique of simulation was developed using Matlab- Simulink software. It was found that crack-induced nonlinearity generated higher harmonics along the bar length, as a function of distance from the crack.

The simulation in MSC Marc Mentat was performed on the cracked bar to characterize the effect of material nonlinearity on the natural frequency. The 2D finite element model of the cracked cantilever bar was modelled to study the effect of crack-tip plasticity on the first three natural frequencies of the cantilever bar. It was found that the presence of the plasticity at the crack tip has no effect on the first natural frequency whereas there was a low level influence on the second and third natural frequencies as the a/h ratio increased. In addition to that there was no effect on the first natural frequency as the d/L ratio increased for different crack depths. On the contrary as the d/L ratio increased second and third natural frequencies were affected for different crack depth. This effect of change in second and third natural frequency for different a/h and d/L ratios is attributed to the change in stiffness due to the crack-tip plasticity. Hence, it was concluded that crack-tip plasticity affected the resonance frequency. This change in resonance frequency depends on the mode shape, a/h ratio and d/L ratio.

The experiments were performed on both the uncracked and the cracked bar. The response of the uncracked bar was obtained at the centre of bar and the responses of the cracked bar were obtained near the crack and away from the crack. The results obtained from experiments performed on both uncracked and cracked bar were analyzed. For uncracked and cracked bar responses were obtained at lower and higher vibration amplitude at the given resonant frequency of excitation. It was found that at lower vibration amplitude, response of uncracked bar showed only resonant frequency of excitation whereas response of cracked bar showed the resonant frequency of excitation along with its higher harmonic. This presence of higher harmonic in the frequency response was due to the crack in the bar which caused sharing of energy between the vibration modes. On the similar ground when the uncracked bar and the cracked bar was excited at higher vibration amplitude at the given resonant frequency of excitation. The response of cracked bar showed resonant frequency and its harmonics along with low frequency component. This low frequency component caused modulation which resulted in the generation of side band frequencies near the resonant frequency. The occurrence of low frequency component and side band frequencies might be attributed to the vibro-impact behaviour of crack. The magnitude of this low frequency component was proportional to the magnitude of resonant frequency. This indicated that crack behaved like a modulator, detector of low frequency component and amplifier as the magnitude of low frequency was proportional to the magnitude of resonance frequency of excitation. To make an analogy with the one of communication system i.e. heterodyne receiver. It can be concluded that the response obtained from bar with a crack is similar to that obtained from heterodyne receiver.

It was concluded from the analytical modelling results and the experimental results that crack-induced nonlinearity were responsible for the generation of higher harmonics. It was observed in both analytical and experimental results that as one moved away from the crack to measure the response; effect of crack-induced nonlinearity reduced. Hence, measuring the response at different location on the cracked bar can help to locate the crack position in the bar by considering magnitude of higher harmonics which decreased as one moved away from crack to measure the response which has the localized effect on the dynamics of the bar.

6.2 Further Work

In the present study Matlab-Simulink program was developed considering the contact force generated due to the cracks faces interaction as a nonlinear feedback. This Matlab-Simulink model can be further developed by incorporating structural damping, plasticity and dry friction. This can also be extended to the multi-dimensional problem and various ultrasonic processes. The finite element model developed can be further improved by using the high performance computing by incorporating the damping in the cracked bar. The experimental study performed in this can be extended to the PMMA specimen after the successful generation of the crack in the PMMA bar. Though the vibro-impact behaviour of crack caused signal modulation. There is a further need to investigate at what stress level crack opens and closes using high speed camera. The technique developed for structural health monitoring can be used in real time using the non-contact measurement technology for response measurement which doesn't affect the dynamics of the structure.

References

ACTIS, R. and DIMAROGONAS, A.D., 1989. Non-linear effects due to closing cracks in vibrating beams, 17-20 September 1989, Vibration and noise pp99-104.

ANDERSON, T.L., 2005. *Fracture Mechanics Fundamentals and Application.* CRC Press.

ANDREAUS, U., CASINI, P. and VESTRONI, F., 2007. Non-linear dynamics of a cracked cantilever beam under harmonic excitation. *International Journal of Non-Linear Mechanics,* **42**(3), 566-575.

BABAKOV, I.M., 1968. *Theory of Vibrations.* Moscow: Fizmatgiz.

BABITSKY, V.I., 1998. *Theory of vibro-impact systems and applications.* Berlin ; New York: Springer.

BAMNIOS, G. and TROCHIDES, A., 1995. Dynamic behaviour of a cracked cantilever beam. *Applied Acoustics,* **45**(2), 97-112.

BAMNIOS, Y., DOUKA, E. and TROCHIDIS, A., 2002. Crack identification in beam structures using mechanical impedance. *Journal of Sound and Vibration,* **256**(2), 287-297.

BARR, A.D.S., 1966. An extension of the Hu Washizu variational principle in linear elasticity for dynamic problems. *Transactions of ASME Journal of Applied Mechanics,* **33**, 465.

BAYISSA, W.L., HARITOS, N. and THELANDERSSON, S., 2008. Vibration-based structural damage identification using wavelet transform. *Mechanical Systems and Signal Processing,* **22**(5), 1194-1215.

BRANDON, J.A. and ABRAHAM, O.N.L., 1995/8/24. Counter-intuitive quasi-periodic motion in the autonomous vibration of cracked Timoshenko beams. *Journal of Sound and Vibration,* **185**(3), 415-430.

ÇAM, E., ORHAN, S. and LÜY, M., 2005/7. An analysis of cracked beam structure using impact echo method. *NDT & E International,* **38**(5), 368-373.

CARPINTERI, A., LACIDOGNA, G. and PUGNO, N., 2007. Structural damage diagnosis and life-time assessment by acoustic emission monitoring. *Engineering Fracture Mechanics,* **74**(1-2), 273-289.

CAWLEY, P. and ADAMS, R.D., 1979. The location of defects in structures from measurements of natural frequencies. *Journal of strain analysis,* **14**(2), 49-57.

CHATI, M., RAND, R. and MUKHERJEE, S., 1997/10/23. Modal analysis of a cracked beam. *Journal of Sound and Vibration,* **207**(2), 249-270.

CHEER GERM GO and YEE SHOWN LIN, 1994/7. Infinitely small element for the dynamic problem of a cracked beam. *Engineering Fracture Mechanics,* **48**(4), 475-482.

CHENG, S.M., SWAMIDAS, A.S.J., WU, X.J. and WALLACE, W., 1999/8/5. Vibrational response of a beam with a breathing crack. *Journal of Sound and Vibration,* **225**(1), 201-208.

CHONDROS, T.G., DIMAROGONAS, A.D. and YAO, J., 1998/8/6. A continuous cracked beam vibration theory. *Journal of Sound and Vibration,* **215**(1), 17-34.

CHONDROS, T.G., DIMAROGONAS, A.D. and YAO, J., 1998/11/12. Longitudinal vibration of a bar with a breathing crack. *Engineering Fracture Mechanics,* **61**(5-6), 503-518.

CHONDROS, T.G., DIMAROGONAS, A.D. and YAO, J., 1998/11/12. Longitudinal vibration of a continuous cracked bar. *Engineering Fracture Mechanics,* **61**(5-6), 593-606.

CHONDROS, T.G., DIMAROGONAS, A.D. and YAO, J., 1997/2/27. A consistent cracked bar vibration theory. *Journal of Sound and Vibration,* **200**(3), 303-313.

CHONDROS, T.G. and LABEAS, G.N., 2007/4/3. Torsional vibration of a cracked rod by variational formulation and numerical analysis. *Journal of Sound and Vibration,* **301**(3-5), 994-1006.

CHRISTIDES, S. and BARR, A.D.S., 1984. One-dimensional theory of cracked Bernoulli-Euler beams. *International Journal of Mechanical Sciences,* **26**(11-12), 639-648.

CHU, Y.C. and SHEN M.-H.H., 1992. Analysis of forced bilinear oscillators and the application to cracked beam dynamics. *AIAA Journal,* **30**(10), 2512-2519.

COOK, R.D., MALKUS, D.S., PLESHA, M.E. and WITT, R.J., 2002. *Concepts and applications of finite element analysis.* John Wiley & Sons, Inc.

DADO, M.H.F. and ABUZEID, O., 2003. Coupled transverse and axial vibratory behaviour of cracked beam with end mass and rotary inertia. *Journal of Sound and Vibration,* **261**(4), 675-696.

DADO, M.H., 1997. A comprehensive crack identification algorithm for beams under different end conditions. *Applied Acoustics,* **51**(4), 381-398.

DADO, M.H.F. and SHPLI, O.A., 2003. Crack parameter estimation in structures using finite element modeling. *International Journal of Solids and Structures,* **40**(20), 5389-5406.

DHARMARAJU, N., TIWARI, R. and TALUKDAR, S., 2005. Development of a novel hybrid reduction scheme for identification of an open crack model in a beam. *Mechanical Systems and Signal Processing,* **19**(3), 633-657.

DHARMARAJU, N., TIWARI, R. and TALUKDAR, S., 2004/1. Identification of an open crack model in a beam based on force–response measurements. *Computers & Structures,* **82**(2-3), 167-179.

DILENA, M. and MORASSI, A., 2004. The use of antiresonances for crack detection in beams. *Journal of Sound and Vibration,* **276**(1-2), 195-214.

DILENA, M. and MORASSI, A., 2002/8/29. Identification of crack location in vibrating beams from changes in node positions. *Journal of Sound and Vibration,* **255**(5), 915-930.

DIMAROGONAS, A.D. and PAPADOPOULOS, C.A., 1983/12/22. Vibration of cracked shafts in bending. *Journal of Sound and Vibration,* **91**(4), 583-593.

DONSKOY, D., EKIMOV, A., LUZZATO, E., LOTTIAUX, J.-., STOUPIN, S. and ZAGRAI, A., 2003. N-SCAN®: New Vibro-Modulation System for Detection and Monitoring of Cracks and Other Contact-Type Defects, 2003, pp400-409.

DONSKOY, D., SUTIN, A. and EKIMOV, A., 2001/6/1. Nonlinear acoustic interaction on contact interfaces and its use for nondestructive testing. *NDT & E International,* **34**(4), 231-238.

DOUKA, E., BAMNIOS, G. and TROCHIDIS, A., 2004. A method for determining the location and depth of cracks in double-cracked beams. *Applied Acoustics,* **65**(10), 997-1008.

DOUKA, E. and HADJILEONTIADIS, L.J., 2005/1. Time–frequency analysis of the free vibration response of a beam with a breathing crack. *NDT & E International,* **38**(1), 3-10.

FRISWELL , M.I. and PENNY J.E.T., 1992. A simple nonlinear model of a cracked beam, 1992, pp516-520.

GOUNARIS, G. and DIMAROGONAS, A., 1988. A finite element of a cracked prismatic beam for structural analysis. *Computers & Structures,* **28**(3), 309-313.

GOUNARIS, G.D. and PAPADOPOULOS, C.A., 1997. Analytical and experimental crack identification of beam structures in air or in fluid. *Computers & Structures,* **65**(5), 633-639.

GOUNARIS, G.D., PAPADOPOULOS, C.A. and DIMAROGONAS, A.D., 1996. Crack identification in beams by coupled response measurements. *Computers & Structures,* **58**(2), 299-305.

GOUNARIS, G.D. and PAPADOPOULOS, C.A., 2002. Crack identification in rotating shafts by coupled response measurements. *Engineering Fracture Mechanics,* **69**(3), 339-352.

GUDMUNDSON, P., 1983. The dynamic behaviour of slender structures with cross-sectional cracks. *Journal of the Mechanics and Physics of Solids,* **31**(4), 329-345.

GUDMUNDSON, P., 1982/10. Eigenfrequency changes of structures due to cracks, notches or other geometrical changes. *Journal of the Mechanics and Physics of Solids,* **30**(5), 339-353.

KAM, T.Y. and LEE, T.Y., 1994. Crack size identification using an expanded mode method. *International Journal of Solids and Structures,* **31**(7), 925-940.

KAM, T.Y. and LEE, T.Y., 1992/5. Detection of cracks in structures using modal test data. *Engineering Fracture Mechanics,* **42**(2), 381-387.

KRAWCZUK, M. and OSTACHOWICZ, W., 1990. Forced vibration of a cantilever Timoshenko beam with a closing crack, 1990, pp1067-1078.

LAMONACA, B.G., VALENTE, C. and BRANCALEONI, F., 1997. Crack Identification in nonlinear vibrating beams, 1997, pp1808-1814.

LEONG, W.H., STASZEWSKI, W.J., LEE, B.C. and SCARPA, F., 2005. Structural health monitoring using scanning laser vibrometry: III. Lamb waves for fatigue crack detection. *Smart Materials and Structures,* **14**(6), 1387-1395.

LOUTRIDIS, S., DOUKA, E. and HADJILEONTIADIS, L.J., 2005. Forced vibration behaviour and crack detection of cracked beams using instantaneous frequency. *NDT & E International,* **38**(5), 411-419.

MALLET, L., LEE, B.C., STASZEWSKI, W.J. and SCARPA, F., 2004. Structural health monitoring using scanning laser vibrometry: II. Lamb waves for damage detection. *Smart Materials and Structures,* **13**(2), 261-269.

MANOACH, E. and TRENDAFILOVA, I., 2008. Large amplitude vibrations and damage detection of rectangular plates. *Journal of Sound and Vibration*, **315**(3), 591-606.

MATVEEV, V.V. and BOVSUNOVSKY, A.P., 2002/1/3. Vibration-based diagnostics of fatigue damage of beam-like structures. *Journal of Sound and Vibration,* **249**(1), 23-40.

MCGRAVIE, A. and WOODWARD, C., 2000. Long Range Ultrasonic Fatigue Crack Detection, 2000, pp261-267.

MEIROVITCH, L., 1997. *Fundamental of Vibraitons.* McGraw- Hill higher Education.

MEIROVITCH, L., 1997. *Principles and techniques of vibrations.* Prentice hall International (U.K.) Limited.

MEYERS, M.A. and CHAWLA, K.K., 2009. *Mechanical behavior of materials.* 2nd Edition edn. Cambridge University Press.

NAGY, P.B., 1998. Fatigue damage assessment by nonlinear ultrasonic materials characterization. *Ultrasonics,* **36**(1-5), 375-381.

NAHVI, H. and JABBARI, M., 2005/10. Crack detection in beams using experimental modal data and finite element model. *International Journal of Mechanical Sciences,* **47**(10), 1477-1497.

ORHAN, S., 2007/9. Analysis of free and forced vibration of a cracked cantilever beam. *NDT & E International,* **40**(6), 443-450.

OSTACHOWICZ, W.M. and KRAWCZUK, M., 1991/10/22. Analysis of the effect of cracks on the natural frequencies of a cantilever beam. *Journal of Sound and Vibration,* **150**(2), 191-201.

OSTACHOWICZ, W.M. and KRAWCZUK, M., 1990. Vibration analysis of a cracked beam. *Computers & Structures,* **36**(2), 245-250.

PAGET, C.A., ATHERTON, K. and O'BRIEN, W., 2003. Triangulation algorithm for damage location in aeronautical composite structures, September 15-17 2003, pp363-360.

PALIT SAGAR, S., DAS, S., PARIDA, N. and BHATTACHARYA, D.K., 2006/7. Non-linear ultrasonic technique to assess fatigue damage in structural steel. *Scripta Materialia*, **55**(2), 199-202.

PANOVKO Y G, 1962. Internal damping during oscillation of elastic systems.

PAPADOPOULOS, C.A. and DIMAROGONAS, A.D., 1987/8/22. Coupled longitudinal and bending vibrations of a rotating shaft with an open crack. *Journal of Sound and Vibration*, **117**(1), 81-93.

PARSONS, Z. and STASZEWSKI, W.J., 2006. Nonlinear acoustics with low-profile piezoceramic excitation for crack detection in metallic structures. *Smart Materials and Structures*, **15**(4), 1110-1118.

PUGNO, N., SURACE, C. and RUOTOLO, R., 2000/8/31. Evaluation of the non-linear dynamic response to harmonic excitation of a beam with several breathing cracks. *Journal of Sound and Vibration*, **235**(5), 749-762.

QIAN, G.-., GU, S.-. and JIANG, J.-., 1990/4/22. The dynamic behaviour and crack detection of a beam with a crack. *Journal of Sound and Vibration*, **138**(2), 233-243.

RIVOLA, A. and WHITE, P.R., 1998/10/8. Bispectral analysis of the bilinear oscillator with application to the detection of fatigue cracks. *Journal of Sound and Vibration*, **216**(5), 889-910.

RIZOS, P.F., ASPRAGATHOS, N. and DIMAROGONAS, A.D., 1990/5/8. Identification of crack location and magnitude in a cantilever beam from the vibration modes. *Journal of Sound and Vibration*, **138**(3), 381-388.

RUOTOLO, R., SURACE, C., CRESPO, P. and STORER, D., 1996/12. Harmonic analysis of the vibrations of a cantilevered beam with a closing crack. *Computers & Structures*, **61**(6), 1057-1074.

SAAVEDRA, P.N. and CUITIÑO, L.A., 2001/6. Crack detection and vibration behavior of cracked beams. *Computers & Structures*, **79**(16), 1451-1459.

SEKHAR, A.S. and PRABHU, B.S., 1992/9/8. Crack detection and vibration characteristics of cracked shafts. *Journal of Sound and Vibration,* **157**(2), 375-381.

SHEN, M.-.H. and CHU, Y.C., 1992/9/17. Vibrations of beams with a fatigue crack. *Computers & Structures,* **45**(1), 79-93.

SHEN, M.-.H. and PIERRE, C., 1994/2/17. Free Vibrations of Beams With a Single-Edge Crack. *Journal of Sound and Vibration,* **170**(2), 237-259.

SHEN, M.-.H. and PIERRE, C., 1990/4/8. Natural modes of Bernoulli-Euler beams with symmetric cracks. *Journal of Sound and Vibration,* **138**(1), 115-134.

SHEN, M.-.H. and TAYLOR, J.E., 1991/11/8. An identification problem for vibrating cracked beams. *Journal of Sound and Vibration,* **150**(3), 457-484.

SHIFRIN, E.I. and RUOTOLO, R., 1999/5/6. Natural frequencies of a beam with an arbitrary number of cracks. *Journal of Sound and Vibration,* **222**(3), 409-423.

SHIH, H.W., THAMBIRATNAM, D.P. and CHAN, T.H.T., 2009. Vibration based structural damage detection in flexural members using multi-criteria approach. *Journal of Sound and Vibration,* **323**(3-5), 645-661.

SINHA, J.K., FRISWELL, M.I. and EDWARDS, S., 2002. Simplified models for the location of cracks in beam structures using measured vibration data. *Journal of Sound and Vibration,* **251**(1), 13-38.

SINHA, J.K., 2009. Higher Order Coherences for fatigue crack detection. *Engineering Structures,* **31**(2), 534-538.

SINHA, J.K. and FRISWELL, M.I., 2002. Simulation of the dynamic response of a cracked beam. *Computers & Structures,* **80**(18-19), 1473-1476.

SINOU, J. and LEES, A.W., 2005. The influence of cracks in rotating shafts. *Journal of Sound and Vibration,* **285**(4-5), 1015-1037.

SOLODOV, I.Y., 1998. Ultrasonics of non-linear contacts: propagation, reflection and NDE-applications. *Ultrasonics,* **36**(1-5), 383-390.

STASZEWSKI, W.J., LEE, B.C., MALLET, L. and SCARPA, F., 2004. Structural health monitoring using scanning laser vibrometry: I. Lamb wave sensing. *Smart Materials and Structures,* **13**(2), 251-260.

SUNDERMEYER, J.N. and WEAVER, R.L., 1995/6/22. On crack identification and characterization in a beam by non-linear vibration analysis. *Journal of Sound and Vibration,* **183**(5), 857-871.

SUTIN, A.M. and NAZAROV, V.E., 1995. Nonlinear acoustic methods of crack diagnostics. *Radiophysics and Quantum Electronics,* **38**(3), 109-120.

TIMOSHENKO, S.P. and YOUNG, D.H., 2002. *Elements of Strength of Materials.* East-West Press Private Limited.

TSAI, T.C. and WANG, Y.Z., 1996/5/9. Vibration analysis and diagnosis of a cracked shaft. *Journal of Sound and Vibration,* **192**(3), 607-620.

TSYFANSKY, S.L. and BERESNEVICH, V.I., 2000/9/7. Non-linear vibration method for detection of fatigue cracks in aircraft wings. *Journal of Sound and Vibration,* **236**(1), 49-60.

VIOLA, E., FEDERICI, L. and NOBILE, L., 2001/0. Detection of crack location using cracked beam element method for structural analysis. *Theoretical and Applied Fracture Mechanics,* **36**(1), 23-35.

VIOLA, E., RICCI, P. and ALIABADI, M.H., 2007. Free vibration analysis of axially loaded cracked Timoshenko beam structures using the dynamic stiffness method. *Journal of Sound and Vibration,* **304**(1-2), 124-153.

ZAITSEV, V., NAZAROV, V., GUSEV, V. and CASTAGNEDE, B., 2006. Novel nonlinear-modulation acoustic technique for crack detection. *NDT & E International,* **39**(3), 184-194.

Appendix A: Theory of Integral Equations for Straight Rods

Note: There has been no literature available on theory of integral equations for straight rods in English. This chapter on theory of integral equations for straight rods has been taken from Russian literature (Babakov) and translated into English.

The Principle of Linear Integral Equation

The simplest continuous system with infinite number of degrees is straight rods, oscillating about the equilibrium position. The oscillation around the position of equilibrium can be longitudinal, torsional or transverse. In all these cases it is assumed that the rod cross-section in all deformations remain flat and that the displacement of points of the axis or related to these points cross section of rod due to external excitation are determined uniquely by the value of one function from $y(x,t)$ of two variables – coordinates x and time t .

The restoring force arising due vibrations of rods for these cases are assumed to be within the proportionality limits, So that the values that determine the deformation of rod are linear functions of these forces. The systems committing these oscillations are called linear systems. The most important feature of linear system could be used in constructing the general theory of linear oscillations is the source-wise presentation of the deformation of system with the generalized force acting on it.

To clarify the meaning of this, consider first the static deformation $y\ (x)$ of system from a distributed load of intensity $f(x)$. For example, consider the static deflection of the rod under its own weight. Let $\overline{K}(x,q)$ denote, displacement of a cross section of the rod with the abscissa x under action of a single generalized force applied at the point with abscissa q. $\overline{K}(x,q)$ is a function of the coordinates x and q, defined over the whole length of the rod l, finite and continuous in $0 \leq x \leq l$, $0 \leq q \leq l$ and it satisfies all the properties necessary to justify the correctness of the following transformations. This function is called the influence function of the rod having a property of symmetry relative to the coordinates of x and q. This is called the *law of reciprocity*. Because of this law, displacement at cross-section-x due to unit force applied to cross-section q is equal to the displacement at cross-section q due to unit force applied cross-section-x.

$$\overline{K}(x,q) = \overline{K}(q,x) \tag{A-1}$$

All other values associated with linear elastic deformations of the linear system have the similar reciprocity. Using the influence of $\overline{K}(x,q)$, static deflection of the $y(x)$ at point x from the load of intensity $f(q)$ can be written as following integral expression:

$$y(x) = \int_0^l \overline{K}(x,q) f(q) dq \qquad \text{(A-2)}$$

This presentation of a $y(x)$ is called *source-wise presentation*. Source-wise representation (Eq. (A-2)) for a deformation is one of the expressions of the principle of superposition of linear elastic deformation of the system. According to the principle of superposition displacement at point x from the distributed load is obtained as the linear sum of elementary displacements of the loads acting on each element dq of the rod.

$$f\ (q)\ dq \qquad \text{(A-3)}$$

From this point of view (Eq. (A-2)) represents the extension of Hooke's law to the system with an infinite number of degrees of freedom. For a system with finite number of degrees of freedom we have the following expression (Eq. (A-4)):

$$y_i = \sum_{k=1}^{n} \alpha_{ik} F_k \qquad (i = 1, 2, \dots \dots \dots k) \qquad \text{(A-4)}$$

Where F_k- concentrated force, α_{ik}- static factors of influence. Thus, the principle of linear superposition and the possibility of imposing source-wise presentation of the strain $y(x)$ – are two equivalent expressions of the same basic properties of a linear system described by (Eq.(A-2)). Thus the existence of the functions of influence of an elastic system within its linear deformation is inextricably linked to its basic properties, expressed by the principle of superposition. If, apart from a distributed load the concentrated forces $F_i (i = 1, 2, \dots \dots \dots k)$ applied to the bar in some sections $x_i (i = 1, 2, \dots \dots \dots k)$ then the deformation at any point x would be the given by

$$y(x) = \int_0^l \overline{K}(x,q) f(q) dq + \sum_{i=1}^{k} F_i \overline{K}(x, x_i) \qquad \text{(A-5)}$$

Application of Linear Integral Equation on Small Oscillations of Straight Rod

This linear integral equation can be applied to the small vibration of straight rod along with d'Alembert's principle. Let the rod be loaded by forces depending on the time, with the intensity denoted as $P(q,t)$.In this case the deformation of the rod in a section x will also depend on time and will be determined by some function of two variables from $y(x,t)$ .This deformation according to the d'Alembert principle can be considered as static, if the load $P(q,t)$, does not includes the force of inertia of the masses of elementary particles of the rod. If $m(q)$ is mass or moment of inertia of unit length of the rod, the force of inertia of a rod element of length dq at point q will be equal

$$-m(q)\frac{\partial^2 y(q,t)}{\partial t^2}dq \qquad \text{(A-6)}$$

we get the equation of oscillations of a rod, if in the Eq. (A-2) we replace $f(q)dq$ for

$$\left[P(q,t) - m(q)\frac{\partial^2 y(q,t)}{\partial t^2}\right]dq \qquad \text{(A-7)}$$

and instead of $y(x)$ to write $y(x,t)$

$$y(x,t) = -\int_0^l \bar{K}(x,q)\frac{\partial^2 y(q,t)}{\partial t^2}\, m(q)dq + \int_0^l \bar{K}(x,q)P(q,t)dq \qquad \text{(A-8)}$$

This is integral equation of small vibrations of the straight rod. When the external load is absent, i.e., $P(q,t) = 0$, the system performs free vibrations. An integral equation of free vibration of rod is:

$$y(x,t) = -\int_0^l \bar{K}(x,q)\frac{\partial^2 y(q,t)}{\partial t^2}\, m(q)dq \qquad \text{(A-9)}$$

One of the most remarkable properties obtained in Eq. (A-9), is the fact that these equations have the same form for all types of vibration of rod - longitudinal, torsion and lateral for all boundary conditions. However, the influence function $\bar{K}(x,q)$ will be different for different types of vibrations and different boundary conditions. It can be built with the rules presented in course of mechanics of materials. The invariance of the

form of Eq. (A-9) in relation to different types of vibrations and different boundary conditions expresses the unique physical nature of small oscillations of linear systems, determining the existence of common properties and justifying the feasibility and desirability of constructing the general theory of vibration. Many principles of this theory significantly associated with the description of vibration by Eq.(A-9) or Eq. (A-8), can serve as interpretations of well-known theorems of the mathematical theory of integral equations with symmetric kernel. This theory, therefore, is particularly suited to identify the general features of different types of oscillations.

Integral Equations of the Free Oscillations of Straight Rod

The integral equations of free oscillation is given by following equation

$$y(x,t) = -\int_0^l \bar{K}(x,q)\frac{\partial^2 y(q,t)}{\partial t^2} m(q)dq \qquad \text{(A-10)}$$

The simplest periodic solution to the Eq. (A-10) is given in the following form

$$y(x,t) = \bar{A}(x)\sin(\Omega t + \alpha) \qquad \text{(A-11)}$$

Here $\bar{A}(x)$ defines a continuous set of amplitude of displacements of sections of rod from their equilibrium. It is therefore called *amplitude function, or modal function.* Substituting Eq. (A-11) in Eq. (A-10) we have

$$\bar{A}(x) = \Omega^2 \int_0^l \bar{K}(x,q)m(q)\bar{A}\,(q)dq \qquad \text{(A-12)}$$

From the theory of integral equations is well known that a nontrivial solution of homogeneous Eq. (A-12) does not exist for any values of Ω^2. Those values of Ω^2 for which there exists a nonzero solution $\bar{A}(x)$ are called *eigenvalues* of the functions $K(x,q)m\,(q)$, and the square roots of eigenvalues are resonance frequency of the system. The function $\bar{A}(q)$ corresponding to the natural frequency is called an *eigenmodes* of oscillations of the system. Eq. (A-12) have the asymmetric kernel

$$\bar{K}(x,q)m(q) \qquad \text{(A-13)}$$

This kernel can be made symmetric by substituting

$$A(x) = \bar{A}\,(x)\sqrt{m(x)} \tag{A-14}$$

Multiplying Eq. (A-12) by $\sqrt{m(x)}$ we have

$$\bar{A}(x)\sqrt{m(x)} = \Omega^2 \int_0^l \overline{K}(x,q)m(q)\bar{A}\,(q)\sqrt{m(x)}dq \tag{A-15}$$

Rearranging the terms, we have

$$\bar{A}(x)\sqrt{m(x)} = \Omega^2 \int_0^l \overline{K}(x,q)\sqrt{m(q)}\,\sqrt{m(x)}\bar{A}\,(q)\sqrt{m(q)}dq \tag{A-16}$$

Using Eq. (A-14), Eq. (A-16) takes the form

$$A(x) = \Omega^2 \int_0^l K(x,q)A\,(q)dq \tag{A-17}$$

Where

$$K(x,q) = \overline{K}(x,q)\sqrt{m(x)m(q)} \tag{A-18}$$

Thus the eigenmode $A(x)$ are fundamental functions of a homogeneous integral equation with symmetric kernel and square of natural frequencies are eigenvalues of kernel $K(x,q)$. From the general theory of integral equations, eigenvalues of the symmetric kernel form discrete infinite set renumbered in ascending order till infinity. It is assumed that eigenvalues corresponds to its eigenmode. They form the so called *complete system*.

Properties of Oscillations of the Straight Rod

Some properties of eigenmode can be found, without solving the Eq. (A-17). Of these properties particularly important in the theory of vibrations are the properties of orthogonality theorems for eigenmodes and decomposition of the mode represented source-wise by means of eigenmodes. These theorems are spread to the system with an infinite number of degrees of freedom of the known properties of systems with a finite number of degrees of freedom.

The Theorem on Orthogonality of Eigenmodes.

Let $A_i(x)$ denote the eigenmode corresponding to natural frequency Ω_i and the $A_k(x)$ corresponding to Ω_k so that

$$A_i(x) = \Omega_i^2 \int_0^l K(x,q) A_i(q) dq \tag{A-19}$$

$$A_k(x) = \Omega_k^2 \int_0^l K(x,q) A_k(q) dq \tag{A-20}$$

Multiply the Eq. (A-19) by $A_k(x)/\Omega_i^2$, Eq. (A-20) by $A_i(x)/\Omega_k^2$, and integrate for x ranging from 0 to l we get:

$$\frac{1}{\Omega_i^2} \int_0^l A_i(x) A_k(x) dx = \int_0^l \int_0^l K(x,q) A_i(x) A_k(q) dx dq \tag{A-21}$$

$$\frac{1}{\Omega_k^2} \int_0^l A_i(x) A_k(x) dx = \int_0^l \int_0^l K(x,q) A_i(x) A_k(q) dx dq \tag{A-22}$$

Double Integrals, on the right hand side of Eq.(A-21) and Eq. (A-22) is equal to each other due to the symmetry of the functions of the influence $K(x,q)$.Subtracting Eq. (A-22) from Eq. (A-21) we have

$$\left(\frac{1}{\Omega_i^2} - \frac{1}{\Omega_k^2}\right) \int_0^l A_i(x) A_k(x) dx = 0 \tag{A-23}$$

If $\Omega_i \neq \Omega_k$ then

$$\int_0^l A_i(x) A_k(x) dx = 0 \tag{A-24}$$

This equality is a theorem about orthogonality of the symmetrisized , to use their eigen forms. Due to the homogeneity of Eq. (A-17) the eigen modes are defined to a value of arbitrary constant multiplier. This factor can be selected so that

$$\int_0^l A_i^2(x)dx = 1 \tag{A-25}$$

The modes satisfying Eq. (A-25) are called as normalized ones. Going back to non symmetrised eigenmodes $A_i(x)$ then to such forms, taking into account the ratio

$$A_i(x) = \bar{A}_i(x)\sqrt{m(x)} \tag{A-26}$$

conditions of orthogonality and normalization will have the form:

$$\int_0^l m(x)\bar{A}_i(x)\bar{A}_k(x)dx = \begin{cases} 0 & i \neq k \\ 1 & i = k \end{cases} \tag{A-27}$$

written in such manner a condition of orthogonality can be seen as an expression of the fact that the mechanical work of the eigenload due to orthogonal eigen mode is equal to zero.

According to the theorem of decomposition, we assume the Eq. (A-17) of the eigenmode

$$A(x) = \Omega^2 \int_0^l K(x,q)A(q)dq \tag{A-28}$$

form a complete orthonormal system of functions

$$A_1(x), A_2(x), \ldots\ldots\ldots, \tag{A-29}$$

renumbered in ascending order of their corresponding natural frequencies

$$\Omega_1 < \Omega_2 < \ldots\ldots\ldots \tag{A-30}$$

In this case, with positive Ω_i^2 for any value of q from the interval $(0, l)$ the kernel $K\ (x, q)$, considered as a function of x only, may be represented by a uniformly convergent series

$$K(x,q) = a_1 A_1(x) + a_2 A_2(x) + \ldots\ldots\ldots\ldots \tag{A-31}$$

Multiplying both sides of this equality by $A_k(x)$ and integrating to x from 0 to l is received by virtue of orthonormality for the functions $A_k(x)$

$$a_k = \int_0^l K(x,q) A_k\,(x) dx \tag{A-32}$$

Comparing this equality with the Eq. (A-28), we have

$$a_k = \frac{A_k(p)}{\Omega_k^2} \tag{A-33}$$

This value of the coefficients of expansion Eq. (A-33) under the assumption that such an expansion exists, and a series is uniformly convergent. Hence,

$$\sum_{k=1}^{\infty} a_k\, A_k(x) \tag{A-34}$$

Now the decomposition of the kernel on its eigenmodes looks as follows:

$$K(x,q) = \sum_{k=1}^{\infty} \frac{A_k(x) A_k(q)}{\Omega_k^2} \tag{A-35}$$

This presentation of the kernel is called bilinear.

In the theory of linear oscillations of the assumptions about the uniform convergence of series Eq. (A-31) and Eq. (A-35) is always implemented as the kernel of integral equations of small oscillations, as functions of the influence of the elementary deformations of the rod, satisfy all necessary conditions for this. Bilinear representation of the kernel Eq. (A-35) is a generalized expression of the theorem about the expansion

coefficients of the inverse equations of small oscillations of systems with a finite number of degrees of freedom.

General Solution of Integral Equations of Free and Forced Vibrations of Straight Rod

Free Vibrations of Straight Rods

The equation of free vibration of rod is given by

$$y(x,t) = -\int_0^l \bar{K}(x,q)\frac{\partial^2 y(q,t)}{\partial t^2} m(q)dq \qquad \text{(A-36)}$$

on substitution

$$u(x,t) = y(x,t)\sqrt{m(x)} \qquad \text{(A-37)}$$

and putting

$$K(x,q) = \bar{K}(x,q)\sqrt{m(x)m(q)} \qquad \text{(A-38)}$$

gives Eq. (A-36) a symmetric form

$$u(x,t) = -\int_0^l K(x,q)\frac{\partial^2 u(q,t)}{\partial t^2} dq \qquad \text{(A-39)}$$

Using Eq. (A-35), Eq. (A-39) can be written in eigen form as follows

$$u(x,t) = -\int_0^l \sum_{i=1}^{\infty} \frac{A_i(x)A_i(q)}{\Omega_i^2}\frac{\partial^2 u(q,t)}{\partial t^2} dq \qquad \text{(A-40)}$$

Rearranging terms

$$u(x,t) = -\sum_{i=1}^{\infty}\frac{A_i(x)}{\Omega_i^2}\int_0^l A_i(q)\frac{\partial^2 u(q,t)}{\partial t^2} dq = \sum_{i=1}^{\infty} F_i(t)A_i(x) \qquad \text{(A-41)}$$

Where

$$F_i(t) = -\frac{1}{\Omega_i^2}\int_0^l A_i(q)\frac{\partial^2 u(q,t)}{\partial t^2}dq \qquad \text{(A-42)}$$

Therefore

$$u(x,t) = \sum_{i=1}^{\infty} F_i(t)A_i(x) \qquad \text{(A-43)}$$

It proves that the solution of Eq. (A-39) can be represented as an infinite sum of products of two functions, one of which is a function of only t, the other function of x which is the general solution of integral equations. The solution of Eq. (A-39) can always be represented in the form of expansion in its eigenmodes of oscillations of the rod. Using the decomposition in Eq. (A-43) it is possible to find the general solution of Eq. (A-39). In fact, the well-known rule for determining the coefficients F_i by the decomposition of Eq. (A-43):

$$F_i(t) = \int_0^l u(q,t)A_i(q)dq \qquad \text{(A-44)}$$

will have:

$$\ddot{F}_i(t) = \int_0^l A_i(q)\frac{\partial^2 u(q,t)}{\partial t^2}dq \qquad \text{(A-45)}$$

on the other hand from Eq.(A-42) we have

$$F_i(t) = -\frac{1}{\Omega_i^2}\int_0^l A_i(q)\frac{\partial^2 u(q,t)}{\partial t^2}dq \qquad \text{(A-46)}$$

consequently,

$$\ddot{F}_i(t) + \Omega_i^2 F_i(t) = 0 \qquad \text{(A-47)}$$

and

$$F_i(t) = C_i \cos \Omega_i t + D_i \sin \Omega_i t \quad (i = 1,2,3, \dots \dots \dots \dots) \tag{A-48}$$

where C_i and D_i- arbitrary constant of integration.

Solution in Eq. (A-43), using the Eq. (A-48) can be represented as follows:

$$u(x,t) = \sum_{i=1}^{\infty} (C_i \cos \Omega_i t + D_i \sin \Omega_i t) A_i(x) \tag{A-49}$$

It can also be written as

$$u(x,t) = \sum_{i=1}^{\infty} H_i \sin(\Omega_i t + \alpha_i)\, A_i(x) \tag{A-50}$$

if you replace the constants C_i and D_i by putting

$$\begin{aligned} C_i &= H_i sin\alpha_i \\ D_i &= H_i cos\alpha_i \end{aligned} \tag{A-51}$$

Eq. (A-50) implies that the vibration of the rod represents the result of superimposing a finite or infinite number of simple harmonic vibrations of their eigenmodes. Thus, the law established for systems with a infinite number of degrees of freedom, remains valid for systems with finite number of degrees of freedom – this is the universal for free oscillations of linear systems without damping. The constant of integration C_i and D_i are determined from the initial conditions, which in the case, for example, the transverse vibrations are expressed as the initial moment $t = 0$ the distribution of displacements of point of the axis of the rod system.

$$u(x,0) = \psi(x) \tag{A-52}$$

and their velocities

$$\dot{u}(x,0) = \eta(x) \tag{A-53}$$

where $\psi(x)$ and $\eta(x)$ some known function of the variable x. The calculation of the constants is as follows. First, we find from (A-49):

$$C_i \cos \Omega_i t + D_i \sin \Omega_i t = \int_0^l u(q,t) A_i(q) dq \qquad \text{(A-54)}$$

Putting here $t = 0$, we obtain:

$$C_i = \int_0^l A_i(x) \psi(x) ds \qquad \text{(A-55)}$$

Taking derivative of (A-54) w.r.t. t and then putting $t = 0$, we have

$$D_i = \frac{1}{\Omega_i} \int_0^l \eta(x) A_i(x) ds \qquad \text{(A-56)}$$

As can be seen from the last formulas, the constant C_i and D_i are the coefficients of expansion given function $\psi(x)$ and $\eta(x)$ on the eigenmodes. We have seen that such decomposition is possible for functions represented by source-wise. The functions $\psi(x)$ and $\eta(x)$ have simple physical meaning - the initial deformation and the distribution of initial velocities. The potential and kinetic energy of initial state of the system is always finite. Thus, the functions $\psi(x)$ and $\eta(x)$ are not arbitrary mathematical functions, and the feasibility and convergence of expansions with respect to its own forms here does not require additional special studies.

Forced Vibrations of Straight Rods

As can be seen from the Eq. (A-49) for the general solution of Eq. (A-39) of free oscillations of a rod, a solution can be constructed, if systems natural frequency is known,

$$A(x) = \Omega^2 \int_0^l K(x,q) A(q) dq \qquad \text{(A-57)}$$

With the help of their eigen form of free oscillations general solution of the equation of forced oscillations can be constructed:

$$y(x,t) = -\int_0^l \overline{K}(x,q)\frac{\partial^2 y(q,t)}{\partial t^2}m(q)dq + \int_0^l \overline{K}(x,q)f(q,t)dq \quad \text{(A-58)}$$

where the external excitation is a function of the load represented by $f\ (q,t)$.

Let

$$u(x,t) = y(x,t)\sqrt{m(x)} \quad \text{(A-59)}$$

substituting Eq. (A-59) in Eq. (A-58) we have

$$u(x,t) = -\int_0^l K(x,q)\frac{\partial^2 u(q,t)}{\partial t^2}dq + \int_0^l K(x,q)Q(q,t)dq \quad \text{(A-60)}$$

where

$$K(x,q) = \overline{K}(x,q)\sqrt{m(x)m(q)} \quad \text{(A-61)}$$

$$Q(q,t) = \frac{1}{\sqrt{m(q)}}f(q,t) \quad \text{(A-62)}$$

From Eq. (A-35) we have

$$K(x,q) = \sum_{i=1}^{\infty}\frac{A_i(x)A_i(q)}{\Omega_i^2} \quad \text{(A-63)}$$

substituting Eq. (A-63) in Eq.(A-60) gives the decomposition by eigenmodes for functions $u(x,t)$:

$$u(x,t) = \sum_{i=1}^{\infty}F_i(t)A_i(x) \quad \text{(A-64)}$$

where

$$F_i(t) = -\frac{1}{\Omega_i^2}\int_0^l A_i(q)\frac{\partial^2 u(q,t)}{\partial t^2}dq + \frac{1}{\Omega_i^2}\int_0^l A_i(q)Q(q,t)dq \quad \text{(A-65)}$$

But

$$F_i(t) = \int_0^l u(q,t)A_i(q)dq \quad \text{(A-66)}$$

$$\ddot{F}_i(t) = \int_0^l \frac{\partial^2 u(q,t)}{\partial t^2}A_i(q)dq \quad \text{(A-67)}$$

substituting Eq. (A-67) in Eq. (A-65), we arrive to the equation

$$\Omega_i^2 F_i(t) = -\ddot{F}_i(t) + \int_0^l A_i(q)Q(q,t)dq \quad \text{(A-68)}$$

which with the help of definition

$$\int_0^l A_i(q)Q(q,t)dq = f_i(t) \quad \text{(A-69)}$$

can be represented as follows:

$$\ddot{F}_i(t) + \Omega_i^2 F_i(t) = f_i(t) \quad \text{(A-70)}$$

The solution of the Eq. (A-70) is

$$F_i(t) = C_i cos\Omega_i t + D_i \sin\Omega_i t + \frac{1}{\Omega_i}\int_0^t f_i(\tau)sin\Omega_i(t-\tau)d\tau \quad \text{(A-71)}$$

where C_i and D_i are constant of integration. Substituting the expression obtained for $F_i(t)$ in Eq. (A-64), we obtain the general solution of Eq. (A-60)

$$u(x,t) = \sum_{i=1}^{\infty} \left[C_i cos\Omega_i t + D_i \sin \Omega_i t + \frac{1}{\Omega_i} \int_0^t f_i(\tau) sin\Omega_i (t-\tau) d\tau \right] A_i(x) \quad \text{(A-72)}$$

when the perturbing load is changed to a harmonic law

$$Q(q,t) = P(q) \sin(\omega t + \alpha) \quad \text{(A-73)}$$

For this case Eq. (A-70) will take the form:

$$\ddot{F}_i(t) + \Omega_i^2 F_i(t) = c_i \sin(\omega t + \alpha) \quad \text{(A-74)}$$

where

$$c_i = \int_0^l P(q) A_i(q) dq \quad \text{(A-75)}$$

and its integral

$$F_i(t) = C_i cos\Omega_i t + D_i \sin \Omega_i t + \frac{c_i}{\Omega_i^2 - \omega^2} \sin(\omega t + \alpha) \quad \text{(A-76)}$$

The general solution of Eq. (A-60) to a distributed harmonic perturbing load get from Eq. (A-72) by re-writing it as follows:

$$u(x,t) = \sum \left[C_i cos\Omega_i t + D_i \sin \Omega_i t + \frac{c_i}{\Omega_i^2 - \omega^2} \sin(\omega t + \alpha) \right] A_i(x) \quad \text{(A-77)}$$

Let us find the arbitrary constants C_i and D_i assuming that

$$u\,(x,0) = \; 0 \;\; \dot{u}\,(x,0) = \; 0 \; \alpha \; = \; 0. \quad \text{(A-78)}$$

From Eq. (A-77) above all we have:

$$C_i cos\Omega_i t + D_i \sin\Omega_i t + \frac{c_i}{\Omega_i^2 - \omega^2}\sin(\omega t + \alpha) = \int_0^l u(x,t)A_i(x)dx \quad \text{(A-79)}$$

Putting $t = 0$, we get $C_i = 0$ .After differentiation w.r.t t and putting $t = 0$, we obtain:

$$D_i = \frac{c_i \omega}{\Omega_i(\Omega_i^2 - \omega^2)} \quad \text{(A-80)}$$

Thus, with zero initial conditions, solution of Eq. (A-79) will take the form:

$$u(x,t) = sin\omega t \sum_{i=1}^{\infty} \frac{c_i A_i(x)}{(\Omega_i^2 - \omega^2)} + \omega \sum_{i=1}^{\infty} \frac{c_i A_i(x) sin\Omega_i t}{\Omega_i(\Omega_i^2 - \omega^2)} \quad \text{(A-81)}$$

The first element of the right-hand side defines the forced oscillations, which form $v\ (x)$ presented in Eq. (A-81) the sum of the series

$$\sum_{i=1}^{\infty} \frac{c_i A_i(x)}{(\Omega_i^2 - \omega^2)} = v(x) \quad \text{(A-82)}$$

The second term refers to the free oscillation, always accompanied by the forced, even with zero initial conditions. These accompanying oscillations depend, as it is forced, from the exciting forces, however, like this free oscillation, they decay in the presence of damping. Substituting in Eq. (A-82) the value c_i of the formula in Eq. (A-75) presented an equation for the shape of forced oscillations of the form:

$$v(x) = \int_0^l \left[\sum_{i=1}^{\infty} \frac{A_i(x)A_i(q)}{(\Omega_i^2 - \omega^2)}\right] P(q)dq \quad \text{(A-83)}$$

and introducing the definition

$$\sum_{i=1}^{\infty} \frac{A_i(x)A_i(q)}{(\Omega_i^2 - \omega^2)} = \Gamma(x, s; \omega^2) \quad \text{(A-84)}$$

even so:

$$v(x) = \int_0^l \Gamma(x, q; \omega^2) P(q) dq \qquad \text{(A-85)}$$

When the perturbing load is concentrated harmonic force $hsin\omega t$, applied at the point $x = a$, then

$$P(q) = h\sigma_1(q - a) \qquad \text{(A-86)}$$

where $\sigma_1(s - a)$ - impulsive function of the first order. In this case,

$$c_i = \int_0^l P(q) A_i(q) dq = hA_i(a) \qquad \text{(A-87)}$$

and the solution (A-81) has the form

$$u(x,t) = hsin\omega t \sum_{i=1}^{\infty} \frac{A_i(x)A_i(a)}{(\Omega_i^2 - \omega^2)} + \omega \sum_{i=1}^{\infty} \frac{hA_i(a)A_i(x)}{\Omega_i(\Omega_i^2 - \omega^2)} sin\Omega_i t \qquad \text{(A-88)}$$

The form of forced oscillations is presented here with

$$\sum_{i=1}^{\infty} \frac{hA_i(a)A_i(x)}{\Omega_i^2 - \omega^2} = h\,\Gamma(x, a; \omega^2) = v(x) \qquad \text{(A-89)}$$

when h = l,

$$v(x) = \Gamma(x, a; \omega^2) = \sum_{i=1}^{\infty} \frac{A_i(a)A_i(x)}{\Omega_i^2 - \omega^2} \qquad \text{(A-90)}$$

The function $\Gamma(x, a; \omega^2)$ is nothing other than the influence of harmonic coefficient of frequency of ω: It is the amplitude of forced oscillations of the point x from a unit harmonic force of frequency ω applied to a point a. Thus, the important concept of harmonic coefficient of the influence imposed by the theory of forced oscillations of systems with a finite number of degrees of freedom has a natural generalization to continuous systems, treated using the integral equation. All the above forms for solution

the equation of forced oscillations of the straight-rods, and also to determine the influence of harmonic influence makes sense if $\omega \neq \Omega_k$, ie, where the exciting frequency does not coincide with any of the natural frequencies of the system. When a capture takes place, it is the phenomenon of resonance. In this case, the solution of the Eq. (A-77) will have a different form. Suppose, for example, $\omega = \Omega_k$ .Then Eq. (A-77) will have a solution

$$F_k(t) = C_k cos\Omega_k t + D_k sin\Omega_k t - \frac{c_k t}{2p_k} cos\Omega_k t \qquad \text{(A-91)}$$

and

$$u(x,t) = \sum_{i=1}^{\infty} \left[C_i cos\Omega_i t + D_i \sin\Omega_i t + \frac{c_i}{\Omega_i^2 - \omega^2} \sin(\omega t + \alpha) \right] A_i(x) + \left[C_k cos\Omega_k t + D_k sin\Omega_k t - \frac{c_k t}{2p_k} cos\Omega_k t \right] A_k(x) \qquad \text{(A-92)}$$

As can be seen from the above studies, in particular from the expressions Eq. (A-72), Eq. (A-82), and others, the general solution of integral equations of free and forced oscillations may be produced, if you will find the eigen modes of the considered systems.

Appendix B: Complete Matlab-Simulink Program

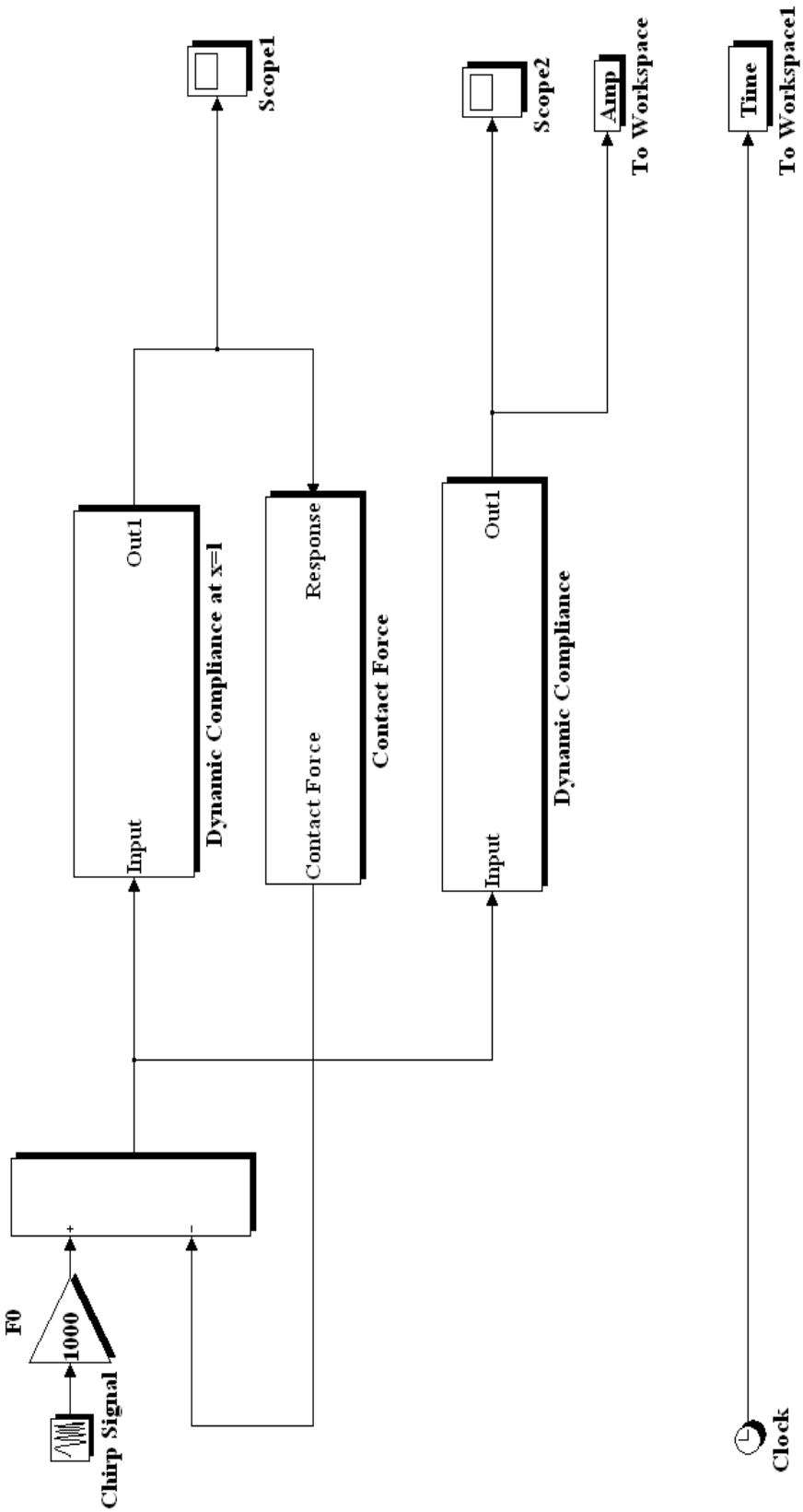

Appendix C: Contact Force Subsystem